UC-4+25
LBL-18554
c.1

Lawrence Berkeley Laboratory

UNIVERSITY OF CALIFORNIA

RECEIVED
LAWRENCE
BERKELEY LABORATORY
NOV 20 1984
LIBRARY AND
DOCUMENTS SECTION

Materials & Molecular Research Division

IMPURITY COMPLEXES IN PURE ELEMENTAL SEMICONDUCTORS

R.E. McMurray, Jr.
(Ph.D. Thesis)

October 1984

For Reference
Not to be taken from this room

LBL-18554
c.1

Prepared for the U.S. Department of Energy under Contract DE-AC03-76SF00098

DISCLAIMER

This document was prepared as an account of work sponsored by the United States Government. While this document is believed to contain correct information, neither the United States Government nor any agency thereof, nor the Regents of the University of California, nor any of their employees, makes any warranty, express or implied, or assumes any legal responsibility for the accuracy, completeness, or usefulness of any information, apparatus, product, or process disclosed, or represents that its use would not infringe privately owned rights. Reference herein to any specific commercial product, process, or service by its trade name, trademark, manufacturer, or otherwise, does not necessarily constitute or imply its endorsement, recommendation, or favoring by the United States Government or any agency thereof, or the Regents of the University of California. The views and opinions of authors expressed herein do not necessarily state or reflect those of the United States Government or any agency thereof or the Regents of the University of California.

LBL-18554

IMPURITY COMPLEXES IN PURE ELEMENTAL SEMICONDUCTORS

Robert E. McMurray, Jr.

Ph.D. Thesis

Lawrence Berkeley Laboratory
University of California
Berkeley, California 94720

October 1984

This work was supported in part by the Director, Office of Energy Research, Office of Health and Environmental Research, U.S. Department of Energy under Contract number DE-AC03-76SF00098, and by the National Science Foundation under grant number DMR-8203430.

Impurity Complexes in Pure Elemental Semiconductors

Robert E. McMurray, Jr.

Submitted in partial fullfillment of requirements
for the degree of Doctor of Philosophy,
to the Department of Physics,
University of California,
Berkeley, CA

ABSTRACT

The physics of shallow impurity levels in semiconductors in many ways corresponds to the physics of simple isolated atoms in free space. Despite the dielectric sceening of the lattice and the necessity of using an effective mass rather than the free electron mass, such questions as the energy spectrum and selection rules for dipole-allowed single photon transitions can be treated rather simply for elemental impurities. However, additional complications arise due to internal structure when an electrically active impurity complex is considered. The theoretical and experimental implications of the multi-atom complex form the basis of this thesis. Although several impurity complexes in germanium had been previously explained in the context of a tunnelling-hydrogen model, additional understanding was needed. Also, several impurity complex centers had still remained unexplained, and three of these in particular, those due to carbon-nitrogen centers, make up a prominent portion of the research for this thesis. In addition to providing a satisfactory model to explain all of the known experimental facts which were discovered in this work regarding these carbon-nitrogen impurity complexes, this dissertation brings together many of the properties of other impurity complexes in a way in which

they can be understood as an overall system of complexes, rather than as isolated cases. Such is the situation for the group II impurity-hydrogen complexes, and for the overcharged acceptors of the groups I and II impurities. Overall, this work brings together the existing knowledge of electrically-active shallow impurity complex centers in elemental semiconductors.

ACKNOWLEDGEMENTS

I would like to express my appreciation to my research advisor, Professor Eugene E. Haller of the Department of Material Science and Mineral Engineering, without whose help and guidance I would not have been able to perform this research. In particular his persistence in regards to care for the fine details which must be understood in order to explain the overall properties of any physical system was extremely useful in a project such as this were one is exploring unknown systems. I would also like to thank my Physics Department faculty advisor, Professor Leo M. Falicov, for many enlightening and encouraging conversations over the course of my research as a graduate student at Berkeley. I gratefully acknowledge Professor Paul L. Richards of the Department of Physics for providing me with continued use of his far-infrared spectrometer facilities throughout the past few years, use of which formed the backbone of the experimental measurements for this thesis. In addition I would like to thank William Hansen and the rest of the staff of the nuclear radiation detector group at Lawrence Berkeley Laboratory for their technical assistance, especially Nancy Haegel for variable temperature Hall effect measurements and Paul Luke for fabrication of nuclear detectors from several of my samples. Thanks also to

Professor Peter Yu of the Physics Department and Professor Nathan Cheung of the Electrical Engineering and Computer Science Department for their help in reading and commenting on this dissertation.

Finally, I especially wish to thank my wife, Sheri, for her patience and understanding at those times when I needed it, and for her continued support of my choice of career as a physicist, despite the amount of time and education necessary.

Funding for this work was provided in part by the Director's Office of Energy Research, Office of Health and Environmental Research, U.S. Department of Energy under contract number DE-AC03-76SF00098, and in part by the National Science Foundation under grant number DMR-8203430.

TABLE OF CONTENTS

Chapter 1 -- Introduction ..... page 1

1.1 Effective Mass Theory 2

1.2 Photothermal Ionization Spectroscopy 6

1.3 Michelson Interferometer 12

1.4 PTIS in Elemental Semiconductors 15

1.5 Spectroscopy of Acceptors 18

Chapter 2 -- Exp. I: Crystal Growth, Characterization and Sample Preparation ..... page 21

2.1 Ultra-pure Crystal Preparation 21

2.2 PTIS Sample Preparation 25

2.3 Quenching, Annealing and Diffusion Procedures for Special Samples 27

2.4 Diagnostic Measurement Techniques 31

Chapter 3 -- Exp. II: Photothermal Ionization Spectroscopy ..... page 35

3.1 Interferometer and Fourier Transformation 35

3.2 Data Acquisition System and Noise Considerations 42

3.3 Sample Holders, Inserts, and Helium Dewar 46

3.4 Stress Insert and Superconducting Magnet Dewar 51

Chapter 4 -- Elemental and Complex Acceptors:

Theory and Experiment ..... page 55

4.1 Characteristic Features of Spectra of Elemental Acceptors 55

4.2 Sensitivity and Signal-to-Noise 61

4.3 Ge and Si Donor Spectra 64

4.4 Impurity Complexes 66

Chapter 5 -- Novel Acceptors $A_{3,4,5}$: Spectroscopy ..... page 71

5.1 Conditions for Existence of the Novel Acceptors 71

5.2 Variable-temperature Infrared Spectroscopy 75

5.3 Piezospectroscopy and Magnetospectroscopy 80

5.4 Interconversion of A_4 and $A_{3,5}$ 82

5.5 $A_{3,5}$ and A_4 Generation by KCN Diffusion into Germanium 90

5.6 ^{14}C Radiotracer Experiments 96

Chapter 6 -- Novel Acceptors $A_{3,4,5}$: Theory ..... page 98

6.1 Group Theoretical Considerations 98

6.2 Models for Impurity Complexes 103

6.3 Agreement of Theory and Experiment 105

6.4 Analysis of Interconversion Kinetics 108

Chapter 7 -- Special Studies ..... page 113

7.1 Magnetic Field Dependences 114

7.2 Ge:Be Spectroscopy 120

7.3 A^+ Centers: Experimental 126

7.4 A^+ Centers: Theory 133

7.5 Ge:Group II-Hydrogen Impurity Complex Acceptors 139

7.6 Absorption Spectroscopy Using A^+ Photoconductors 148

Chapter 8 -- Discussion, Conclusions, and Future Work ..... page 153

8.1 Effectiveness of the Current Models for Tunnelling-hydrogen Complexes 154

8.2 Models for C-N Impurity Complexes and their Predictions 156

8.3 Comparison of Acceptor-plus Centers to Atomic Models 158

8.4 Absorption Spectroscopy Using A^+ Photoconductors 159

8.5 Future Plans and Speculations 159

Appendix A -- Effective Mass Theory ..... page 163

References ..... page 168

FIGURES

Figure 1 -- Band structure of Ge 3

Figure 2 -- PTIS two-step process 7

Figure 3 -- Absorption vs. PTIS 9

Figure 4 -- Michelson Interferometer 36

Figure 5 -- Interferogram and Fourier Transformation 39

Figure 6 -- Transconductance Amplifier 43

Figure 7 -- Liguid He Cryostat 47

Figure 8 -- Exchange Gas Insert 50

Figure 9 -- Stress Insert 52

Figure 10 -- Excited States of Elemental Acceptors 56

Figure 11 -- PTIS of Al 57

Figure 12 -- PTIS with Band-edged Light 64

Figure 13 -- PTIS of Si:P 66

Figure 14 -- Tunnelling H Impurity Center 68

Figure 15 -- Impurity Complex Ground State Manifold 69

Figure 16 -- PTIS of carbon-nitrogen grown Ge 73

Figure 17 -- PTIS of Mixed-gas grown Ge 75

Figure 18 -- Sample Temperature Dependence 77

Figure 19 -- Thermal Distribution in Manifold 79

Figure 20 -- Sum of States in Manifold 80

Figure 21 -- Spectroscopy with Interconversion 83

Figure 22 -- Interconversion Annealing Equilibrium 85

Figure 23 -- Free Energy in Configurational Coordinates . 86
Figure 24 -- Interconversion at 50°C 88
Figure 25 -- Interconversion at 120°C 88
Figure 26 -- Time constants vs. 1/T 90
Figure 27 -- Substitutional A(C,N) 91
Figure 28 -- Interstitial A(C,N) 92
Figure 29 -- Magnetospectroscopy of Al and A(H,C) 115
Figure 30 -- Zeeman Splitting of Al D and C Lines 117
Figure 31 -- Field Dependence of C Line Component 118
Figure 32 -- Crossing of Lines of the Same Symmetry 119
Figure 33 -- Ge:Al,Be PTIS Lines 122
Figure 34 -- Be Absorption Lines in Ge:Al Continuum 123
Figure 35 -- Ge:B,Al Absorption Lines in the Continuum . 128
Figure 36 -- Li Compensated Ge:Be Spectra 130
Figure 37 -- Stress Removal of Acceptor-plus Centers ... 132
Figure 38 -- Ge:Cu-plus Center 135
Figure 39 -- Comparison of Group I,II,III-plus Centers . 137
Figure 40 -- PTIS of A(Be,H) 141
Figure 41 -- Thermal Population of A(Be,H) 142
Figure 42 -- PTIS of Stressed Ge:A(Be,H) 143
Figure 43 -- PTIS of A(Zn,H) 145
Figure 44 -- PTIS of Stressed A(Zn,H) 146
Figure 45 -- Isothermal Annealing of A(Zn,H) 147
Figure 46 -- Variable-temperature Hall Effect of A(Zn,H) 148
Figure 47 -- PTIS of Zn^+ 149

Figure 48 -- Absorption Spectrum of Ge:Sb,As 150

Figure 49 -- Absorption Spectrum of High Conc. Sb 151

Figure 50 -- Linear Absorption Coefficient of Ge:Sb 152

TABLES

Table 1 -- Tetrahedral Double Group 100

Table 2 -- Multiple Acceptor Plus Centers 133

Table 3 -- Variational Calculation of Energies 139

Chapter 1 -- Introduction

Any study of impurity complexes in elemental semiconductors must begin with a description of the behavior of the normal elemental impurities. Those atomic impurities of most interest in this work are the single acceptors (donors) which occur when a group III (group V) impurity assumes a substitutional position in an otherwise perfect diamond-structure lattice of group IV atoms. Such an impurity can then be most easily described in terms of an effective mass theory (EMT), as proposed by Kittel and Mitchell (1954) and by Luttinger and Kohn (1955). When this theory is applied to a single elemental substitutional acceptor (donor) which binds a hole (electron) in a dielectrically screened coulomb field, the binding energy is found to be roughly three orders of magnitude smaller than that of the electron in a hydrogen atom (Faulkner, 1969).

For the most part the concern of this thesis will be with impurities in the elemental semiconductor Ge. Although donors will sometimes be mentioned, as well as other host materials such as Si, the Ge acceptor impurities will be focused upon. In particular, results will be given for both substitutional elemental impurities as well as impurity complexes involving two or more atoms. Two of the main reasons for the renewed interest in the long-studied

semiconductor Ge are the recently achieved extremely low impurity concentrations, which are unmatched by any other semiconductor (impurity concentrations as low as 10^9 cm^{-3}), and the discovery of novel complex impurity centers in this material. The high purity sample provides an ideal host for the high resolution spectroscopy of essentially isolated impurities. An in-house ultra-pure Ge crystal growing facility makes possible a wide variety of experimental studies.

1.1 Effective Mass Theory

In an elemental semiconductor such as germanium, the diamond-structure symmetry of the lattice gives rise to the band structure shown in Figure 1. At the top of the valence band there exists a four-fold degeneracy of the energy bands having the Γ_8 symmetry from the $\bar{T}_d$ point group of the Ge atoms. These degenerate states can be characterized by an effective average band curvature (second derivative of E(k), suitably averaged over all directions in reciprocal space) which causes a hole in the band occupancy to react to a force as if it had a mass equal to the inverse of the curvature. That is to say, the hole obeys a force equation of the form

$$F = m^* \left(\frac{dv}{dt}\right) \quad \text{where} \quad m^* = \hbar^2 \left(\frac{d^2E}{dk^2}\right)^{-1} .$$

The value m^* defined in this equation is known as the effective mass of the energy band. Strictly speaking it is an anisotropic tensor quantity, but we will consider an appropriately averaged value of m^* as a scalar.

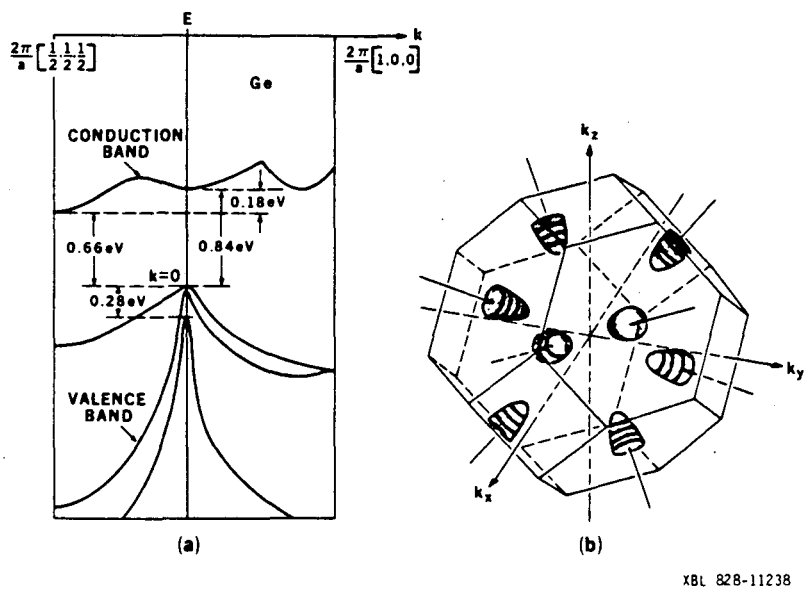

Figure 1 -- Band structure of Ge

One can make good use of the simplicity of the effective mass approximation (Kohn 1957) described above to calculate binding energies of charged carriers at impurity sites. In the case of a single acceptor (donor) the hole (electron) is bound to the impurity by a coulomb field due to a single ionic charge. However, this charge is screened by the dielectric constant of the lattice material (≃16 for

Ge, ≃12 for Si) reducing the binding energy from that of a free hydrogen atom by a factor of ε^{-2}. This energy is further reduced by the effective mass of the carrier (of the order of 0.1 m_e for holes in Ge) resulting in a final EMT energy of the order of 10 meV for single acceptors in Ge (see Appendix A). Thus the obvious terminology of group III (V) impurity atoms as "shallow" acceptors (donors).

Not only is the ground state binding energy scaled down by the factors just given, but all of the excited state energies as well. Each of these states is basically a manifestation of a single charged carrier (hole or electron) in the coulomb field of a singly-charged ion, just as in the hydrogen atom. The spectrum of bound excited states is similar to those of hydrogen (except for the complications of the crystal lattice symmetry and the energy band degeneracy) and so shallow impurity states are known as "hydrogenic". It is therefore possible to perform spectroscopic studies on these shallow hydrogenic impurity states. Spectroscopy from the ground state ((1s) hydrogenic manifold) would correspond to dipole-allowed transitions of the Lyman series in hydrogen. The very small binding energies require photons in the far-infrared spectral range; additionally, cryogenic temperatures (of the order of 6 K for Ge) are required to reduce thermal ionization and line

broadening.

Although this EMT method provides a reasonable estimate for the binding energies of most single acceptors (donors), there is always an impurity-specific correction to this estimate due to the incomplete screening of the ionic charge by the core states in the vicinity of the impurity site. This charge is not simply a single point charge in a uniform dielectric, as the model assumes, but rather a substitutional singly-ionized atom of a different species from that of the host lattice. The requirement of orthogonality of the shallow level's wave function to the core states of the impurity is responsible for this effect, which is most pronounced in the ground state energy due to the large probability density of the (1s) state at r=0. The optically accessible excited states are essentially p-like, having a node in their wave functions at r=0, and so are much less affected. The reduced screening causes the binding energy of the hole (electron) to be somewhat higher than estimated by EMT. The exact correction is very difficult to calculate, but usually increases as the impurity element descends in its column of the periodic table, acquiring more full shells of core electrons.

Additional information that we are able to obtain from an effective mass calculation is the approximate orbital radius of the shallow hole (electron). This radius scales

from the Bohr value with the value of the dielectric constant and inversely with the effective mass. For Ge the shallow acceptor radius is therefore roughly 80 A. The wave function radius is much larger than the lattice spacing (2.2 A nearest neighbor distance for Ge) and so justifies the EMT assumption of a uniform dielectric screening by the lattice. The ground state wave function extends over a volume of thousands of lattice sites; the excited states reach even further. In fact, for even moderately high concentrations of impurities, the excited state wave functions overlap significantly, causing the formation of bands of impurity states.

Several recent review articles concerning the physics of shallow levels in semiconductors have been given in the literature (Ramdas and Rodriguez, 1981; Haller, Hansen and Goulding, 1981).

1.2 Photothermal Ionization Spectroscopy

A large amount of the information obtained in this research project came as a result of a spectroscopic technique known as photothermal ionization (Lifshits and Nad', 1965; Kogan and Sedunov, 1967). This process is aptly named because it occurs as the result of two steps (Figure 2): i) the absorption of a far-infrared photon by the shallow impurity in its ground state, and ii) the

further absorption of a lattice acoustic phonon of relatively low energy from the thermal bath of phonons available. Since the phonons are always more plentiful than the photons at the optical fluxes used in these experiments, the population of the excited states will always be thermally small. Therefore spectroscopy from an excited state does not occur, because the probability of phonon absorption is much greater than that for a second photon to be absorbed.

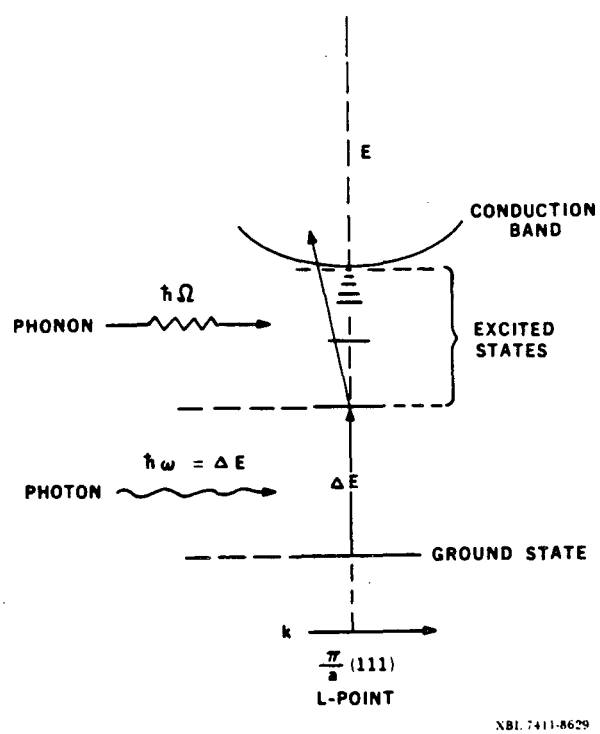

Figure 2 -- PTIS two-step process

Photothermal ionization spectroscopy (PTIS as it is generally known) of shallow levels in Ge requires photon

energies in the far-infrared. As mentioned earlier, binding energies from EMT are only of the order of 10 meV (equivalent to a wavenumber of 80.65 cm^{-1}) for these impurities. Since the spectrum is assumed to be hydrogenic, this means that the first optically accessible excited state (in the (2p) manifold) is expected to be bound by only 1/4 of this energy; the theoretically determined value for this binding energy in acceptors is actually 2.88 meV (Baldereschi and Lipari, 1976). Photon energies in the range of energies down to less than 8 meV are required in order to observe bound-state to bound-state transitions for these impurities. It is also quite obvious that the samples under investigation must be maintained at temperatures which allow the capture of small (less than ≈3 meV) acoustic phonons by the optically-excited hole states but which do not allow ground state ionization by capture of higher energy (≈10 meV) phonons. These temperatures are in the temperature range easily accessible with liquid helium cryostat techniques.

The PTIS method itself is a very sensitive but simple technique. It requires a high-resolution source of far-infrared photons, a method of coupling the photons to the sample (light pipe), a variable-temperature liquid helium cryostat, and electronics to measure the effect of the photothermal ionization process. This last step is

crucial, as it provides the signal by which the spectroscopy is performed. This signal is comprised of conductivity measurements on the sample itself while illuminated by the far-infrared radiation. The sample's conductivity is a function of its temperature and the spectrum of the far-infrared light, among other parameters, since the number of free carriers in the sample is dependent at low temperatures on the degree of ionization of the shallow impurity centers. If measurements are then made of the sample conductivity as a function of the frequency of the infrared radiation for a monochromatic source, a spectral response is obtained.

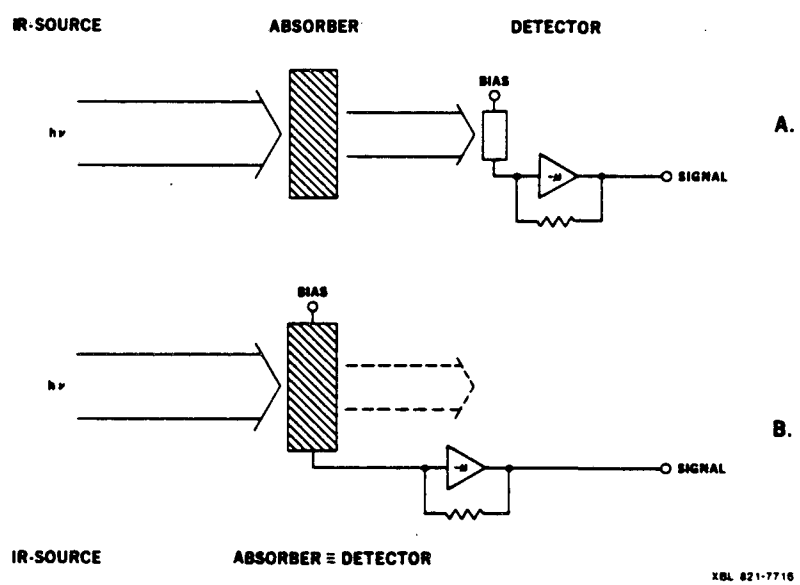

Figure 3 -- Absorption vs. PTIS

Implementation of the PTIS technique thus requires photothermal conductivity measurements of the sample under study. From that point of view, the sample being measured is also the detector of the infrared radiation. This is in marked constrast to absorption spectroscopy, in which the detector is external to the sample being measured (Figure 3). In the case of absorption measurements, the photon stream being measured is that which is transmitted by the sample, with only the small missing flux due to absorption providing the desired signal. The signal to noise ratio can become extremely low at small concentrations of absorbers. In fact, there is a lower limit on the noise in the detection of the transmitted photon stream due simply to statistical fluctuations in the number of photons in the beam. This limit is independent of the internal detector noise.

It was previously believed that the lower limit of detection of electrically active shallow impurities by absorption spectroscopy was a concentration on the order of 10^{13} cm^{-3} (Reuszer and Fisher, 1964; Lifshits, Likhtman and Sidorov, 1968). However, we have demonstrated using a $Ge:Zn^{+}$ photoconductor that a detection limit in the mid-10^{10} range is possible. This experimental point is discussed in Chapter 7 of this dissertation, in relation to measurements of acceptor-plus centers. The full implications of this

very high sensitivity with regard to measurement of low-concentration, non-interacting impurities by absolute absorption techniques have not yet been established. Measurements of absolute oscillator strengths for dipole-allowed bound-state transitions should be easily possible. This would be an important contribution to the theoretical understanding of shallow impurity levels.

In the photoconductivity measurement, the usual technique to allow suppression of low frequency noise is to chop the infrared source alternately on and off by mechanical means (a rotating chopper blade). This allows measurement of an a.c. component of the conductivity which has a well-defined frequency and phase. Since we are then measuring the fractional change in conductivity of the sample with and without the additional infrared illumination from the spectrometer, our signal size is determined by the ratio of sample conductivity with the infrared source (given by source plus background conduction) to that with the source chopped off (background only). Each of these conductivities is proportional to the number of net uncompensated shallow impurities in the sample, so their ratio is totally independent of impurity concentration. It is this particular fact that is responsible for the remarkable sensitivity of PTIS to small concentrations of impurity atoms (as low as 10^6 cm^{-3} for Ge).

Other complementary measurement techniques can be used in addition to PTIS, as will be mentioned in Chapter 2, section 4. These include Deep Level Transient Spectroscopy (DLTS) and Hall effect measurements. Although DLTS is a spectroscopic technique, it does not provide nearly as high a resolution as far-infrared spectroscopy of bound-state to bound-state electric dipole transitions, and yields only the approximate ground state ionization energy. Likewise, Hall effect measurements provide only approximate values for the binding energies of the various impurity species, but the concentrations measured are absolute.

1.3 Michelson Interferometer

As a matter of practical interest, it is presently not possible to obtain high intensity tunable monochromatic far infrared sources (such as semiconductor laser diodes) in the energy range necessary for PTIS of shallow levels in Ge. This leaves us with the possibilities of either grating spectrometers or interferometers. A grating instrument for this spectral range requires line spacings in the submillimeter region, implying a total grating size for a reasonable number of lines of about a meter. Although such an instrument is feasible (Reuszer and Fisher, 1964), it is slow to acquire data with and has several disadvantages with respect to an interferometer in regard to signal to noise.

A Michelson interferometer (Bell, 1972), as was used in the experiments of this thesis, is capable of greater throughput (Jacquinot advantage) due to the lack of collimating slits, and also yields information on all frequencies at one time (multiplex or Fellgett advantage). These combined advantages can yield spectral recording time reductions of up to a factor of 10^4 under otherwise identical circumstances. For these reasons and the fact that a computerized data acquisition system for the recording of interferograms and performance of on-line fast-Fourier transformation is already in existence, the interferometer approach was taken in this study.

An interferometer provides a beam of light whose frequency content is dependent on the relative optical delay between two mirrors, one fixed and one movable. Broadband light is divided by a beamsplitter into two beams which undergo different length paths, recombining with either constructive or destructive amplitudes, depending on the frequency of each component and the optical path difference. The output beam after interference is thus modulated at any given light frequency by the position of the movable mirror according to a factor $\cos(2\pi x/\lambda)$, where x is the total optical path difference of twice the mirror displacement from the zero path difference position. A detector that responds with delta-function response to that one frequency

would also show the same modulation of its output with mirror position. A detector with simultaneous response to many frequencies would respond with modulation that is a sum of many cosines at different wavelengths, each cosine weighted by the strength of the detector's response at that frequency. This Fourier sum results in an interferogram, from which the detector's actual spectral response can be obtained by a Fourier transformation.

The resolution obtainable from an interferometer is inversely proportional to the size of the path difference between the two arms. If we simply Fourier transform the interferogram directly for a finite optical length L of interferogram recorded, each delta-function of frequency (equivalent to a particular cosine in the interferogram, $\cos k^{\circ}x$) will produce a $(\sin \Delta kL)/\Delta kL$ function in wavenumber space, where $\Delta k=k-k^{\circ}$. If our criterion for resolving two frequencies is that their half-maximum positions $\Delta k=(1.89/L)$ just meet, then the difference in their wavenumbers $\lambda^{-1}=(k/2\pi)$ is just $2(1.89/2\pi L)=0.601/L$. Of course this is only true for a perfectly aligned interferometer with a true point source and no optical aberrations of the mirrors, so that in practice the limit will be somewhat higher than this.

One complication arises in interferometry from the sampling theorem due to Nyquist. Since we can only acquire

measurements at a discrete set of mirror displacements, as opposed to an entire continuum of values, we are restricted in the possible oscillation wavelengths that we can determine by Fourier transformation. The shortest wavelength possible to recover from the discrete data samples is twice the optical path difference of the sampling interval. Any information at a wavelength shorter than this is simply aliased back into the spectrum below the minimum recoverable wavelength. This means that if we are not careful to remove all higher-frequency information from the spectrum (by infrared filters or by choice of detector response) this additional information will be aliased into the desired spectrum, resulting in unwanted superpositions. It is usually sufficient to scan to higher frequencies briefly by choosing smaller sampling lengths in order to confirm that no information beyond the maximum wavenumber is present.

1.4 PTIS in Elemental Semiconductors

In the elemental semiconductors Si and Ge, the valence band maximum occurs at the center of the Brillouin zone (Γ point) and has four-fold degeneracy. This means that holes at the top of the band transform according to the Γ_8 representation of the $\bar{T}_d$ group (in the notation of Bethe), in the same manner as a state of 3/2 spin. Any

substitutional elemental acceptor has the full tetrahedral symmetry of the host lattice, and so the electronic levels of such an acceptor have symmetries determined by the direct product of the hydrogenic envelope state (s,p,d,f) with the Γ_8 band symmetry. For the (1s) ground state this symmetry is simply $\Gamma_1 x \Gamma_8 = \Gamma_8$, a four-fold degenerate state. However the excited states of p-like envelope functions have symmetry $\Gamma_5 x \Gamma_8 = \Gamma_6 + \Gamma_8 + (\Gamma_7 + \Gamma_8)$, which yields two Kramers doublets and two quartets in the tetrahedral double group's irreducible representations. This leads to complications in the final-state assignments in a photothermal ionization spectrum. The assignments and nomenclature that are used in the present dissertation for the energy levels are those due to Baldereschi and Lipari (1976), who calculated in detail the sizes of the splittings involved for each of the excited states in Ge. In order to obtain results which are in good agreement with experiment, both the split-off valence band and the conduction band had to be included in the calculation. Notation for the bound state transition line series in Ge is that of Jones and Fisher (1965). For Si the nomenclature is different from that of Ge because the spin-orbit interaction (which determines the energy separation of the lower band) is proportionately much smaller than the ionization energies. This results in different relative spacings of the set of discrete bound

states for acceptors in Si.

Nevertheless, for all single acceptors in Ge (also in Si) the p-like excited state energies relative to the valence band are essentially identical, with no central cell correction, due to the node of the envelope wavefunction at the impurity site. This means that the spacings between these excited states for all acceptor species are identical, and that the spectrum obtained of transitions from the ground state to these p-like excited states will contain a series of lines with identical spacings for all acceptors. The only difference between spectra of different acceptors is the overall shift of the entire pattern of lines due to the central cell shift of the (1s) ground state. This gives a great deal of redundancy to the identification of a particular initial ground state in a spectrum, for if one of the bound-state to bound-state transitions is seen, the entire set of such transitions should appear.

A similar situation occurs for donors, except that the symmetry of the conduction band is different. In both Si and Ge there are multiple conduction band minima, 6 and 4 respectively, and the inter-valley interaction is large, causing the band symmetries to split into A_1+E+T_2 for Si and A_1+T_2 for Ge. In each case the singlet state, denoted A_1 in the conventional molecular notation commonly used in this field, is actually the lowest lying state (an exception

occurs for the interstitial donor Li).

Other PTIS studies have been performed by various research groups, including those on diamond (Collins and Lightowlers, 1968), and several III-IV and II-VI compounds such as GaAs (Stillman, Wolfe, and Dimmock, 1969), AlSb (Ahlburn and Ramdas, 1968-9), GaP and HgCdTe. Since diamond is difficult to obtain with sufficient purity (as a naturally occurring crystal it is usually rather impure, $N \simeq 10^{17}$ cm^{-3}), of the elemental semiconductors only Ge and Si were studied here thus far. The only III-V compound available in sufficient purity was GaAs, and an attempt at PTIS failed due to unacceptalby poor electrical contacts; these were formed by ultra-sonic indium soldering technique. HgCdTe was attempted at several different alloy compositions, each yielding a different size direct band gap. No shallow impurity levels were seen, as these samples again had very poor electrical contacts for low-temperature PTIS.

1.5 Spectroscopy of Acceptors

In a group IV semiconductor the ground state of the substitutional elemental acceptors transform, as mentioned already, according to the Γ_8 representation of $\bar{T}_d$. Under a uniaxial stress in any direction, the four-fold degenerate states are split into a pair of two-fold degenerate Kramers

doublets. This is because the stress introduces an axis of symmetry $D_{\infty h}$ whose largest common subgroup with $\bar{T}_d$ occurs for the case of ⟨111⟩ stress and is C_{3v}. No four-fold irreducible representations exist in this or smaller subgroups. However, the time-reversal degeneracy cannot be removed by stress, and no additional splitting can occur.

For the case of Ge as a host lattice, quite a number of acceptor impurity complexes are known to exist (Haller, Hansen and Goulding, 1981). These are centers comprised of two or more atoms (one constituent could instead be a vacancy in some cases) in which the relative positions of these atoms provide an extra degree of freedom to the system. If this extra symmetry axis between the atoms were frozen in its orientation, as in the extreme limit of a hindered rotor system, there would be a reduction in the symmetry of the site, resulting in a pair of doublet states for even the unstressed case. Moreover the application of stress in an arbitrary direction would affect sites frozen in different orientations by different amounts, resulting in many different line series in the spectrum of such an impurity type due to transitions from these various different ground state energy levels. However, if the internal axis is not frozen, as in a free rotor, the extra degree of freedom is incorporated in the system and the symmetry remains tetrahedral, but with an increased manifold

of states. That is, if the rotor is free to assume four tetrahedrally equivalent orientations at its site, the symmetry of these states is given by $\Gamma_1+\Gamma_5$. This symmetry, in direct product with the Γ_8 band symmetry of the holes, yields an overall manifold of $\Gamma_6+\Gamma_7+3\Gamma_8$ (Joós, Haller and Falicov, 1980). This manifold contains, besides the three Γ_8 quartets, two Kramers doublets (Γ_6 or Γ_7) which are unsplittable under stress. Such Kramers doublets in the ground-state manifolds of several impurity complexes were used to interpret several series of unsplittable lines which were first reported by Haller (1978) in PTIS of ultra-pure Ge samples.

Thus far, models exist which satisfactorily explain the spectra of several of these impurity complexes (Haller and Falicov, 1978; Haller, Joós and Falicov, 1980) to the full extent of the experimentally observed phenomena. Several additional sets of non-elemental impurity complexes have not yet been modelled, and a careful study of the behavior of three of these centers, those related to the presence of carbon and nitrogen in the crystals, has yielded substantial new information. This study and the models and explanations produced by it provide the main thrust of this thesis.

Chapter 2 -- Exp. I: Crystal Growth, Characterization and Sample Preparation

2.1 Ultra-pure Crystal Preparation

The experimental measurements which make up a large portion of this thesis rely heavily upon the availability of a source of single-crystal germanium of extremely high purity. Also, the growth environment of the crystal must be tailored to meet specific needs in terms of melt container and ambient gas, while still retaining high purity. Such a need for the control of all aspects of the history of the crystal is met only with the in-house crystal growing facilities that exist in the germanium nuclear radiation detector group at Lawrence Berkeley Laboratory. It is in this way that we can be sure of the chemical nature of any possible impurities in a given sample of germanium.

The starting material for all of our crystals is commercially refined polycrystalline Ge bar stock. This raw material is chemically etched to remove dirt and contaminants on the surface, and then cast into shape in a graphite boat by melting in a casting furnace. The cast material is then ready for a zone-refining procedure, in which a short zone (less than an inch) of a three foot long bar is melted and the melted region is swept slowly over a period of several hours to one end of the bar. This process

is repeated typically 18 to 20 times, until the bar has nearly reached its equilibrium impurity distribution for the particular zone size and speed of motion used. At this point those impurities with segregation coefficients greater than one (e.g., boron, silicon) are predominantly concentrated at the front end of the bar (the end first melted) and those with coefficients less than one are distributed toward the back end. The limiting purity is obtained from the equilibrium segregation between the molten Ge and the container material, which is always a source of contaminants.

The zone-refined bar that results from this process is then cut into segments with a diamond saw. Both ends of the bar are first removed and saved for later analysis if needed, as these pieces contain the majority of the impurities from the raw starting material. The remainder of the bar is then cut into typically three 850-900 gram sections which will each be used to grow one ultra-pure single crystal. Impurity concentrations in the crystal charge (that is, the material from which the crystal is formed) at this time are typically only of the order of 10^{10}-10^{11} cm^{-3}. In the best of zone-refined material, the net concentrations are even lower, and the compensation by minority carrier-type impurities (usually phosphorus for aluminum-dominated p-type crystals) is very small (less than

or of the order of ten percent).

The polycrystalline zone-refined charge for growth of a new crystal is first pre-cleaned with a hydrofluoric-nitric acid etchant mixture to remove initial surface impurities. The material is then transferred to a laminar flow chemical hood consisting only of plastics (no metals), where it is further etched in a mixture of $HF:HNO_3$, followed by $HCl:HF:H_2O$. Rinsing between etchings is done with deionized water. The final rinse is performed with electronic grade methanol that has been distilled in silica. The charge is blown dry with boil-off nitrogen gas and is then transferred into the Czochralski type crystal growing apparatus where it is melted and grown into a single crystal.

Details of the crystal growth itself depend to an extent on the type of environment desired for the particular crystal. Some typical conditions are: the Ge melt is contained in a crucible of synthetic silica, which for certain cases may also be coated with pyrolytic graphite from methane decomposition, or in the carbon susceptor directly; the atmosphere in the crystal puller is typically flowing purified hydrogen gas diffused through palladium, or nitrogen, argon or helium, or a vacuum of approximately 10^{-5} torr. In all cases the crystal growing chamber is first pumped down to the above mentioned vacuum while the susceptor, charge and crucible are being heated, in order to

out-gas the apparatus. A gas flow, if used, is then established before the charge is melted by r.f. inductive heating of the carbon susceptor. After complete melting, the liquid is brought to a temperature just above the freezing point as a small rotating seed crystal of the desired crystallographic orientation is slowly dipped into the center of the melt. By proper control of applied r.f. power, gas flow, pull rate of the seed and other variables a large single crystal with the given seed orientation can be grown with very low or no dislocation density and very high purity. The process requires several hours and the finished crystal is allowed to cool in place in the grower to room temperature for several hours afterwards. The crystal growing apparatus is then opened and the cooled crystal is broken away from the seed and removed. A resistivity measurement at 77 K is performed on the entire crystal in order to determine the axial profile of the impurity distribution, using the well-known values for the mobilities of electrons and holes for pure material at that temperature ($\simeq$40,000 cm^2/V-sec).

A silicon crystal growth capability does not exist as yet at either Lawrence Berkeley Laboratory or the University of California at Berkeley. This means that silicon samples cannot be prepared in a completely controlled environment as can germanium; therefore the impurities which may exist and

their concentrations cannot be predicted as readily for such samples. However, very high purity material is available commercially as nuclear radiation detector grade single crystals. This in principle allows some experiments of the type performed here on germanium to be extended to silicon in the future.

2.2 PTIS Sample Preparation

The germanium samples used in the photothermal conductivity experiments were obtained from the large single crystals grown as above by slicing with a diamond saw blade. The typical cross-sectional area perpendicular to the axis of infrared light propagation was 7x7 mm^2, and the normal sample thickness was 3 to 7 mm. In cases when application of uniaxial stress was to be employed, the sample was cut in such an orientation that the desired crystallographic stress axis was parallel to the 7x7 mm^2 face and perpendicular to a side face. In all cases the sides were cut in such a way as to be perpendicular at all corners. Special high-stress samples of size 1x1x6 mm^3 with desired axis along the 6 mm direction were used in some cases.

After cutting by diamond saw, the rough-cut saw-damaged faces were lapped flat using first 600 grit followed by 1900 grit silicon carbide on an optically flat glass plate. The lapped surfaces of the sample were then polished to optical

smoothness by chemical etchant. A solution of 4:2:1 proportions of HNO_3:HF:Red fuming HNO_3 was used, followed by quenching of the etchant with methanol. The etched samples were dried by compressed dry nitrogen jet and electrical contacts were applied to two opposing faces.

The electrical contacting procedure was carried out in one of two ways: i) a liquid eutectic of InGa alloy (freezing point 20°C) was applied to the surface by a cotton swab, rubbing the surface strongly, and then removing excess liquid to avoid a thick layer of material with a thermal expansion coefficient different from that of Ge, or ii) an ion-implantation machine was used to implant $2x10^{14}$ cm^{-2} 25 keV boron ions (for p-type samples) or phosphorus (for n-type samples) ions into the first few hundred angstroms from the surface of the sample, which was then thermally annealed to activiate the dopant impurities and to remove structural damage from the implantation. In either case, a layer of In metal was then pressed onto the surface over the electrical contact to insure a large-area metallic surface with which to connect the signal-carrying cables in the PTIS measurement apparatus.

In most cases, the electrical contacts are applied to side faces of the sample, allowing current to flow transverse to the axis of the infrared light propagation. However, for samples used specifically for magnetic field

dependence studies, in which the magnetic field axis is parallel to the light propagation, this sample geometry would lead to large transverse magnetoresistance in the conductivity measurements. This effect can be circumvented only by a geometry in which the current flows parallel to the magnetic field axis, for which the longitudinal magnetoresistance is not a strong effect. To achieve this configuration, ion-implanted contacts were applied to the large 7x7 mm^2 faces of thin (2 to 3 mm) samples. These implanted layers were not covered by In metal pads, but rather formed a transparent electrical contact whose plane was normal to the common optical and magnetic field axes. Electrical connection to this plane conducting layer was formed by soldering with In to alloy a small connection point to one corner of the implanted layer. Copper wires brought out from these points were attached to the signal-carrying leads of the apparatus.

2.3 Quenching, Annealing and Diffusion Procedures for Special Samples

Many of the acceptor complexes of interest do not appear in as-grown germanium crystals. Special thermal treatments of the material are required in order to generate these centers as electrically active species, in sufficient concentration to become observable. The most commonly used

method is that of a thermal "quench", a procedure in which a small sample of material is heated above room temperature and very rapidly cooled to room temperature or below. Such a procedure is used to provide thermal energy to mobile species (hydrogen, lithium, vacancies or interstitials), allowing them to move through the lattice and sample various locations at the elevated temperature. The quenching process then removes that thermal energy rapidly, causing the species to become trapped at a site of a local minimum of energy. In this way centers can be created which are not global energy minima, but are nonetheless very stable at the reduced temperature. A quench of this type usually requires cooling rates of the order of hundreds of degrees per second in order to reduce the chance of diffusion of the mobile species away from the desired site.

In quenching samples for studies of most known impurity complexes in germanium, the usual temperature for the first step is taken as 400°C. Quenching is usually accomplished by application of jets of high-pressure (80 psi) argon gas from two opposite sides of the sample. For thin samples of thickness 2 to 3 mm, this causes cooling rates estimated to be several hundred degrees per second. In certain special cases, samples were quenched by being dropped into either water, ethylene glycol, mineral oil, or liquid nitrogen. In all cases the sample actually measured was not cracked by

the quenching procedure, although it is not known what defect concentrations are introduced. Finally, some samples then required storage at low temperatures (77 K) until they could be evaluated spectroscopically by PTIS, in order to not destroy those of the quenched-in centers with very low thermal stability.

Although impurity complexes of the type found in germanium have not yet been generated in silicon by quenching from high temperatures, the temperatures necessary to achieve a similar result would be expected to be several hundred degrees higher. The thermal stability of such centers would be expected to be dependent upon the strength of the H-Si (or Li-Si) bond and the H (or Li) diffusion barrier in Si.

Additional information for many of the impurity complexes can be obtained from the rates of disappearance of their spectral line features as a function of annealing time and temperature. The temperatures used for these studies vary from just above room temperature up to 400°C. Low-temperature annealing (below 200°C) was accomplished on hot-plates with suitable thermal isolation and automatic temperature regulation. Higher temperature procedures required the use of a quartz-lined tube furnace, with the sample placed on a carbon block in the center of the quartz tube, under flowing argon atmosphere. Both isothermal and

isochronal annealing were performed on some of the samples. For impurity complexes which disappeared by annealing, 77 K Hall-effect measurements were performed after each step of the heat treatment in order to determine the remaining concentration of electrically active impurities. For those special impurity centers discussed in chapters 5 and 6 which convert from one electrically active form to another, no information is obtained by a Hall-effect measurement. A complete liquid helium temperature (4.2 K) PTIS procedure must be performed at each step in the heat treatment in order to determine which spectral features increase in intensity and which decrease.

A number of germanium samples were prepared for PTIS studies by diffusion of cyanide from the surface at 600°C. The samples were first lapped to 1900 grit smoothness as in the normal sample preparation, but were not polish-etched in acid solution. Instead they were rinsed alternately with methanol and deionized water to remove the lapping compound, then soaked for 10 minutes in a 2 Molar solution of KCN in deionized water. These samples, without being rinsed or dried, were then placed on quartz plates which had been etched with HF and rinsed with KCN solution. They were then annealed in air on the quartz plates in either a tube furnace or a brick furnace with a quartz bell jar housing at 600°C for periods of 1 to 24 hours. Many of the samples

prepared in this way were then quenched as above, while others were allowed to cool to room temperature more slowly. A few special samples were diffused with isotopically pure $K^{14}CN$ ($2x10^{-2}$ M solution) or $KC^{15}N$ (2 M solution) in an otherwise identical manner to the normal KCN diffusion.

2.4 Diagnostic Measurement Techniques

It is sometimes the case that a particular sample of germanium may not behave in the expected manner during infrared spectroscopy; that is, either some line series that was expected to be seen is not, or additional unexpected lines are found. In these cases, it is necessary to have at one's disposal a number of additional techniques for sample characterization that enable identification of the unexpected species. The methods most often used include variable-temperature Hall effect and Deep Level Transient Spectroscopy (DLTS -- Lang, 1974). These two techniques allow one to identify quantitatively many impurities which do not appear in PTIS. In particular, deep levels have rather small infrared absorption cross-sections and are frequently impossible to see in PTIS, but often give rise to impurity complexes which affect the spectrum. These impurities can be easily identified with spectroscopic accuracy by DLTS from comparison of the signal peak positions as a function of temperature and time constant

with spectra of known impurities.

Measurements of the transverse Hall voltage as a function of sample temperature at currents of 1 nA-1 mA were performed on germanium samples in the Van der Pauw geometry (Van der Pauw, 1958). The measurements allow calculation of both the sample resistivity and Hall mobility as a function of the temperature. From these quantities, the concentration of free carriers as a function of temperature can be calculated. An Arrhenius plot was then made of the logarithm of the carrier concentration versus inverse temperature, from which the impurity energy levels can be deduced.

Hall effect measurements give information about the energies (from the slope of the freeze-out curve) and the concentrations (from the plateau) of the various impurity levels. Additionally, an estimate of the amount of impurity compensation can be obtained from the change in slope of the shallowest level's freeze-out curve. These data can be extremely useful in determining whether or not an undesired impurity is present in a germanium crystal, either as-grown or due to an annealing procedure. Such an impurity can affect the mobility and lifetime of free carriers in the sample, and can form complexes with other impurities to create new energy levels in the band gap. By identifying the energies and concentrations of such levels it is

possible to fully characterize the semiconductor.

Deep Level Transient Spectroscopy is a technique which allows determination of the energy levels of states that exist near mid-gap, a region of energies inaccessible to PTIS. The determination is accomplished by preparing a semiconductor sample as a diode with n^+ and p^+ contacts on opposite faces. These contacts are usually ion implanted, although Li-diffused or Schottky barrier metal contacts sometimes perform adequately. The diode is placed in a variable-temperature cryostat and cooled, while both a d.c. reverse bias and either a forward (for minority carrier type centers) or reverse biasing pulse train are applied to the contacts. The depletion region of the diode has a bias-dependent thickness. From the a.c. capacitance of the diode, measured with a high-frequency capacitance bridge, the concentration of impurities can be determined as a function of temperature. More importantly, the applied pulses of bias voltage allow one to measure how rapidly those deep levels which are filled by the pulses can return to their equilibrium states. The time constant for the process is a function of the temperature of the sample and of the type of impurity center. By correlating the sample's exponential emission rate with a synthetic exponential function of a known time constant, a signal can be obtained which peaks at the temperature for which both time constants

are the same. This process is in principle simply an inverse Laplace transformation, but in practice it is difficult to obtain better energy resolution than that from an exponential correlator. Such a signal vs. temperature gives a spectrum of the energy levels in the bandgap of the semiconductor, one level per DLTS peak. The peak positions can be obtained as a function of the reference time constant and plotted in an Arrhenius plot in order to determine the actual energy of the deep level.

An additional measurement that can be carried out with a DLTS-prepared sample is a capacitance profile. By varying the applied fixed bias, and measuring the capacitance as above with a high-frequency bridge, the impurity concentration as a function of depth from the contact surface can be obtained. Once again the measured concentration is dependent on the sample temperature, and so it can be determined whether deep levels or shallow ones are being measured merely by changing the sample temperature to a point above the ionization temperature for the shallow levels.

Chapter 3 -- Exp. II: Photothermal Ionization Spectroscopy

3.1 Interferometer and Fourier Transformation

The interferometer used for this research was designed by Prof. P. L. Richards of the University of California Department of Physics, and is shown schematically in Figure 4. It consists of a far infrared radiation source (high pressure Hg arc lamp), a collimating mirror, one of several possible thicknesses of dielectric (mylar) beamsplitter, fixed and movable mirrors, and a converging mirror for collection of the beam into a 1/2-inch diameter output light pipe. The entire apparatus is housed in a pyrex vacuum enclosure to eliminate water vapor absorptions in the infrared beam. A chopper blade interrupts the light pipe at a known frequency in order to provide an a.c. component of infrared output signal, and a filter wheel is placed immediately below the chopper to allow a variety of low-pass far-infrared filters to be selected. The useful spectral range of the instrument is determined by the thickness and index of refraction of the beamsplitter. For 25 μm thick mylar, the first zero in frequency of the beamsplitter's output, occurring when its transmittance vanishes from Fabry-Perot type interference effects in the dielectric, is at 125 cm^{-1}. This therefore provides a very useful range for shallow level spectroscopy in Ge.

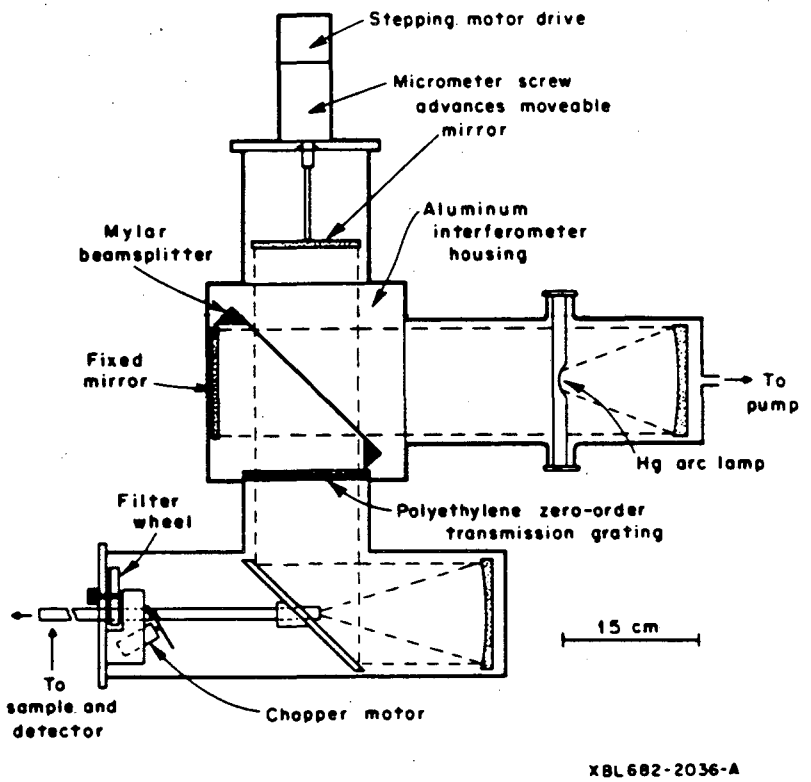

Figure 4 -- Michelson Interferometer

Because of the sampling theorem (Nyquist), it is possible that spectral information that exists in a high-frequency (large wavenumber) region will be folded back or "aliased" into a lower-frequency region if one is not careful to sample at least twice per wavelength of the shortest-wavelength information in the spectrum. The highest frequency reproducible for a given sampling interval, called the Nyquist frequency, is determined by exactly this criterion. Any higher frequency will be undersampled and so will alias to a value below the Nyquist

frequency. Since this could lead to confusing results in a spectrum, the spectral information must be restricted (cut off) to a particular maximum value for a given sampling interval. This is done by means of infrared low-pass filters of the Yoshinaga or similar type. In addition, since all filters of this type eventually open their transmission at frequencies above the reststrahl band of the ionic crystal used, additional filter material must be incorporated, usually a scatter or absorption element such as black polyethylene, so that very high frequency light (near-infrared to ultraviolet) does not pass through to the sample.

Although it does not cause confusion if one oversamples a spectrum, it is a waste of time and effort as the information obtained will exist only in the lower region of the spectrum. Only the noise content of the signal is increased, as it requires more data points (which contain noise components) to achieve the same resolution. Therefore there exists an optimum sampling interval for a given spectral response, beamsplitter, and filter set. In most cases the beamsplitter and filters are chosen to maximize the photon flux at a given photon energy of interest for a particular sample. The sampling interval is then chosen as a convenient value which will not cause aliasing of information to occur but will provide full resolution of the

spectrum in the smallest total number of data points.

In Fourier Transform Spectroscopy (FTS) the data actually recorded are not a direct spectral response (as a function of frequency) but are interferograms, or sample response as a function of mirror displacement of the movable mirror of an interferometer. This is related to the actual spectral response by a simple Fourier transformation, as shown in Figure 5. For the case of an interferometer with sufficient positioning precision to cause one of the data points to be taken at precisely the zero path position, and therefore at equal intervals on either side of zero path, only one side of the interferogram need be recorded (a single-sided interferogram). This is because the pattern of interference is exactly symmetrical with respect to the zero path position. Only a cosine transform need be calculated in such a case, as the function is even about zero path. For the instrument used in this study, we were able to align the optics sufficently well in all cases to be within a few percent of the maximum signal possible at the zero-path peak. In most cases this peak of the interferogram was 24 or 48 possible mirror positions wide for Ge samples, so that positioning within 1/2 of the smallest sampling interval, which was done in all cases, always produced a zero path peak value which was within a few percent of the theoretical maximum. This made it unnecessary to perform the sine

Fourier transformation in order to phase-correct the data for incorrect zero path position.

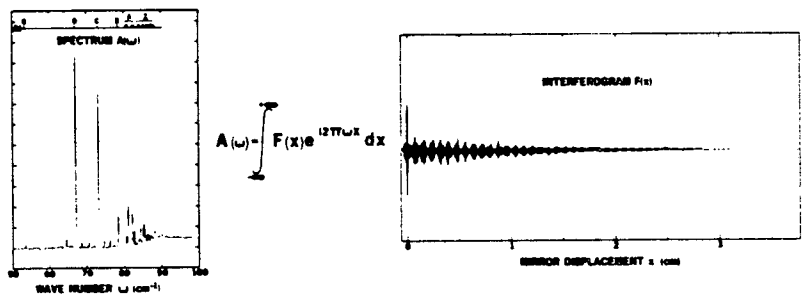

Far-infrared Fourier Transform Spectroscopy of Shallow Levels in High-Purity Semiconductors

XBL 808-11004A

Figure 5 -- Interferogram and Fourier Transformation

The maximum resolution obtainable in practice with a FTS interferometer is a function of both the maximum path difference available for the arms of the instrument and of the source size and precision of the optics. With exactly precise optics and only a point source of radiation the resolving power is linearly proportional to the path difference. As more data are accumulated, by moving further away from zero path, the resolution increases. The limit of resolvability for two precise delta-function peaks is determined by the half-width of the sinc function (sin x/x) produced in the discrete Fourier transformation of the finite sample of data collected. This limit is just a difference in wavenumber (for the two peaks to coincide at half-maximum positions) of 0.601/L where L is the optical

path difference or twice the mirror displacement. In order to avoid transformations having negative-amplitude "feet" (pods) on either side of the sinc function, one can resort to the mathematical technique of apodization, which is a multiplication in real space (interferogram) by a diminishing function of the mirror displacement. Triangular apodization (1-x/L) is the most commonly used, as the Fourier transformation of the triangular envelope is simply a sinc^2 function, which is positive definite. This procedure, however, limits the resolution somewhat: the minimum wavenumber difference between two sinc^2 $(\Delta kL/2)$ peaks now becomes $2(1.391/\pi L)=0.886/L$ for the condition of exact matching of half-maximum positions. As this is only a 47% penalty to pay and the resolution is usually limited by the optics rather than the mirror displacement, apodization was employed with the spectra discussed in this dissertation. For the interferometer used in this research, the movable mirror was mounted on a 5 cm long translation stage, with the zero path position set approximately one cm from the end of travel. This provided a single-sided interferogram of 4 cm mirror displacement or 8 cm optical delay. Such an optical path difference can in principle, barring finite source size and imperfect optics, yield a resolution of $(0.601/8\ \text{cm})=0.0751\ \text{cm}^{-1}=0.0093$ meV.

The effect of a finite source size is to limit the resolution of an optical instrument. In the case of a Michelson interferometer, the limiting resolving power R can be defined as $R=(f/h)^2$, where f is the focal length of the collimating mirror and h is the source diameter. This is a fractional resolution, equivalent to the wavenumber of a line divided by its width. Imperfect mirror optics have a similar effect upon resolution as an extended source, as they introduce non-parallel rays (off-axis from the translation stage motion) and so corrupt the interference pattern at large displacements. The effect in either case is to introduce somewhat of a self-apodization of the interferogram. The interference pattern (cosine wave) due to a particular delta-function response in wavenumber of a sample will in fact decrease in amplitude as path difference increases. This decrease in signal determines a practical limit on the fractional resolution at any given wavenumber, regardless of the possible optical path difference. A limit of this type (fractional) only becomes important on an absolute scale for high frequency signals. If we combine the source and optical effects into one effective resolving power R_{eff}, the resolution limit due to an 8 cm optical delay becomes comparable on an absolute scale to the fractional limit due to finite R only above a wavenumber of roughly 50 cm^{-1} for this particular interferometer.

3.2 Data Acquisition System and Noise Considerations

The signal from the sample consists of a measurement of the conductivity at constant voltage bias. This bias is supplied by the trans-conductance amplifier (TCA) circuit shown in Figure 6. In this circuit a regulated, filtered d.c. power supply provides the voltages required by the ultra-low-noise operational amplifier (OP-27). The amplifier is configured in such a way as to maintain the voltage across the sample at a constant level, set by the 10-turn bias potentiometer. In an earlier design of this circuit, only one field-effect transistor (FET) was used, in the sample input leg, to minimize leakage current into the op-amp input. That design, used for several years, required an offset voltage to overcome the source-gate potential of the FET. The new circuit design which is presently being implemented compensates for the offset by using a selected matched pair of very low voltage-noise FET's (2SK147) in a differential input configuration. This introduces an additional noise source in the channel of the second FET, but the noise can be filtered with a long time constant so that only very low frequencies of noise are added, which will be shown below to be unimportant for a chopped signal. The current through the sample, from both thermally and optically generated carriers, passes through the amplifier's feedback resistor to generate a voltage which is directly

proportional to the current. The size of the resistor is chosen to provide an average output voltage of several volts d.c.

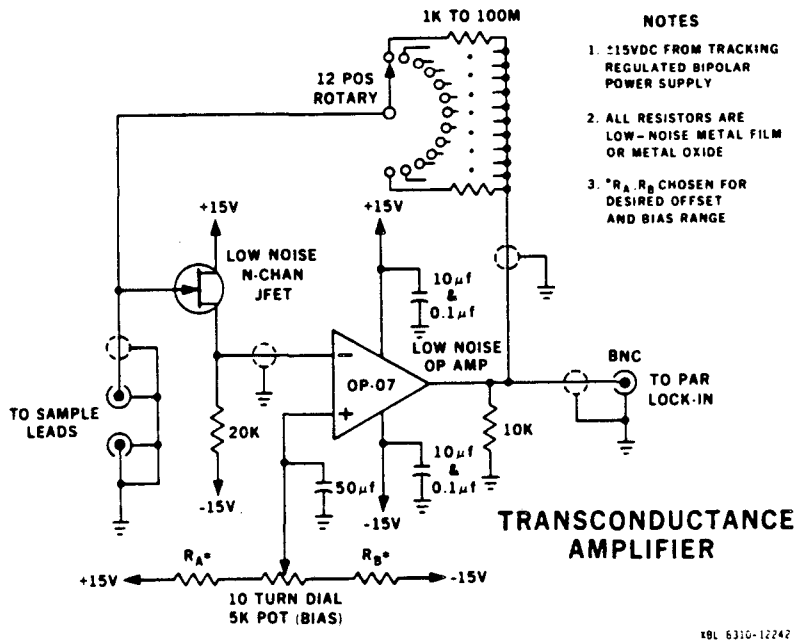

Figure 6 -- Transconductance Amplifier

The signal voltage from this amplifier contains a component due to thermally generated carriers (very small at a few degrees K), a d.c. component due to carriers generated from background radiation entering the light pipe (mostly 300 K blackbody radiation from warm filters, windows, and the light pipe itself), and a photocurrent (the desired signal) due to the infrared output of the interferometer. Since we are only interested in the small changes that occur in the photocurrent as the mirror is moved to change the interference effect, and not in the large d.c. background

conduction, it is most advantageous to chop the beam on and off mechanically in order to cause the photoconductive signal to be an a.c. component on a d.c. background. This component is then recovered simply by a.c.-coupling the output of the signal voltage from the TCA. This method substantially enhances the signal-to-noise ratio and allows rejection of changes due to very low frequency (1/f) noise or drifts in the parameters. In addition, the digitization error for a large d.c. voltage signal would be comparable to the size of the changes in voltage due to mirror motion.

The signal-to-noise ratio can be further improved by pre-filtering the a.c.-coupled signal with a circuit that is resonant at the chopping frequency. This eliminates noise in frequency bands away from that of the desired chopped light beam signal. Typically a filter of Q=10 or 20 is used in this capacity. Additionally a synchronously-locked rectifier ciruit is employed to detect the component of the a.c. signal that varies exactly in phase and frequency with the chopped beam. Usually, the chopping motor is driven by the reference frequency at which the rectifier is switching. This procedure eliminates all noise conponents which are not in the proper phase. The resulting signal is a rectified sine wave which must be filtered to recover its average d.c. value, proportional to the original a.c. signal. The filter used consists of a 2-pole (12 db/octave) low-pass

filter having a time constant of usually 30 ms which again removes high-frequency noise from the d.c. signal. Any component of noise not at an odd integer multiple of the chopping frequency which passes through the Q=10 prefilter does not have a d.c. average value after synchronous rectification at the chopping frequency, and is thus greatly reduced by this post-filter. All of these filter and rectifier components are contained in a PAR model 124A lock-in amplifier. The amplifier also contains an adjustable-gain preamplifier which can be used to scale the size of the a.c. input for maximum allowable d.c. output to the computerized analog-to-digital (A/D) converter in order to minimize digitization error. Finally, the d.c. output of the lock-in amplifier is averaged by computer for typically 1 second at each mirror position, with a 200 ms wait time between mirror steps to allow damping of any vibrations induced (causing mirror or beam splitter motion) and to allow at least five time constants for the filter circuit.

The input to the computer A/D circuit then consists of an average d.c. component proportional to the desired photoconductive signal, plus some undesired noise and ripple components from the rectifier. The 30 ms time constant post-filter enables a 1 ms sampling interval to be easily sufficient for following any ripple voltage variations. Usually an A/D conversion is performed once every

millisecond and 1000 samples (1 sec total time) are averaged to obtain each data point at the current mirror position. This is essentially equivalent to a digital low-pass filter of a 1 sec time constant, which serves to further reduce noise that is away from the chopping frequency. For noise frequencies which are commensurate with the 1 sec time interval, there is exact cancellation of the output component due to this averaging process.

3.3 Sample Holders, Inserts, and Helium Dewar

The geometry of the cryostat used in these experiments is detailed in Figure 7. It is a pyrex liquid helium cryostat surrounded by a liquid nitrogen heat shield. The central space of the dewar holds up to 2 liters of liquid He, which can if necessary be pumped to a vacuum of less than one torr, leaving nearly a liter of liquid He at a temperature of 1.2 K. It is more common in this series of experiments to maintain a He pressure of 1 atm and corresponding liquid temperature of 4.2 K. In all cases this liquid bath provides the sink of heat for cooling the sample apparatus. Although the sample can be maintained at a temperature warmer than the bath by means of heaters, it cannot be cooled below the liquid's boiling point at the selected operating pressure. The holding time for liquid He in this dewar can be as long as 18 hours if heating is not

used and samples are not changed.

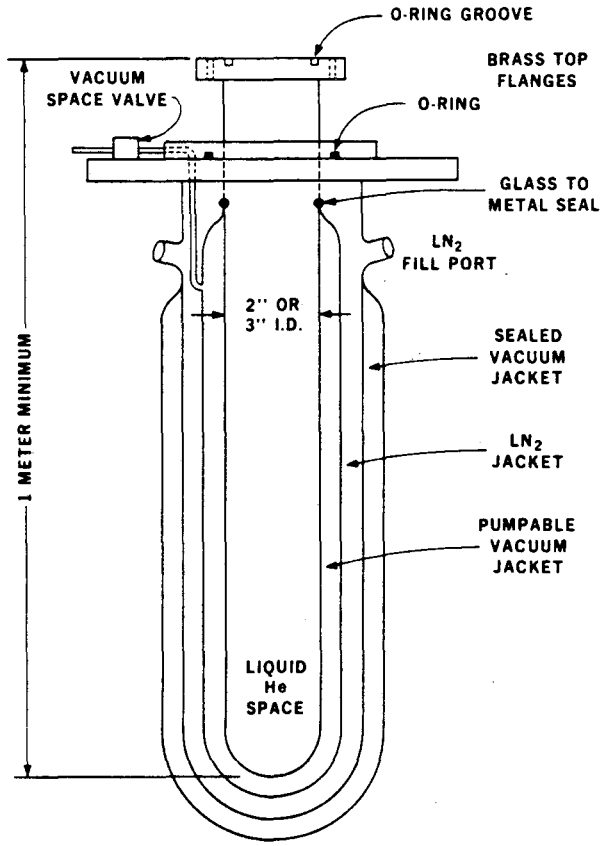

PYREX CRYOSTAT

XBL 8310-12244

Figure 7 -- Liquid He Cryostat

The majority of the spectroscopy discussed in chapters 4, 5 and 7 of this dissertation was performed using a sample holder and dewar insert of the type depicted in Figure 8. This consists of a brass sample cavity with indium electrical contacting pads and a stainless steel spring of just enough force to maintain physical contact between the sample and the In pads attached to the signal cable pads

without causing stress effects. Teflon insulated coaxial cables with graphite coating on the teflon surface to reduce microphonic noise due to static charges was used throughout. The sample cavity contains an adjustable plunger to accomodate various sample thicknesses and a filter position, which usually contained a black polyethylene sheet to provide cold (4.2 K) low-pass filtering of the warm incident radiation, at the exit of the light pipe. The light pipe itself consists of 1/2" diameter brass and stainless steel (for thermal isolation) tubing segments which were polished mechanically on the inside surfaces until several optical rings were visible when sighting through the pipe. Since the light propagation in the infrared is essentially conductivity limited, this polishing procedure was sufficient to insure good optical coupling to the sample chamber. The top of the light pipe is fitted with a polyethylene window as a vacuum seal to the outside when not coupled to the interferometer. Additional warm filters can be placed in the coupling fitting to the output pipe of the interferometer. A temperature sensing resistor (68 ohm Allen-Bradley carbon composition) calibrated at several temperatures down to liquid He temperature is placed in a hole drilled into the brass sample cavity immediately adjacent to the sample position. A heater resistor (10 ohm metal oxide) placed similarly provides controlled heating of

the entire sample cavity and the sample itself, using a Thermac temperature controller modified to provide a smooth d.c. low voltage output at a maximum current of 300 mA. The leads for the heater and sensor resistors are very small gauge (No. 39) copper wire to minimize heat leakage, and are routed through their own separate shield to minimize cross-talk to the signal leads. These leads pass out of the vacuum space through a separate glass-epoxy 6-pin Bendix connector from that of the signal coaxial cables. This design essentially eliminates the pick-up of stray 60 Hz a.c. fields in the signal circuit. The entire sample holder and light pipe assembly is surrounded by a 17/16" outer diameter #306 stainless steel vacuum jacket which enables filling with only a small quantity of He heat exchange gas for minimal coupling to the liquid He bath when operating at elevated temperatures (to 20 K). The brass sample chamber is wrapped with several turns of waxed string to insure that no metal-to-metal contact is made with the 4.2 K stainless steel wall. This sample insert allows samples to be changed easily. After a new sample is inserted, the air is pumped out and He gas is filled back before recooling. This procedure prevents air and water vapor from freezing onto the walls of the light pipe, which would severely block the infrared beam.

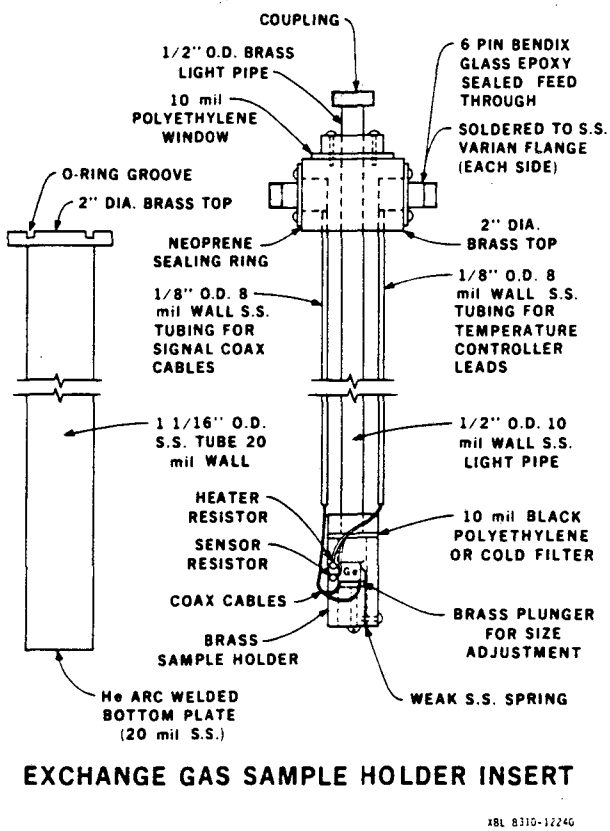

Figure 8 -- Exchange Gas Insert

The light-pipe connection to the interferometer is made in one of two ways: either a straight section of brass pipe with a pumping port to eliminate the air and water vapor from the path, or a coupling consisting of a pair of 45° mirrors and a horizontal section of brass pipe with a pumping port. The mirror arrangement is used when it is required to introduce band-edged light (discussed in chapter 4) into the sample from outside through a small hole in one of the mirrors. This necessitates removing the cold black polyethylene and introducing a warm (300 K) black

polyethylene sheet ahead of the mirrors in the beam. The warm filter then blocks all chopped high-frequency radiation while the d.c. band-edged light is introduced behind it along the beam line. In most cases the straight pipe was used when band-edged light was not needed, to minimize reflection losses of the available infrared beam power.

3.4 Stress Insert and Superconducting Magnet Dewar

An important piece of experimental information is obtained from the behavior of a sample's line spectrum when uniaxial compressional stress is applied to the sample. This has been accomplished for samples of interest in this thesis by an apparatus shown schematically in Figure 9. It is a cryostat insert which consists of a light pipe, heater and temperature sensor as before, although there is now no exchange gas jacket, but rather a copper cold finger reaching down into the liquid He. This sample insert does not allow easy changing of more than 2 samples in a single day. The major difference from the other holder is in the sample chamber which contains a sliding brass plunger with a point contact (for uniform distribution of the stress) to a lever arm which can be pulled inward toward the sample by a stainless steel wire. The other end of this wire passes out of the dewar to a floating calibrated spring unit, from which the desired force can be applied. The stiffness of

the brass plunger and backing block spread the stress across the entire sample surface, while both indium and cardboard pads compress to allow for non-planarity of the sample. The result is a reasonably uniform single axis for the applied stress causing only minor degradation of the linewidths of stressed sample spectra. The additional broadening due to inhomogeneous stress components is small compared to the stress-splittings of the initial and final states of the transitions.

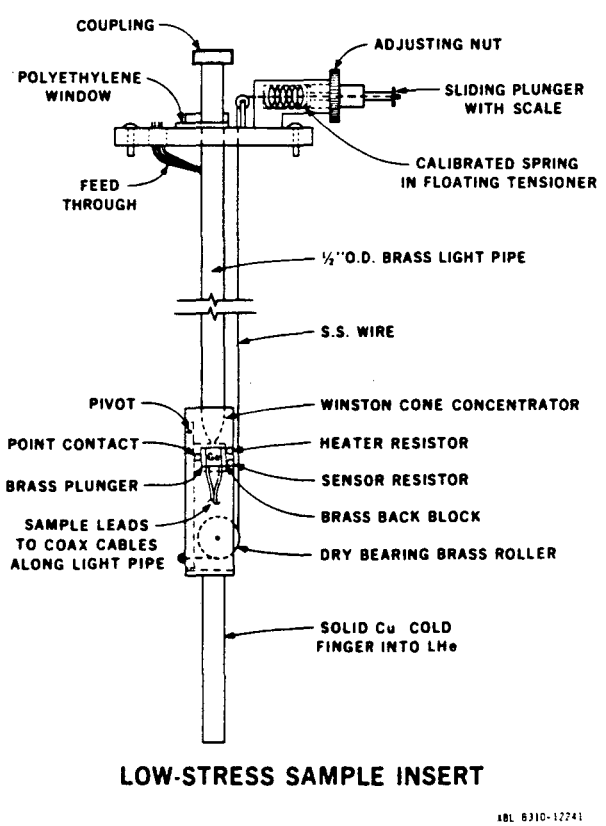

Figure 9 -- Stress Insert

One other important apparatus is the superconducting magnet and dewar used for magnetic field splitting studies (Zeeman effect). These consist of a steel dewar with a copper-walled liquid nitrogen heat shield and a 50 kG (maximum field) superconducting niobium wire solenoid suspended in the liquid helium space. The magnet has a very uniform field distribution (<1% variation, as measured by a Gaussmeter using an axial Hall probe) over a sample volume of a cubic centimeter, which was always larger than the actual sample used. A superconducting shunt wire and heater exist which are used (in normal mode, shunt heated) to apply current to the magnet from an external supply and (in persistent mode, shunt superconducting) to isolate the coil from any outide influence during data acquisition. The bore of the magnet is >1 1/16" allowing insertion of the exchange gas sample holder, which has already been described. That holder was designed to be used with this system, having a light pipe length so as to place the sample at the center of the coil. This superconducting magnet dewar allows measurements of samples with applied fields of a few hundred gauss up to 50 kG with good field uniformity. The axis of the field is in all cases parallel to the light pipe, and so nearly parallel to the propagation direction of the infrared radiation (Faraday geometry). The holding time for liquid He in this dewar is typically 3 or 4 hours due to the

substantial heat leakage of the magnet supports and wiring.

Chapter 4 -- Elemental and Complex Acceptors: Theory and Experiment

4.1 Characteristic Features of Spectra of Elemental Acceptors

Spectroscopy of the hydrogenic levels of ordinary elemental acceptors has been well known for many years, both in absorption (Jones and Fisher, 1965) and photothermal ionization (Lifshitz and Nad', 1965). Such spectroscopy occurs by dipole-allowed transitions from the (1s)-like ground state of the hydrogenic envelope function into one of the p-like excited states. A unique feature in the spectroscopy of shallow levels is that all acceptors have the same spectrum of excited p-state energy levels (as do all donors) by virtue of the large spatial extent of the state and the node in the wavefunction at the impurity position, or central cell. As shown in Figure 10, this immediately implies that the relative energy spacings between transitions for a single impurity are exactly the same as for any other shallow impurity of the same carrier type, although the absolute positions are in general different. The extreme redundancy in such spectra then allows one to isolate whole series of transition lines as due to a single species with great confidence, even if several of the lines are weak or obscured by other spectral

features. Therefore a very complicated spectrum can be reduced to simply a few different initial states for the dipole transitions. An example of one such spectrum is shown in Figure 11. The markings along the top of the figure indicate the entire series of strongly allowed transitions for the single elemental acceptor ground state of aluminum in the notation of Jones and Fisher (1965).

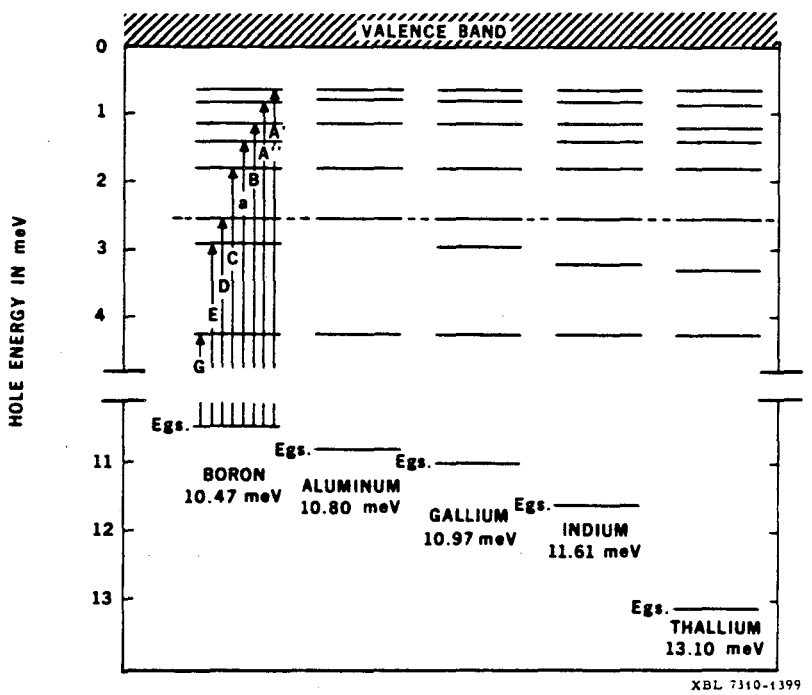

Figure 10 -- Excited States of Elemental Acceptors

The resolution with which the spectral lines are obtained is determined in part by the instrumental resolution as explained in section 3.1, but in addition there are several broadening effects which can occur. For ultra-pure semiconductor material such as that used in the

studies performed for this thesis, there are not enough ionized atoms to contribute greatly to the overall electric field at the site of another impurity. Such a field, being inhomogeneously distributed in the solid by random impurity positions, would lead to Stark broadening in less pure material due to shifts in the ground state energies for various atoms of a given species. We do not experience such broadening for impurity concentrations of the order of 10^{11} cm^{-3} or less.

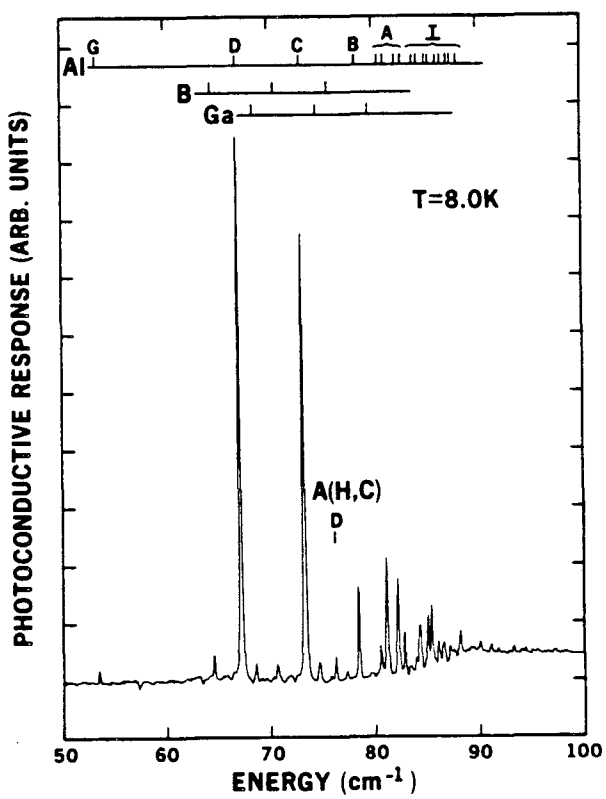

Figure 11 -- PTIS of Al

Another major contribution to a spreading of the ground state energies is having an inhomogeneous strain field present in the crystal. In even the best single-crystalline material there exist sufficient quantities of point and line defects to cause some small random stress components at any given impurity atom site. These stresses cause the bound states to split slightly, reducing their symmetry and partially lifting the ground-state degeneracy. The net effect for the spectrum is a broadened lineshape formed from a distribution of impurities with slightly different energies. Broadening of this type is responsible for most of the linewidth for lines of the elemental shallow acceptors in spectra carried out to the full resolution of our instrument. This is not true for impurity complexes, discussed below.

In heavily doped samples, prepared for special studies, both broadening mechanisms occur and it is not necessary to record an interferogram to full machine resolution. These samples have the additional problem of excited state overlap causing broadening of the excited state energy levels, which reflects directly in the line spectrum. The only additional broadening mechanism that is significant for semiconductors having only weak electron-phonon interactions is the so-called "lifetime broadening" proposed by Kane (1960), which accounts for the rather small natural linewidth in the

absence of all other effects.

Stress can be additionally applied to a sample from the exterior, as detailed in section 3.4 of the last chapter. When samples are chosen with faces perpendicular to the major crystallographic axes, symmetry information regarding the shallow levels can be obtained from spectra taken under applied uniaxial stress. This occurs because the stress axis is a $D_{\infty h}$ axis imposed upon the sample. Therefore the overall symmetry group at an impurity site is reduced to the common subgroup of the tetrahedral group and the group of the applied stress vector. For stress along ⟨111⟩, this is just the C_{3v} group, while stress along the ⟨100⟩ axis leads to the group D_{2d} and ⟨110⟩ stress to C_{2v}. None of these reduced symmetries allow four-fold degeneracy to exist, unless an accidental degeneracy. Therefore in all cases of applied uniaxial stress (including the extreme case of stress in a non-symmetry direction giving overall C_1 symmetry) the four-fold degenerate ground and excited states of a shallow acceptor must split into two Kramers doublets. If a particular energy state were to not split under such a stress it would be evident that it did not originally (in the full tetrahedral double group) have Γ_8 symmetry, as normal shallow acceptors do.

If we consider the stress tensor as a perturbation of the normal unstressed single-particle Hamiltonian for a

hydrogenic shallow hole state, we can write the perturbation, to first order in ε as

$$H_{stress} = \Sigma V_{ij}\varepsilon_{ij}$$

where the V_{ij} are interaction potential operators. Since the stress tensor is by definition a real symmetric second-order tensor, it has only 6 independent components in general. However, since the point symmetry operations of the tetrahedral group leave the unperturbed wavefunctions invariant (commute with the unperturbed Hamiltonian) and these functions form our basis set for the first-order degenerate perturbation theory, we need only consider those parts of the stress tensor which are invariant under T_d. There are only three such components for a real symmetric tensor, and so only three independent paramaters: a singlet, a doublet, and a triplet matrix, each with its own amplitude. In first order perturbation, the singlet component shifts the energies of all eigenstates equally, and so is just a change in the zero point of measured energy, but the doublet and triplet components have nonzero matrix elements between only certain specific states. In particular, both components perturb states of Γ_8 symmetry, causing a linear splitting of the quartet into two Kramers doublets as expected, but neither component causes a first order shift of states having Γ_6 or Γ_7 symmetries. This simply means that, while a quartet state must split, there

is no first order (linear in stress) effect on a Kramers doublet of states.

Similar symmetry considerations apply to the case of an externally applied magnetic field, except that the new symmetry axis is now of the $C_{\infty v}$ type, and time reversal symmetry is now destroyed. Kramers doublets then are split linearly with magnetic field, and in fact all degeneracy is lifted. It then becomes possible to count how many states existed in the original unsplit multiplet. In principle this is a very simple idea, but nature does not cooperate with us very well in this area. The measured (Tokumoto and Ishiguro, 1977) g-factors for the ground state are much lower than those for the excited states. While the excited states of a shallow acceptor readily split into all components, resolvable at only a few kilogauss, the ground state splits very little even at 50 kG. This makes it very difficult to experimentally determine the multiplicity of a ground state by magnetic field splitting.

4.2 Sensitivity and Signal-to-Noise

As mentioned in chapter 1 of this dissertation, the PTIS technique is a very sensitive tool for use with shallow levels in semiconductors. With chopped infrared radiation the signal measured is actually the fractional change in conductivity of the sample, a quantity essentially

independent of the absolute number of impurities. However, the overall signal amplitude is set by the majority impurity, and this does limit the sensitivity for additional impurities which coexist in the sample at lower concentrations. The ultimate absolute sensitivity, in terms of impurities per cubic centimeter, is determined by the net impurity concentration $|N_A-N_D|$ and the signal to noise ratio for that particular spectrum. Much of the signal amplitude is due to broad-band continuum photoconductivity with only a small percentage due to the integrated intensity of the discrete line transitions. As the temperature of the sample is raised, creating more phonons, the line strengths increase relative to the continuum, but many more carriers are ionized, contributing to the background conduction and noise. An optimal temperature for Ge appears to occur at approximately 6 K (15 K for Si), at which the lines are strong, but not much ground-state ionization occurs thermally. In such a case, with data acquisition parameters as given in chapter 3, a sample with "good" contacts (injecting and extracting carriers with low energy barrier) can easily achieve a signal to noise ratio for bound excited state transition lines of 100 to 1. With residual impurity concentrations of the order of 10^{10-11} cm^{-3} we could in principle observe electrically active shallow impurities at concentrations of 10^8 cm^{-3}. The noise from a particular

sample is usually caused by the carrier injection process and is very nonlinearly dependent on the sample bias. This can be adjusted to maximize the S/N ratio, a typical bias being 50 mV for Ge but several hundred millivolts for Si for 7 mm sample thickness.

Although this allows us to see very small fractional concentrations of impurities of the majority carrier type, it does not at all enable spectroscopy of minority carrier type impurities. To get around this difficulty, one can shine band-edged light on the sample in addition to the infrared beam from the interferometer (Bykova, Lifshits, and Sidorov, 1973). This light beam contains photons of sufficient energy to promote electrons from the valence band to the conduction band, creating both free holes and free electrons. A carrier of the minority type can be trapped locally by a phonon cascade process at a minority impurity site, from whose ground state PTIS can be performed. This enables one to see line spectra from minority type impurities superimposed on the majority carrier conduction spectrum, as shown in Figure 12. The existence of many free carriers from the band-edged light can sometimes decrease the noise due to carrier injection in a poorly-contacted or high-impedance sample by reducing space charge, and so the barrier to injection. For high-purity Ge samples, the minority lines under band-edged light are negative-going

with respect to the majority spectrum, most likely due to a decrease in conductivity from annihilation of a minority by a majority carrier (Van de Steeg et al, 1982; Darken and Hyder, 1983). In Si however the spectral lines are all positive-going, indicating an increase in conductivity from the minority free carrier.

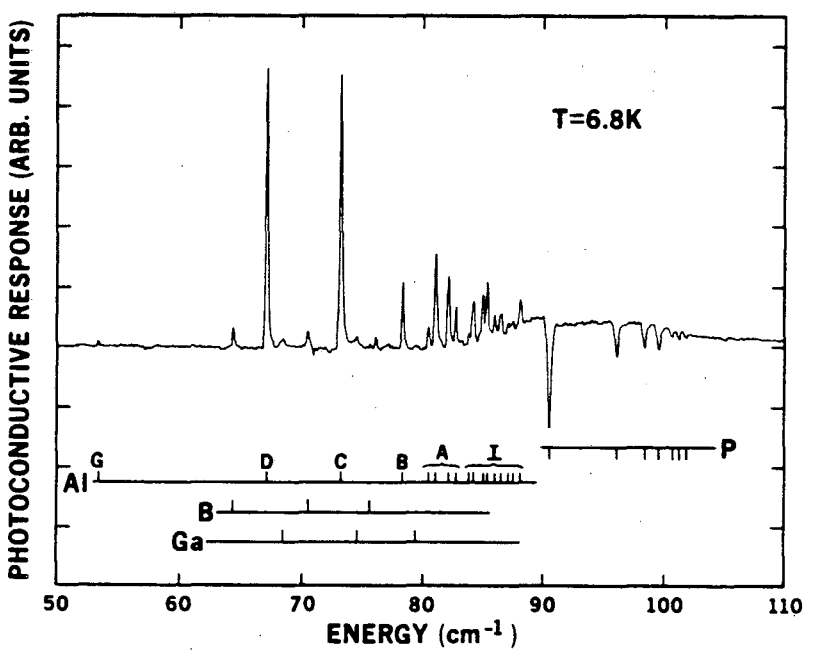

Figure 12 -- PTIS with Band-edged Light

4.3 Ge and Si Donor Spectra

The spectrum already seen as Figure 11 in section 4.1 is one of acceptors in p-type Ge. Spectroscopy of donors in n-type material is performed identically (except for the contact procedures discussed in chapter 2) but must be

interpreted in a different theoretical light. The conduction band of Ge has four equivalent valleys (6 for Si) which cause the symmetry of the states to be singlet plus triplet (plus an additional doublet for Si). In Ge the splitting due to valley-orbit interaction is large and we are generally concerned with only the singlet A_1 ground state of the shallow donor. However for Si the donors have much larger energies and the doublet E and triplet T_2 states can be thermally populated from the singlet ground state. The spectrum in Figure 13 shows phosphorus in Si, doped by the neutron transmutation technique (crystal donated by Topsil), at T=15 K where all three series of lines are seen simultaneously. The excited state energy differences can be very accurately determined spectroscopically and are in agreement with theoretical calculations (Faulkner, 1969). The doublet and triplet states have nodes at the central cell and so feel the least impurity-specific correction to their effective mass energy values. The singlet state has the largest probability at the impurity sight, causing a large central-cell correction lowering its energy, and so it remains the overall ground state.

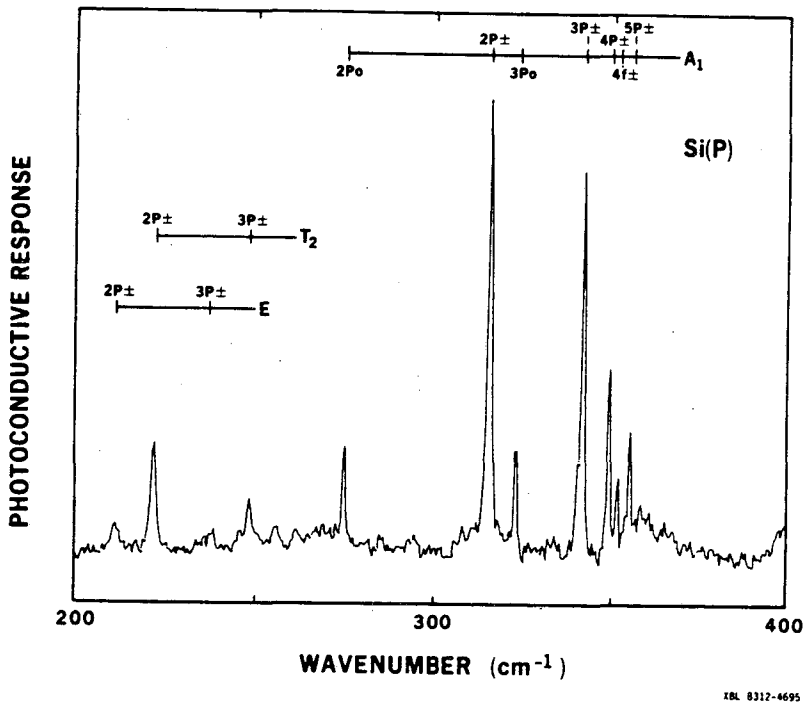

Figure 13 -- PTIS of Si:P

Stress applied to n-type samples (in all but the ⟨100⟩ direction in Ge) causes the valleys to become non-equivalent and so decreases the degeneracy of the states. Piezospectroscopy of elemental donors in Si and Ge is again in agreement with the symmetry assignments of Faulkner.

4.4 Impurity Complexes

Over the last several years, many impurity spectra have been seen in PTIS of ultra-pure Ge which cannot be explained by normal substitutional shallow impurities (Haller, Hansen and Goulding, 1981). Firstly they occur at energies different from all of the known elemental single shallow dopants, and secondly they show symmetry properties under

applied uniaxial stress that are different from those of ordinary substitutional impurities. Most of these spectra have been explained by the existance of impurity complexes, consisting of a substitutionally coordinated atom plus a light tunnelling species, H or Li (Haller and Falicov, 1978; Haller, Joós, and Falicov, 1980; and Joós, Haller and Falicov, 1980) as shown schematically in Figure 14. The additional symmetry provided by the extra degrees of freedom of the tunnelling atom, trapped in the strain field of an impurity which is smaller than the host atom, causes the (1s) hydrogenic ground state to expand into a multiple ground state manifold. In the cases of acceptor complexes in Ge the tunnelling atom is expected to sample four equivalent positions, tetrahedrally symmetric, probably in the antibonding directions of the substitutional atom. This leads to 4x4=16 states of the manifold. Group theory demands that the four-fold positional wavefunction of the light atom consists of a singlet and a triplet state. Simple direct product formation of the group of the bound carrier wavefunction with that of the light atom position gives a basis state of two Kramers doublets plus three quartets, shown in Figure 15.

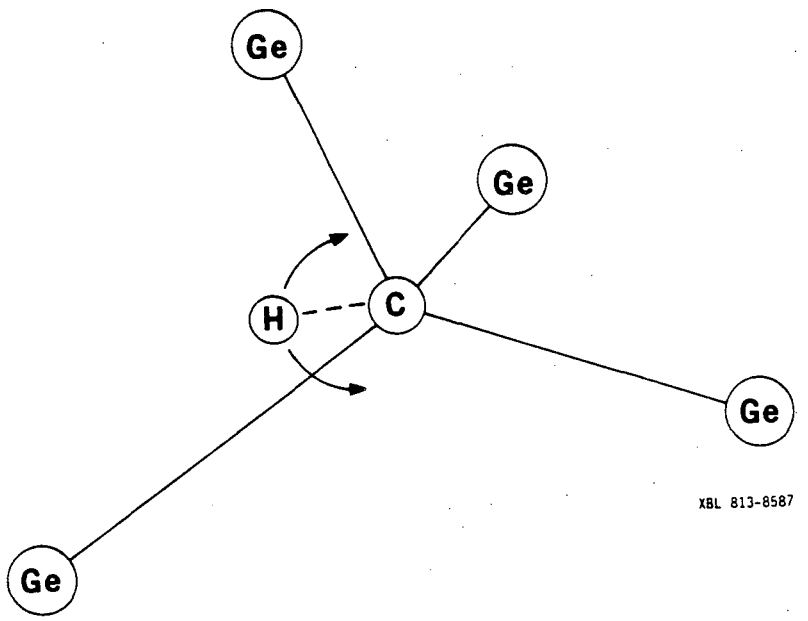

Figure 14 -- Tunnelling H Impurity Center

A set of seven new acceptors centers were originally discovered during the spectroscopic studies referenced above. Of these, four have been established as centers involving tunnelling hydrogen of the type described above, of which two are formed with Si as the substitutional atom and two with carbon, denoted A(H,Si) and A(H,C) respectively. Each of these pairs of states were shown to be split ground states of a single acceptor complex, and both states were of the stress-independent type. This implied that the states seen in PTIS as the lowest-lying in the manifold are actually the two Kramers doublets, while the three quartets are not seen by thermal population at T=8 K or lower.

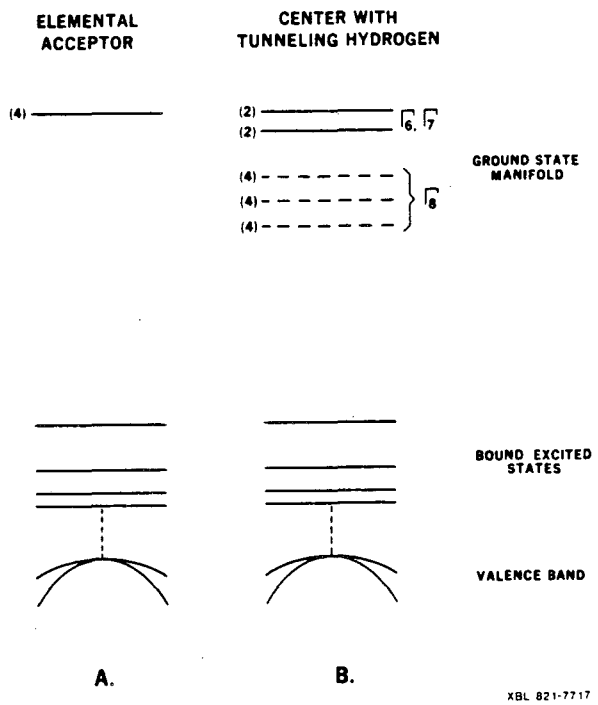

Figure 15 -- Impurity Complex Ground State Manifold

Additionally there were several donor complexes described in the above references which were all attributed to oxygen as the sustitutional species with H or Li tunnelling around. The oxygen atom is thus stabilized in this position by the formation of such a complex, since isolated substitutional oxygen in germanium has never been seen. In each of these cases all of the experimental facts are accounted for by the theoretical model described above. The presence of the extra H atom in both the donor and acceptor complexes appears to make available an additional empty orbital for accomodation of one electron from the valence band. It thus acts in such a way as to shift the

position of the substitutional atom one element to the left in the periodic table. Oxygen therefore becomes a single donor when one H atom is present, while C and Si become single acceptors in Ge.

Three of the new acceptor states, labelled A_3, A_4, and A_5, were not studied extensively and were not modelled by the above theory. Some of the states behave in much the same way as the A(H,C) and A(H,Si), with many of the same thermal and piezo properties, but there are some differences. These differences are the basis of much of the experimental endeavors of this thesis, and will be described in the next two chapters. This work builds on the above-mentioned material, and has in certain ways strengthened the model for the cases already reviewed. Also, additional experimental work was performed on the acceptor complexes already mentioned in order to further elucidate a comparison of the three new centers with the previously known ones.

Chapter 5 -- Novel Acceptors $A_{3,4,5}$: Spectroscopy

5.1 Conditions for Existence of the Novel Acceptors

The three series of lines labelled A_3, A_4, and A_5 always and only appear in as-grown single crystal ultra-pure germanium samples grown from a carbon or pyro-carbon coated silica crucible and in a nitrogen growth atmosphere. Many variations in the crystal growth environment have been explored, but only the carbon-nitrogen combination gives rise to these centers. The relative concentrations of the three spectral line series depends on the thermal history of the sample. A given sample exhibits in general a mixture of all three sets. After specific annealing conditions it shows only A_4 in addition to aluminum or other unrelated impurity acceptors, or it may contain only A_3 and A_5 besides the residual impurity acceptors. Most of the as-grown samples contain, shortly after growth, approximately a 1:1 ratio of line intensities of A_4 and A_5 with only a very small amount of A_3.

For samples that were stored at room temperature for a very long time (4 to 5 years), the spectra taken afterward were different from the ones taken from identical samples shortly after crystal growth. In all of the long room-temperature-stored samples, the spectral series A_4 had completely disappeared, while the other two novel acceptor

series had increased in strength. It became clear that these centers are indeed very strongly related, and it appeared that a conversion had taken place between electrically active centers of one type and those of the other. This has not been observed before for any shallow levels in Ge, making the new acceptors very novel indeed.

A photothermal ionization spectrum of an as-grown crystal sample containing all three line series A_3, A_4 and A_5 plus the lines of aluminum is shown in the bottom trace of Figure 16. It can be noticed from such spectra that the lines of the new center A_5 are much sharper than those of aluminum, a phenomenon familiar from the A(H,C) and A(H,Si) line series. This indicates an independence of the ground-state energy on random inhomogeneous stress within the crystal. Such an assumption is borne out by the upper trace of the same figure in which a uniaxial stress is applied, showing that while spectral series A_4 splits under stress as a normal elemental acceptor such as aluminum, the series labelled A_3 and A_5 do not split with stress. Such stress-independent centers are reminiscent of the tunnelling hydrogen impurity complexes.

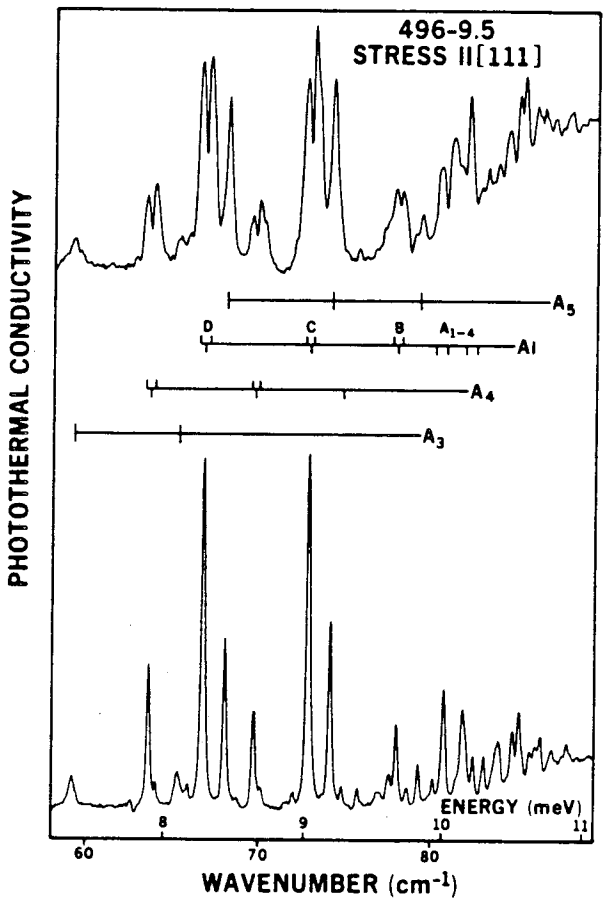

Figure 16 -- PTIS of carbon-nitrogen grown Ge

To prove that hydrogen is not involved in this novel series of three acceptors, a special crystal was grown from a carbon susceptor, initially under a pure nitrogen atmosphere. Partway through the growth of the crystal, hydrogen gas was added in a 1:1 ratio with the nitrogen. If hydrogen were necessary for the formation of the three novel centers it would be available only in trace amounts under the normal nitrogen atmosphere in which the centers appear. Growing a crystal in a mixed-gas environment should provide

much more hydrogen, leading to the formation of additional centers of this type. However, this turns out not to be the case at all. Spectra of samples taken from the pure nitrogen-grown region (lower trace) and the mixed-gas region (upper trace) are shown in Figure 17. It can be seen from these spectra that in fact the hydrogen introduction has completely eliminated the novel centers, while the acceptor complex A(H,C) has been formed instead. It appears that the hydrogen competes for the carbon which may be involved in the carbon-nitrogen related centers and does not directly play a role in these novel impurities.

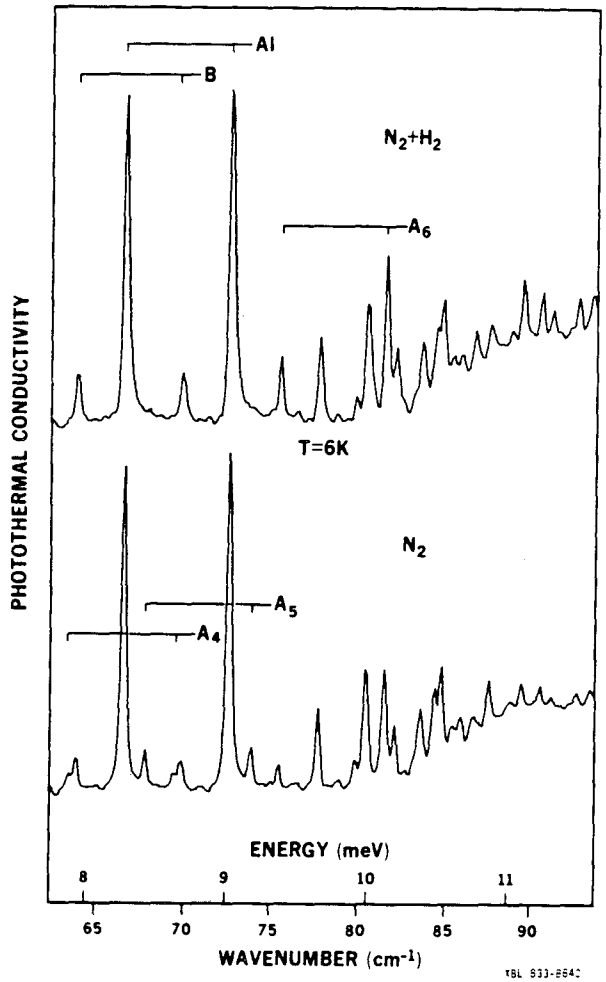

Figure 17 -- PTIS of Mixed-gas grown Ge

5.2 Variable-temperature Infrared Spectroscopy

As discussed in previous chapters, the spectrum of bound-state to bound-state transition lines in photothermal ionization is a function of the temperature of the sample during the time the interferogram is being recorded. This is due to the phonon absorption step of the process, whose

rate depends on the phonon population in the sample. However, one thing that is independent of the sample temperature is the ratio of two equivalent integrated line strengths (for, say, two D lines, $1\Gamma_8^+ \rightarrow 2\Gamma_8^-$ transitions) of two different species of shallow elemental acceptors in the same sample. Since the excited states are identical for all of these acceptors, as shown in Figure 10 in Section 4.1, the phonon absorption step is identical once the bound hole is promoted to a given excited state.

States of even the non-elemental single acceptors will have the same spectrum of energy levels of excited p-states, so that this ratio between a given transition line's integrated strength for two different line series again has the property that the phonon excitation from the final state into the band is identical. The ratio then is simply the relative concentrations of holes in the ground states of the two centers. This property is used to advantage as an internal calibration for the concentrations of complex impurity centers whose ground states are split into manifolds of several states, having temperature-dependent populations. Samples containing such impurity centers always have in addition a background concentration of at least one elemental impurity, typically aluminum in p-type germanium. The aluminum acceptors, whose ground states are not thermally ionized at low enough temperatures, thus have

a temperature-independent ground state population which is taken as a reference concentration for the spectral lines of the complex impurities. This neglects the effects of both compensation and of direct thermal ionization at higher temperatures (Darken, 1982). In this way we obtain the temperature dependence of the ground state manifold levels, independently of the phonon process of PTIS. We can then determine whether or not a pair of line series belong to a single impurity center having a split ground state, as in A(H,C) and A(H,Si).

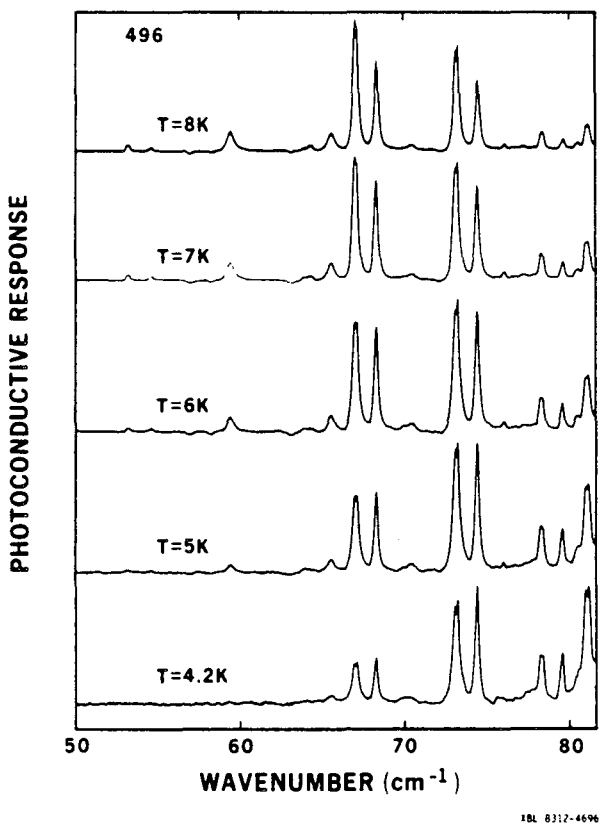

Figure 18 -- Sample Temperature Dependence

This procedure was carried out for samples containing the spectral series A_3, A_4, and A_5, as shown in Figure 18. All such samples contained a certain residual aluminum background concentration which was used as a reference value in the ratio. The D lines of each series were used as the strongest and best understood in terms of final state symmetry (which may be more complicated for the C lines, $1\Gamma_8^+ \rightarrow 2\Gamma_8^- + 1\Gamma_7^-$ transitions). Even at 4.2 K there is sufficient signal to noise to enable one to ratio D lines for the various acceptors. The result is that the ground state population of A_4 is independent of temperature at low temperatures, ionizing in the same way as aluminum at higher T. This indicates that there are no nearby states in any multiple level manifold due to this impurity center. However, the lines of spectra A_3 and A_5 are temperature dependent in ratio to aluminum, indicating that both are due to initial states in multiple-level manifolds. In fact, the relative populations of the two initial states is just given by a Fermi-Dirac distribution function with Fermi energy very close to the lower-lying ground state A_5 (Figure 19), while the sum of the two populations is constant with T (Figure 20). This clearly indicates that the two line series are due to initial states belonging to the same impurity center, and that it has a split ground-state manifold. We will henceforth denote this single impurity

center, giving rise to these two series of spectral lines, as $A_{3,5}$.

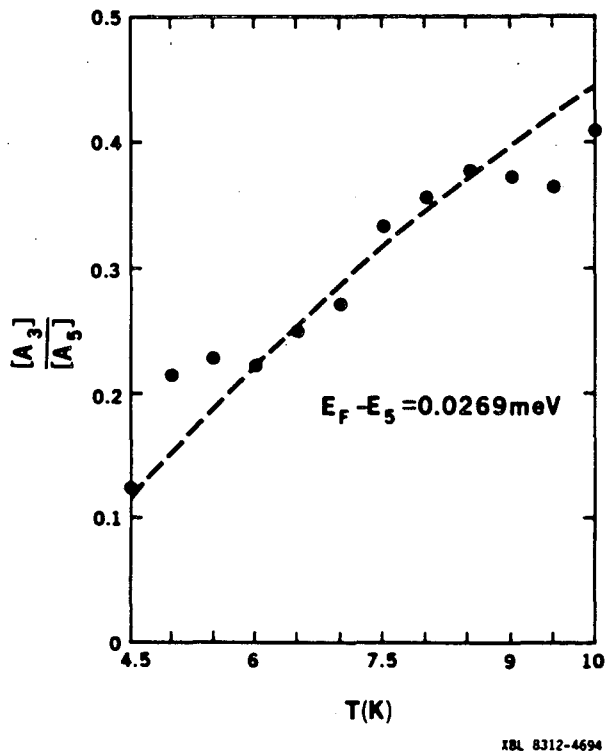

Figure 19 -- Thermal Distribution in Manifold

The poor fit in Figure 19 at low temperatures is due to the large errors in integrated line strengths for such weak lines. At high temperatures, ionization of the Al ground state relative to the $A_{3,5}$ states becomes important.

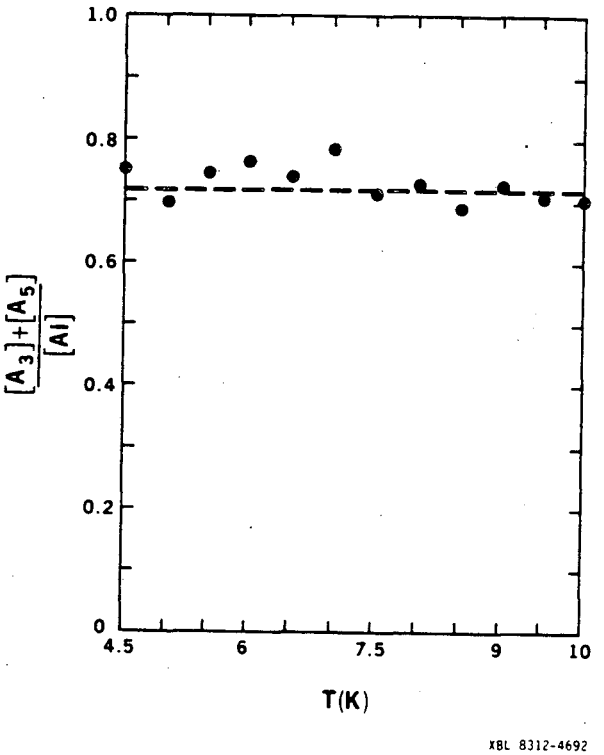

Figure 20 -- Sum of States in Manifold

5.3 Piezospectroscopy and Magnetospectroscopy

Photothermal ionization spectroscopy of the three novel acceptors presented in this chapter was carried out using single-crystal Ge samples cut in the ⟨111⟩ and the ⟨110⟩ orientations for use in the low-stress insert shown in Figure 9. The sample temperature was typically maintained at 6 K to obtain reasonable line strengths with good signal to noise, as discussed in section 4.2. In all cases, including spectra of several accidentally inhomogeneously stressed samples, the line series due to $A_{3,5}$ were totally

insensitive in the ground state component to the applied stress, broadening only slightly from excited state splittings. However, the line series A_4 splits and/or broadens in a manner identical to the residual aluminum impurity, indicating that it is a center with a ground state having a Γ_8 symmetry identical to the elemental acceptors. This clearly indicates that the two types of impurity centers responsible for the different symmetries of line series both exist in a site in the host Ge crystal which has the full tetrahedral symmetry of the lattice; if not, uniaxial stress fields would cause splittings characteristic of the underlying local reduced symmetry, as explained in section 4.1. In particular, centers with fixed internal axes would exist as an ensemble of several non-equivalent orientations, which would produce dichotomies in the spectra under applied uniaxial stress. No states of reduced symmetry remain unshifted in energy by such stress.

Magnetospectroscopy was also performed on a sample of carbon-nitrogen-grown Ge containing the three novel centers, but no additional information was gained due to the lack of significant splitting of the ground states of these centers, as explained in section 4.1 for other acceptors. With the present experimental apparatus we are unable to gain additional information from piezomagnetospectroscopy. If the capability of using higher magnetic field strength (to

100 kG) becomes available, ground-state splittings of reasonable size may be observed. The use of polarized infra-red light would greatly aid in classifying the symmetries of the states involved in each transition.

5.4 Interconversion of A_4 and $A_{3,5}$

As mentioned in section 5.1, a sample containing these two novel impurity centers in the as-grown crystal will, after several years, revert to a condition of containing only $A_{3,5}$. This is shown in the lower trace of Figure 21, where the position of the missing series A_4 is marked and the small peaks very close to these positions are just a trace amount of residual boron acceptors. In the upper curve of the same figure, however, it is seen that the same sample, when heated for 5 minutes to a temperature of 400°C, converts back to a large quantity of A_4 and essentially no amount of $A_{3,5}$. Thus there is an essentially complete interconversion from one center to the other and back again, all of which can be done reversibly, conserving total number of acceptor states. It is only with a time constant of over a hundred hours ($\tau \simeq 107$ hr) at 400°C (Hall and Soltys, 1977) that the centers irreversibly disappear. This is a new effect in that both forms of the center are shallow single acceptors and the interconversion occurs to completeness in either direction at the proper sample temperature.

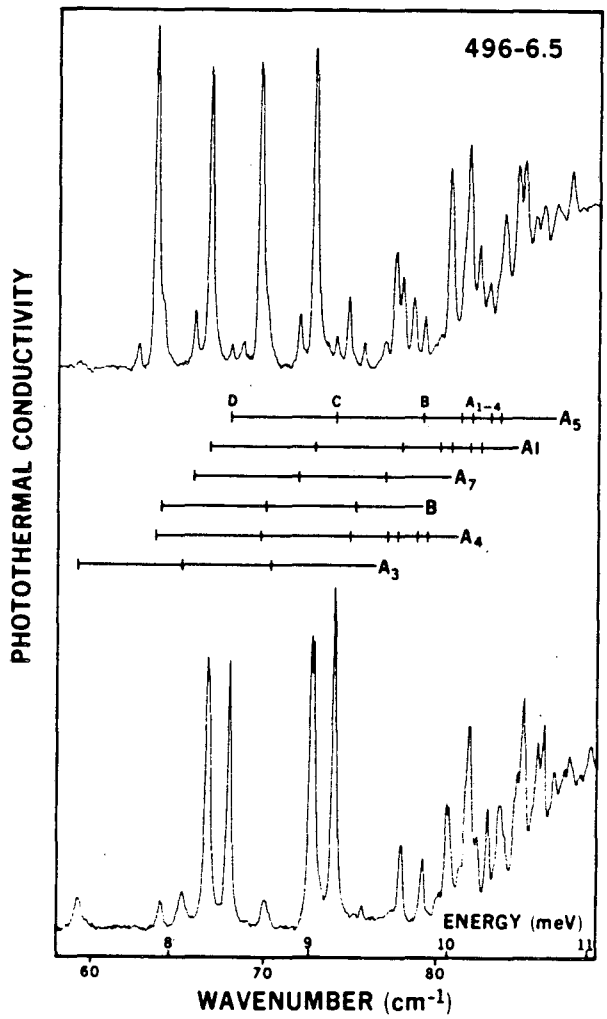

Figure 21 -- Spectroscopy with Interconversion

Further study into the annealing behavior of these centers reveals that at any given temperature the interconversion process achieves an equilibrium ratio of concentrations between A_4 centers and $A_{3,5}$ centers. This equilibrium can be characterized by the curve shown in Figure 22, in which the fractional concentration of the $A_{3,5}$ centers relative to the total is shown as a function of the

temperature at which the equilibrium is allowed to occur. It can be seen that the overall ground state of the system (low-temperature preferred state, that with lowest internal energy E) is that of $A_{3,5}$ while the thermally populated higher-lying state is the A_4 center. It is evident from a curve of this type that this system is not a simple two-level system having Boltzmann population of the higher-lying state; this would lead at most to equal populations of the two at high temperatures. Instead, it can be seen from the steepness of the transition region of the curve that a very large degeneracy, such as that due to a continuum state, exists for the higher-lying of the two states. Such a relative degeneracy "g" for the upper state is equivalent to producing an entropy term in the free energy of the system, allowing this state to lower its free energy F=E-TS with temperature.

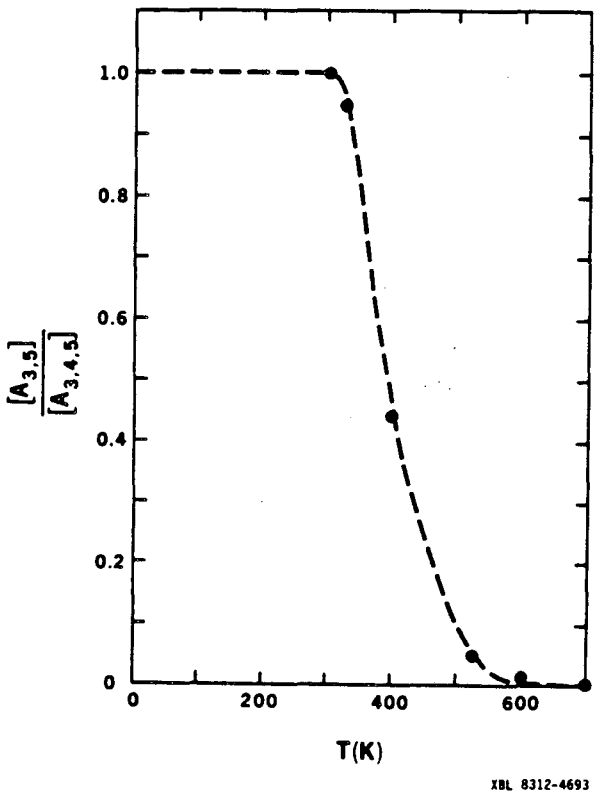

Figure 22 -- Interconversion Annealing Equilibrium

If one fits an exponential Boltzmann curve to these data, allowing only the activation energy ΔE and the relative degeneracy "g" of the upper state as free parameters, one finds that a degeneracy of at least 10^6 exists for that state in order to account for such a steep slope; a higher degeneracy is easily possible due to the limited precision of the data for such a large value in the calculation. The fraction of centers in the $A_{3,5}$ configuration is given by $1/(1+g \exp-\Delta E/kT)$ while that for

the A_4 state is $(g \exp{-\Delta E/kT})/(1+g \exp{-\Delta E/kT})$. Since the two endpoints of the curve in Figure 22 have poor accuracy (room temperature fraction >99%, fraction above 300°C <1%), only the three central points provide data for fitting the parameters. Of these, the two lower-temperature points (50°C and 120°C) are most accurate due to the very short time scales involved at higher temperatures. The result of a weighted fit is then $g=1.56\times10^{6\pm0.5}$ and $\Delta E=0.45\pm0.03$ eV. Such a degeneracy corresponds to an entropy $S=k(\ln g)$ of approximately one millivolt per degree K. With these values it can be easily calculated that the room temperature fraction is >99% and the fraction at 300°C is <1%, in agreement with experiment.

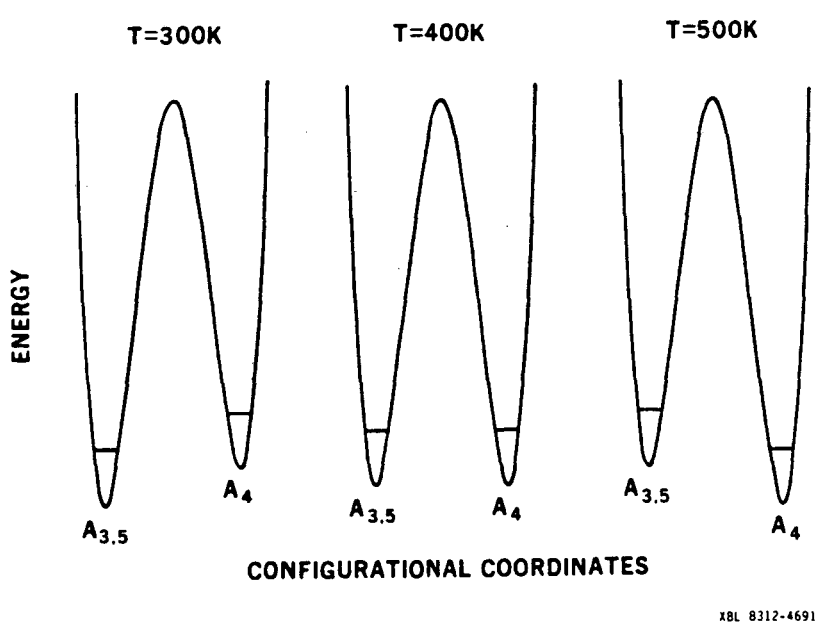

Figure 23 -- Free Energy in Configurational Coordinates

In terms of a free-energy minimization picture in configurational coordinate space, the experimental result can be stated as a lowering of the total free energy of the A_4 state at higher T. As shown in Figure 23, this is just a diagrammatic representation of the entropy factor that comes from a generalized configuration with a high degeneracy, such as was found above. At any given temperature there will be an equilibrium concentration of centers in each of the two stable configurations. Such an equilibrium ratio is reached only after an exponential decay from some initial ratio of states. Ratios of centers as a function of annealing time, determined by PTIS, are shown for two different temperatures in Figures 24 and 25. In both cases, the equilibrium is reached by a first-order exponential process in time, indicating that the rate is determined solely by the concentrations of active centers present in the sample. A time constant for the decay can then be determined at each temperature. An Arrhenius plot of the time constants as a function of inverse temperature gives an estimate of the activation energy (barrier height for interconversion) of the process, as shown in Figure 26. Although the error bars for the measurements are large at both high and low temperatures, a slope of approximately 0.7-1.0 eV/K yields a satisfactory fit to the data points.

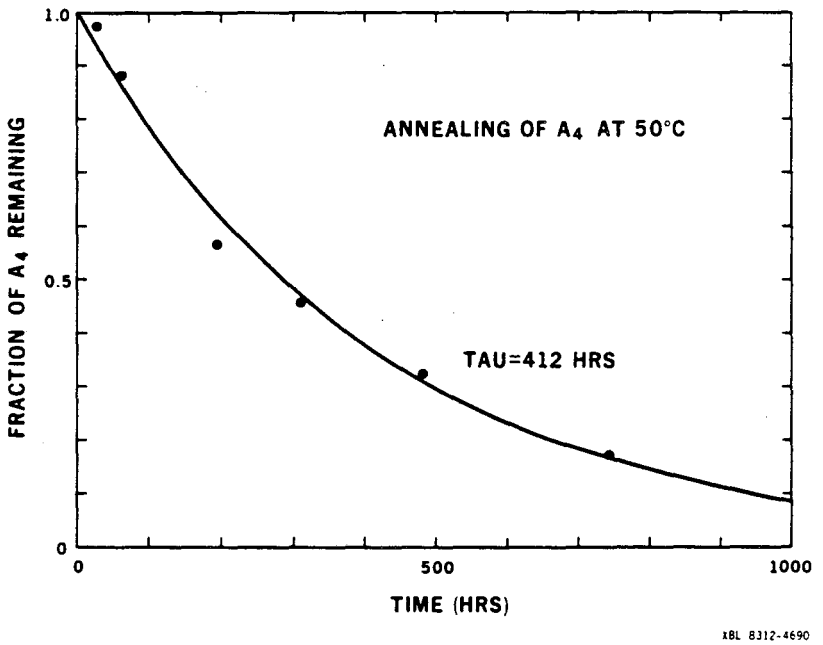

Figure 24 -- Interconversion at 50°C

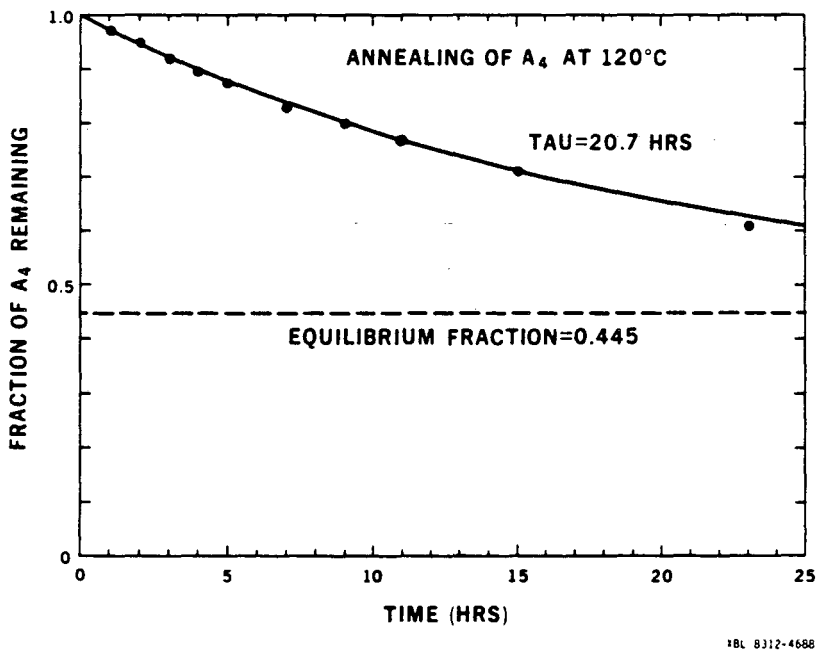

Figure 25 -- Interconversion at 120°C

This information leads one to the assumption that what exists in these samples is a carbon-nitrogen center having two independent positions within the lattice, both with full tetrahedral symmetry, and able to interconvert by moving from one such environment to the other. The most likely candidates for such a system, and the only simple models having the proper number of electron states for a single acceptor, are shown schematically in Figures 27 and 28. These consist of a single carbon and a single nitrogen atom, with a tunnelling or rotational orientation degree of freedom to accomodate the symmetry of the Kramers doublet states, existing either at a substitutional lattice site or with large degeneracy at the site of a tetrahedral interstitial void in the lattice. These models account for all of the known experimental facts pertaining to the novel shallow acceptor centers.

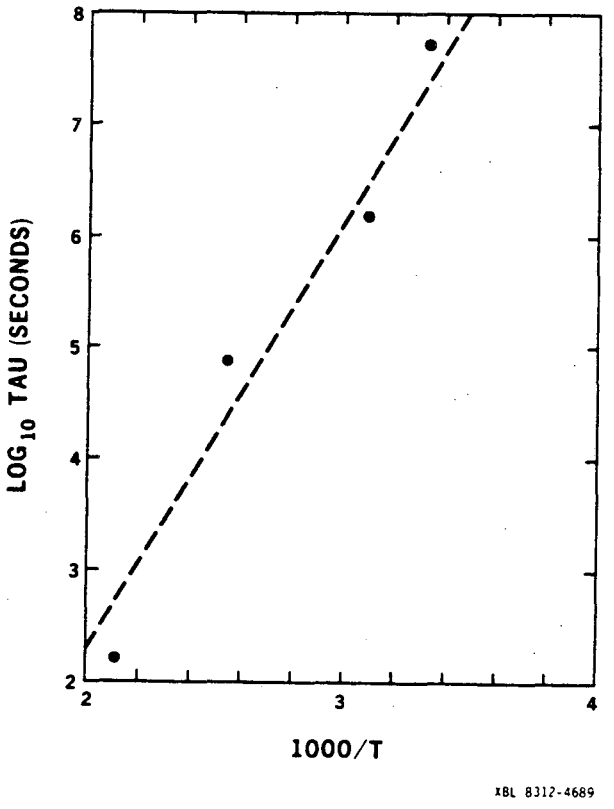

Figure 26 -- Time constants vs. 1/T

5.5 $A_{3,5}$ and A_4 Generation by KCN Diffusion into Germanium

The above models for the novel centers, along with the chemical information that they are carbon-nitrogen related, leads one naturally to the possibility that the centers are formed simply from a cyanide ion CN^- located interstitially in the lattice, where it would prefer to remain ionized to maintain a full valence shell. In this configuration it could travel from one interstitial tetrahedral site to another by a charge-state aided diffusion mechanism such as

the Si self-interstitial may do (Frank, Seeger and Gosele, 1981), passing through the hexagonal ring by valence band electron relaxation. If a substitutional site were found it could form the second type of impurity complex configuration. Such a hypothesis leads one naturally to experiment with the diffusion of cyanide ions in the germanium lattice. The ions are expected to diffuse rapidly, as does copper, lithium or atomic hydrogen, because of the above arguments. If they can be introduced into the bulk from an external source, they are expected to produce centers of the types $A_{3,5}$ and A_4 in the Ge lattice. These centers should then be indistinguishable in all properties from the as-grown centers in carbon-nitrogen grown crystals.

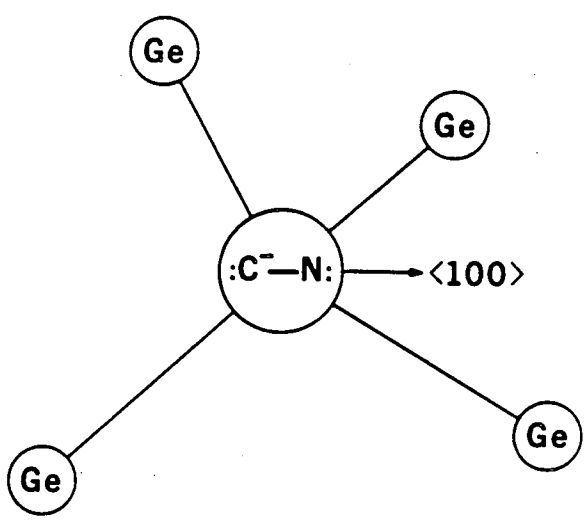

$A_{3,5} = A_S$ (C,N) SUBSTITUTIONAL T_d

XBL 8310-12045

Figure 27 -- Substitutional A(C,N)

It should be noted that the CN^- intersitial was first suspected as the species causing the $A_{3,4,5}$ line series after a series of experiments performed by Darken (1982). In this instance, pure Ge samples which were quartz-hydrogen grown showed no trace of $A_{3,4,5}$ in PTIS of as-grown material. After annealing for 24 hours at 600°C in air and rapidly quenching to room temperature, these samples showed spectral line series A_4. Additional annealing (for InGa contact regrowth) at lower temperatures (275°C, slow cool) caused creation of the A_5 center. Samples slow cooled from 600°C also showed both A_4 and A_5. These results were not understood, until it was realized that the samples had been treated with KCN solution before annealing.

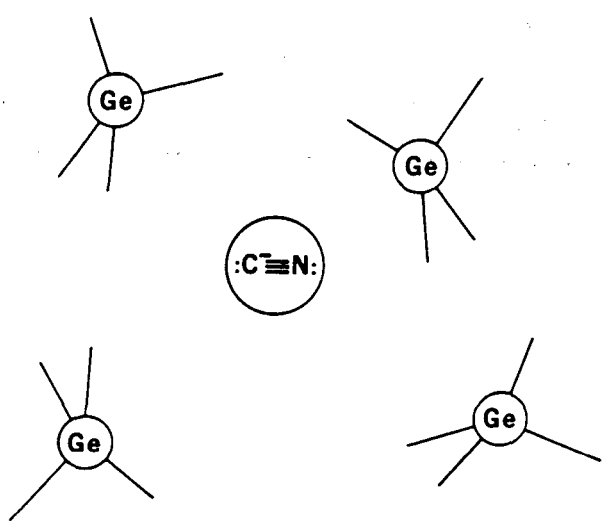

$A_4 = A_I$ (C,N) INTERSTITIAL T_d

IBL 8310-12243

Figure 28 -- Interstitial A(C,N)

Experiments were performed in order to verify these assumptions. Germanium samples from several crystals with different chemical histories, none of which involved a carbon-nitrogen environment, were soaked in a KCN aqueous solution, as detailed in section 2.3. These samples were heated on similarly treated quartzware in furnaces at 600°C for periods of one to 24 hours. PTIS performed on these samples revealed that the three novel impurity spectra, which did not exist before treatment in these samples, were now strongly evident. For most samples, removal from the furnace was followed immediately by a rapid quench to room temperature by argon jets. The spectra obtained were thus (by virtue of the interconversion facts presented in section 5.2) those of A_4 without the other two line series. However, as expected, the samples showed acceptor $A_{3,5}$ after gentle annealing treatments of 24 to 48 hours at 120°C. This leads one to the conclusion that the chemical nature of the novel acceptors is that of the cyanide ion species, barring secondary effects between cyanide and other possible components.

As control samples, germanium samples of carbon-nitrogen grown material were heated in the same conditions both with and without cyanide coating for 24 hour periods. The samples without cyanide showed complete loss of the novel acceptor PTIS series, while the samples with

cyanide showed very little change in concentration before and after heating. This is taken to indicate that the impurity complex centers, now presumed to be cyanide, diffuse out of the sample under these heating conditions unless a source of cyanide exists at the sample surface. This diffusion would have to occur at the rapid rate of an interstitially diffusing species.

In order to characterize the diffusion more quantitatively, samples were diffused for short periods of time (up to one hour). These samples showed surprisingly high average concentrations of the novel centers. The samples were carefully lapped and re-etched a total distance of 300 microns from each of the two major faces (a total of 0.6 mm thickness reduction), resulting in a new spectrum containing only half of the total average concentration of novel centers, relative to the known constant aluminum concentration. This indicates that the cyanide-based centers were able to diffuse into the crystal with a profile whose characteristic distance for an integrated concentration of half the initial value is only of the order of a few tenths of a millimeter. The diffusion constant D for such a profile, if first-order as expected, would have to be of the order of 10^{-5} cm^2/sec, which is very similar to that of the known interstitial diffusers such as copper and lithium in this temperature range ($D_{Cu}=3x10^{-5}$ cm^2/sec,

$D_{Li}=5x10^{-6}$ cm^2/sec at 600°C).

Additional evidence for such a diffusion profile also comes from the capacitance profile of a sample prepared as a diode for DLTS measurement. This profile indicates an extrapolated surface concentration of 10^{13} cm^{-3} with a depth to half-maximum concentration of 200-300 microns. This is in very good agreement with the depth obtained from the lapped sample measurements, and gives the additional information of the absolute concentration of the novel acceptors at the surface of the sample. Based on this value, it would appear that an average concentration of only a few times 10^{10} cm^{-3} in a sample of thickness several millimeters is entirely reasonable. Also, the low average concentrations for samples diffused for 24 hours is explained by a depletion of the semi-infinite source at the surface followed by out-diffusion of the cyanide from the bulk germanium. This may occur because the diffusion is performed in air, in which free cyanide is known to form many products at these temperatures (such as cyanates and oxides whenever a reducible oxide such as that of Ge is present). A sample from which 300 microns were removed from the surface after a 24 hour cyanide diffusion was measured to have a relatively higher concentration of A_4 to aluminum than before being lapped, indicating an out-diffusion profile which peaks in the center of the sample rather than

at the surfaces. This confirms the hypothesis that the diffusion was first carried out to high concentration from the semi-infinite source, followed by some out-diffusion as the source became dissipated, leaving a higher internal than surface concentration.

5.6 ^{14}C Radiotracer Experiments

As additional proof of the in-diffusion of CN from external sources, a few samples were prepared by diffusion with isotopically pure $K^{14}CN$, and were then fashioned into diodes by P. Luke for use as nuclear radiation detectors. Such diodes detect not only unwanted background radiation, but also the internal beta decays of the radioactive carbon. If ^{14}C from the external KCN source does actually diffuse into the Ge lattice rapidly in the form of CN, it will provide a characteristic beta decay spectrum. Since carbon has such a long half-life, very few counts were expected at the concentrations thought to exist in the Ge sample from diffusion. In addition, the diodes were only able to achieve depletion depths of a few hundred microns, due to the high concentrations of electrically active impurities near the surfaces ($\approx 10^{13}$ cm^{-3}). Therefore, the detectors were operated in an ultra-low background radiation facility, existing at Lawrence Berkeley Laboratory (using all specially selected low radioactivity materials), in an

effort to achieve sufficient signal to noise ratio for the internal decays. The detectors were set to automatically record the energy spectrum of detected events using a multi-channel analyzer and computer interface. These spectra were carried out over a period of several months of counting, to increase statistics (average event rate was only one count per several hundred seconds). Even with such long counting times, and using a control sample treated with normal KCN as a background detector for background subtraction, convincing statistics for a ^{14}C beta spectrum were not in evidence.

Chapter 6 -- Novel Acceptors $A_{3,4,5}$: Theory

6.1 Group Theoretical Considerations

In order to develop a group-theoretical analysis of the behavior of the novel acceptors discussed in chapter 5, we must first consider the analysis of a normal substitutional acceptor, a group III atom. In the case of a third-column element, the valence shell is exactly one electron short of the required number to participate in four tetrahedrally-directed bonds to the elemental host lattice. Since it is energetically favorable to form such bonds, a valence band electron from the solid as a whole will become deeply bound at the site of the impurity, resulting in a coulomb field due to the single excess charge, which can bind a shallow hole in a hydrogenic orbital.

The valence band of the group IV elemental semiconductors is made up of bands of p-states from the individual atoms which are split by the spin-orbit interaction mechanism into states of $p_{1/2}$ symmetry (Γ_7 states) and states of $p_{3/2}$ (Γ_8) symmetry. The doublet state is lower in energy by 300 meV in Ge (50 meV in Si) than the quartet, which is the state of the valence band top. At the center of the Brillouin zone, the k=0 or Γ point, the states at the top of the valence band have the full tetrahedral symmetry of the lattice. For a point defect, the impurity

states produced by hydrogenic binding of a shallow hole take on the symmetry of the point defect, T_d. These states appear in the energy gap of the semiconductor as shallow hole levels at the center of the zone. The symmetry of the electronic state produced from a hydrogenic acceptor is that of the valence-band hole state in direct product with the hydrogenic-orbital envelope function symmetry.

Consider first the set of operations which leave a regular tetrahedron invariant. If we inscribe the tetrahedron in a cube with four corners matching, the symmetry rotations are the eight three-fold rotations about the ⟨111⟩ axes which pass through a corner and a face midpoint, the three two-fold and six improper four-fold rotations about ⟨100⟩ axes, six diagonal mirror planes which pass through a tetrahedral edge and are normal to a cube face, plus the identity transformation. These twenty four operations form a group, denoted T_d, and there exist only five irreducible representations of this group, whose character table is shown in the top section of Table 1 (and neglecting the rotations labelled R). This produces the constraint, as mentioned previously, that there exist only singlet, doublet, and triplet states with the symmetry of this point group. The multiplicity of the representation is the character of the identity transformation (column E of the table). One of the two possible triplet symmetries is

that of the p-state of the hydrogen atom (Γ_5 symmetry).

$\bar{T}_d$	E	R	$8C_3$	$8RC_3$	$3C_2+3RC_2$	$6\sigma_d+6R\sigma_d$	$6S_4$	$6RS_4$
Γ_1	1	1	1	1	1	1	1	1
Γ_2	1	1	1	1	1	-1	-1	-1
Γ_3	2	2	-1	-1	2	0	0	0
Γ_4	3	3	0	0	-1	-1	1	1
Γ_5	3	3	0	0	-1	1	-1	-1
Γ_6	2	-2	1	-1	0	0	$\sqrt{2}$	$-\sqrt{2}$
Γ_7	2	-2	1	-1	0	0	$-\sqrt{2}$	$\sqrt{2}$
Γ_8	4	-4	-1	1	0	0	0	0

Table 1 -- Tetrahedral Double Group

In addition to the above, for states of odd half-integral spin (fermions) one must consider operations in which rotations by 2π (denoted R in the character table) leave the wavefunction inverted in sign from rotations by 0 or 4π. Such operations can be accounted for by formation of the double group $\bar{T}_d$, which gives rise to three additional "doubled" irreducible representations for fermionic states (doublets Γ_6 and Γ_7, and quartet Γ_8). These are the symmetries of interest for the case of single-hole states in a diamond-lattice semiconductor. Hole states of this type

must always have at least two-fold (time-reversal) symmetry and are therefore either Kramers doublets or quartets. The full character table for the tetrahedral double group is given above in Table 1.

The normal elemental shallow acceptor, such as boron or aluminum in Ge or Si, has a ground state of four-fold symmetry equivalent to a state of 3/2 spin, transforming like the Γ_8 representation of the tetrahedral double group. When this "spin-3/2" hole is in a p-like hydrogenic envelope function state, its symmetry is seen to be $\Gamma_8 x \Gamma_5$ which is a mixture of several states with doublet and quartet symmetries. These various excited states cause the spectrum of an acceptor to have relative spacings quite different from that of an ordinary hydrogen atom. Identification of the symmetries of these excited states is made by piezo- and polarized light spectroscopy of carriers into each state. The assignments of Baldereschi and Lipari will be taken to be correct for these states.

Allowed dipole transitions from the normal elemental ground state Γ_8 include any transitions with final states having odd half-integral effective spin, i.e. those whose final state is that of a single hole having the symmetry of one of the doubled irreducible representations. These include transitions to states having Γ_7 doublet symmetries such as the $1\Gamma_7^-$ state suggested to be assigned as

accidentally degenerate to the $2\Gamma_8^-$ quartet responsible for the C-line transition in far-infrared spectroscopy of germanium. Such an additional state could in principle give rise to different selection rules from initial states having other than Γ_8 symmetry, such as the doublet states of the impurity complexes. In such a case, a state of Γ_7 symmetry would not connect by first-order dipole matrix element to the $1\Gamma_7^-$ doublet component of the C-line final state, whereas a state of Γ_6 symmetry would have an allowed transition. This difference in principle could enable the assignment of the symmetry of the doublet ground-state.

An additional complication exists for silicon, in which the spin-orbit splitting of the valence band is much smaller than in germanium and the shallow levels are four times deeper in energy. Therefore all six states of the p-bands of the host atoms must be included in the identification of the symmetries of impurity hole states. Thus a different scheme for the labelling of lines exists for acceptor spectroscopy in silicon.

There exists an incompatibility between the demonstrated split ground states (which can be thermally populated) of impurity complexes and the usual assignment of the Γ_8 symmetry of the ground state. Piezospectroscopy has shown that the ground states for the complex acceptors of chapter 4 and acceptor $A_{3,5}$ of chapter 5 do not split or

shift with stress, indicating doublet rather than quartet symmetry. This incompatibility can be resolved by resorting to a model with an internal degree of freedom in the impurity.

6.2 Models for Impurity Complexes

The simplest model for extra internal symmetry resulting in a manifold of states for the (1s) hydrogenic envelope function is that of one atomic species, usually a light atom such as H or Li, tunnelling around the position of a second, heavier substitutional atom. In this "tunnelling hydrogen" model, previously shown schematically in Figure 14, the hydrogen (or lithium) atom can exist in at least four equivalent positions, such as the antibonding orbital directions from the substitutional atom. This is the minimum number of non-tetrahedrally symmetric positions which can be combined linearly to obtain a state having full tetrahedral symmetry. If we assume that this is indeed the configuration for the hydrogen-related impurity complexes of chapter 4, then we can construct a set of properly symmetrized wavefunctions for the ground state manifold by taking direct products of four basis states for the valence band hole symmetry with four basis states for the internal nuclear motion to obtain 16 total states. Reduction of this 16-fold basis by standard group theoretical techniques leads

to a decomposition into irreducible representations consisting of two Kramers doublets of symmetries Γ_6 and Γ_7, plus three quartets having Γ_8 symmetry. This simplest possible state of full tetrahedral symmetry then leads to a manifold of states having the proper pair of doublets required by piezospectroscopic studies of the impurity complexes. However, it does not immediately explain the observed interconversion of acceptor species in the three novel line series of chapter 5.

The next more complicated model possible for internal symmetry would be one having six degenerate orientations for the direction to the tunnelling atom, giving rise to 24 states in the ground state manifold of which four are Kramers doublets. This is precisely the case expected for a diatomic impurity complex in which both atoms are of nearly equal size and neither is as small as a hydrogen atom. In such a system the atoms exist in a diatomic dumbell arrangement in which stearic hindrance and bond stiffness would be expected to prevent either atom from orienting in a lattice bonding direction. The least hindered configuration would be along a ⟨100⟩ axis for which the atoms fall exactly between two bonding directions. This is the proposed model for the substitutional configuration of the novel centers of chapter 5, as is shown in Figure 27. This configuration for a carbon-nitrogen dumbell results in a reduced mass of

6.5 amu which is little more than that of lithium, a known tunnelling species. If such a C-N impurity were able to tunnel between the six equivalent positions, the symmetries of the ground state manifold levels for $A_{3,5}$ can be easily explained. The assignment of particular doublet irreducible representation symmetries may become possible by examining the difference between transition strengths of the C-line transitions from each of the two ground states, which may be only partially allowed for one of the doublets since states of Γ_7 symmetry do not connect to the accidentally degenerate doublet portion of the C-line final state by first-order dipole matrix elements. Note especially that in the case of a six-fold orientational degeneracy, two each of the Γ_6 and the Γ_7 symmetry states exist in the manifold. Thus, unlike for tunnelling-hydrogen centers, the two observed ground-state doublets may both have the same symmetry.

6.3 Agreement of Theory and Experiment

The models put forth in Figures 27 and 28 and the previous chapter can very readily explain the piezospectroscopic data. These spectra require only that two states exist in the ground state manifold which are Kramers doublets and have full tetrahedral symmetry (i.e. either Γ_6 or Γ_7 irreducible representations). The spectra do not in any way indicate the presence of additional

states, and give only a lower limit of about 2-3 meV for the energy difference to the next lowest lying unseen state. This is not at all to say that such states cannot exist for these complex impurity centers, only that they are higher-lying. It is one of the shortcomings of any purely group-theoretical analysis that the ordering of states in energy cannot be predicted, so that we cannot say whether the doublet states or the quartets are a priori lower lying. We know only that the states actually observed as the lowest lying are compatable with the model in terms of allowed symmetries and degeneracies of states. In fact, for a six-fold orientational symmetry such as that proposed in section 6.2, there are actually four doublets in the manifold, any of which could possibly be the observed doublet states. We cannot distinguish at this point between seeing two states of Γ_6 symmetry, two states of Γ_7 symmetry, or one of each.

The A_4 center, on the other hand, is made up of a ground state with the Γ_8 quartet symmetry of the normal substitutional elemental acceptor. The model proposed in Figure 28 is not a substitutional center at all, but rather an interstitial center which sees the full tetrahedral symmetry of the surrounding Ge lattice. If this center is also of the tunnelling or rotationally reorientable type, then the extra orientational degree of freedom will provide

a complete manifold of states for the (1s) hydrogenic envelope function. It must then be the case for this one center that the absolute ground state is a quartet. This has never been the case in the past for any acceptor complex which has been successfully modelled. In defense of the unusual case presented here, it is also true that no previous complex has been interstitially coordinated, which may be reason enough to expect a different ordering of the states in the manifold. Once again the proposed model does not contradict any of the experimental findings, and in fact seems to be the only model which accounts for not only the piezospectroscopy but also the interconversion kinetics described in the next section. Additionally, diffusion data and carbon-14 radiotracer experiments concerning cyanide in Ge can only be explained by a very rapidly diffusing species, such as an interstitial diffuser. This center is thus the first known interstitial acceptor which not only diffuses interstitially, as does copper, but also remains interstitially in an electrically active form, which copper does not. It is therefore, if properly modelled, a never-before-seen variety of acceptor in an elemental semiconductor.

It is our hope that the same type of center can be created in Si by diffusion of cyanide from an external source in a manner similar to that done in Ge. If this were

to occur as predicted here, the new center would then be the first such interstitial acceptor in Si. Because of the higher melting point of the silicon lattice, it is unclear whether or not such a center can be formed at accessible temperatures, without risk of contamination from other fast diffusing impurities such as the noble metals. It should be pointed out, however, that cyanide solutions have long been used as a "rinse" for conditioning a sample of semiconductor material in order to avoid copper contamination during diffusions (Evwaraye, Hall, and Soltys, 1979). The utility of a solution of this type has been demonstrated in these diffusion experiments, as copper has never become a problem, even at 600°C for 24 hours. The explanation may be that the cyanide ion attaches to the copper (or other metal) forming an insoluble or slowly-diffusing metallic cyanide compound, and can in fact act as a getter for copper already in the lattice by diffusing to it quickly and forming an electrically inactive complex. Since the term "solubility" on the scales considered here (one part in 10^{12}) is not very meaningful, and since interstitial impurity diffusion is highly charge-state dependent (Barraf, Schluter, and Allan, 1982), in all likelihood the cyanide complex is simply a more slowly diffusing (vacancy assisted) species or one which is heavily favored at equilibrium over separation of the cyanide and copper as ions.

6.4 Analysis of Interconversion Kinetics

One of the most interesting and difficult to explain features of the experimental data regarding the three novel line series is the way in which one center can be totally eliminated (at least 100:1 S/N ratio) in favor of the other, or vice versa (again over 100:1 ratio). The extreme steepness of the equilibrium concentration curve as a function of temperature cannot be explained by a two-state system unless one state has a huge degeneracy, such as occurs with a species in a continuum. Thus the interstitial model for one of the centers of this novel impurity group is essential. This is the only mechanism, within the other constraints of the data, which can produce a state of the proper degree of freedom by interstitial motion.

The rates of interconversion between the two complex impurity sites are consistent with an activation energy of approximately 0.7-1.0 eV, as determined from an Arrhenius plot of rate vs. inverse temperature (Figure 26). The rates were obtained from exponential fits to a series of experimental curves at a given annealing temperature as a function of time (Figures 24 and 25). The only two free parameters for such a many-point fit were the time constant and the long-time asymptotic equilibrium concentration. These fits were made over time scales of from several minutes for temperatures of the order of 150°C up to several

years for room temperature. While the Arrhenius plot is not a precise straight line fit, the tendency is clearly seen. An activation energy of this order is consistent with the model given for the two sites for a CN group, in that this conversion requires only the breaking of two of the pi-bonds of the triple C-N bond of the interstitial form, with formation of four Ge-cyanide bonds for the substitutional form. This electronic rearrangement is performed in the highly polarizable ($\varepsilon \simeq 16$) Ge lattice in passing from a tetrahedral hollow site (void of the diamond lattice) to a substitutional site. Notice that since chemical bonds are both made and broken, the final state energy is not vastly different from the initial state, on a scale of electron volts. This is an extremely unique aspect of the diatomic impurity complex, totally unlike a single atomic center, that enables both substitutionally bonded and interstitial internally bonded configurations to have comparable energies. In both cases the one additional electron required to form the fourth bond is taken from the lattice and is rather deeply bound at the CN site, leaving a singly-charged screened coulomb potential for formation of a shallow acceptor. It may be the case that the CN group remains ionic during the interconversion process between different sites, or it may change charge states during diffusion to a vacancy.

Although the kinetics of this interconversion do yield some interesting information relating the two types of CN sites, the equilibrium concentrations obtained as a function of temperature yield the most insight into the nature of the two sites. It is not possible to explain the total interconversion in both directions without relying on two such related sites. The fact that an equilibrium point is reached at any given temperature, and can be approached from either side, indicates a dynamic process in which centers continually interconvert at temperature-dependent rates. The degeneracy of the interstitial state causes ultimately lower free energy at the higher temperatures, but it is obvious from the data that the substitutional site is the lower total internal energy site, as it is the equilibrium state at low (room) temperatures. Any successful model of the entire system must account for the extreme temperature dependence of this equilibrium. It is not clear at the present time whether the interconversion proceeds by a vacancy-assisted process (very unlikely at the lower temperatures, even for such slow rates of conversion) or by a "kick-out" mechanism (creation of a Frenkel pair) in which the Ge atom becomes interstitial and possibly wanders away athermally. The latter mechanism would require a substantial amount of energy (several eV) to produce the pair, which could perhaps be provided by the unsaturated

bond of the interstitial cyanide. In this event, the substitutional singly-bonded C-N center would have only a small energy barrier to becoming interstitial by creating a vacancy (leaving its lattice site) since approximately 4 eV of energy is gained in formation of each of the additional Π-bonds within the cyanide ion. Note, however, that the very small size of the cyanide ion (interatomic C-N distance of only 1.1 A) as compared to the Ge-Ge covalent bond distance (2.2 A) or the lattice parameter (5.5 A) allows it to move relatively freely, as evidenced by the high diffusion constant explained in the previous chapter. This could enable it to find an interconversion site, which may in fact be a vacancy, via purely interstitial diffusion without requiring vacancy motion at all. This may be the best candidate for the microscopic mechanism of the interconversion process.

Chapter 7 -- Special Studies

Additional information has been obtained from special samples, using the PTIS technique, which does not belong to the class of data used in identifying new impurity complexes. It does however shed new light on some aspects of the physics of shallow levels in semiconductors and so will be included here in some detail. The first such information concerns the behavior of the line spectra (ground state to bound state transitions), and in particular a component of the C-line of acceptors in Ge, under the application of strong magnetic fields of up to ≃50 kG. This behavior is unique in that it allows the tunability with field of the position of a very strong photon absorption line over a moderately wide range in the far-infrared. The second piece of new and exciting information relates to the discovery of many additional positively-charged acceptor centers (denoted A^+) in Ge and Si doped intentionally with acceptors. Proof as to the nature of these centers will be discussed for the case of the beryllium acceptor, but many more such new centers will be enumerated.

7.1 Magnetic Field Dependences

PTIS has been performed on ultra-pure Ge samples in the Faraday configuration under magnetic fields at strengths of up to 50 kG. It was discovered that the very large transverse magnetoresistance for such pure samples, with their inherent very high mobility and long scattering times, caused extreme signal to noise degradation at field strengths above ≈20 kG. The problem occurs because the sample conductivity is usually measured transversely to the direction of light propagation (which for this series of experiments was parallel to the magnetic field) and the very low conductivities caused a severe decrease in the strength of the available PTIS signal. This appears to have been the limiting factor in previous studies (Broecx et al, 1979) of this type, in addition to the ever-present problem of producing current-injecting contacts with low energy barriers at cryogenic temperatures. We solved both of these problems at once by creating samples with optically thin ion-implanted boron contacts for p-type Ge studies. These degenerately-doped contacts provided excellent carrier (hole) injection and extraction at 4.2 K, and in addition allowed us to utilize a sample geometry in which the hole-current flow was parallel to the applied magnetic field. For the Faraday geometry, k parallel to B, this requires the light propagation to be along the direction of

current flow, and thus photons must pass through the contact to enter the sample. Only a transparent contact (depth of the boron implant was 0.06 micron) suffices, allowing increased signal to noise due to the much lower longitudinal than transverse magnetoresistance of the sample.

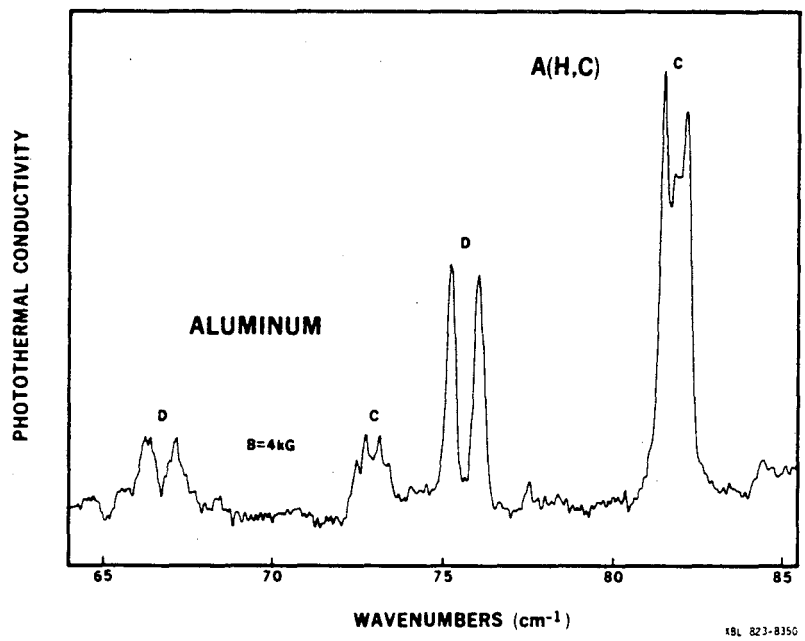

Figure 29 -- Magnetospectroscopy of Al and A(H,C)

Spectroscopy was performed on samples containing mainly aluminum, or aluminum plus A(H,C) centers in comparable concentrations (Figure 29). In both cases it was found that with the available field strength and instrumental resolution it was not possible to resolve completely the splitting of the ground state. It has been shown by magneto-acoustic resonance attenuation measurements (Tokumoto and Ishiguro, 1977) that the ground state

g-factors are significantly smaller than those of the p-like excited states to which the optical transitions occur. In fact, although the components of the excited states were well resolved for the fields applied, only two components for the aluminum ground state quartet were resolved (Figure 30), making it impossible to discern a difference between such a quartet of states and the theoretical prediction of doublet states for the model of the A(H,C) center. In order to achieve such a differentiation of the two types of states, higher field strengths and/or higher resolution are necessary, and are indeed feasible with these sample contacts as the signal to noise ratio was still very good at the highest available field strength.

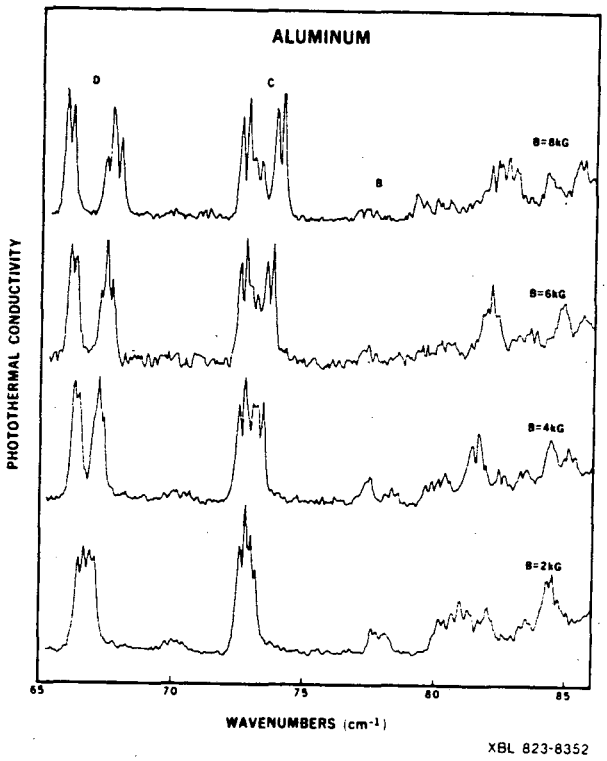

Figure 30 -- Zeeman Splitting of Al D and C Lines

However, additional information as to the behavior of the line spectrum of aluminum was obtained at the higher fields available with these superior sample contacts, compared to previous data. The foremost experimental fact is the large energy dependence of one of the components of the C-line, which shifts linearly with magnetic field and incorporates most of the strength of this multi-component transition. It is therefore a very strong field-tunable absorption line, which could in principle also be used as an emission line if properly optically pumped. This would provide a tunable narrow-band source of far-infrared

radiation over a spectral range from 73 to well over 100 cm^{-1} if the equivalent A(H,C) line is also used (Figure 31).

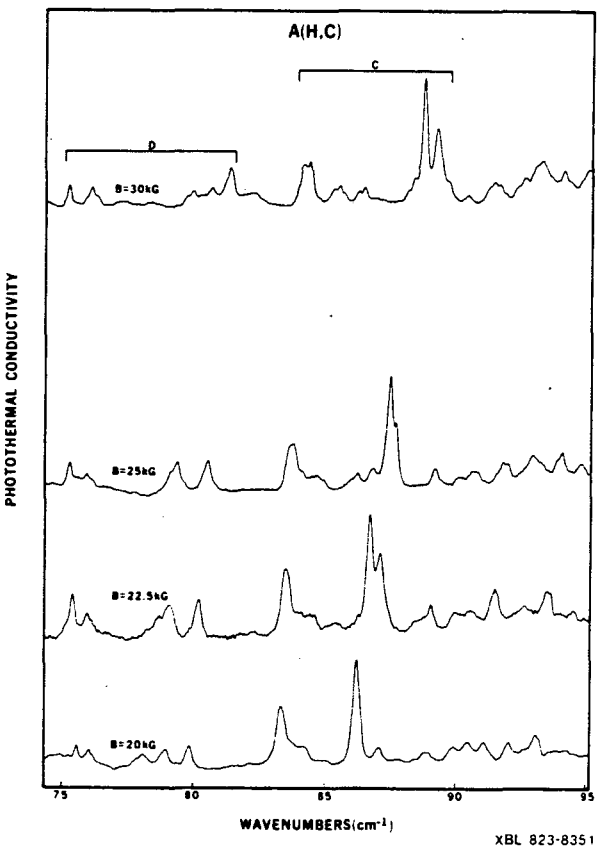

Figure 31 -- Field Dependence of C Line Component

One of the more interesting aspects of the behavior of this line is its "crossing" of other lines in the spectrum. As the field strength is varied, the transition energy for this particular strong transition, which has a much larger field dependence than any of the other transition lines, approaches that of another line of the same symmetry. The

two lines mix, increasing the strength of the weaker one at the expense of the "crossing" line. At still higher fields as the lines separate, a weak line is left at the position of the original weak line, while a very strong line continues shifting linearly with field strength to higher energies (Figure 32). This phenomenon points out the transitions with the same overall symmetry under applied field as the strong component of the C-line of the spectrum, and is a very clear physical example of the phenomenon of mixing of states of the same symmetry.

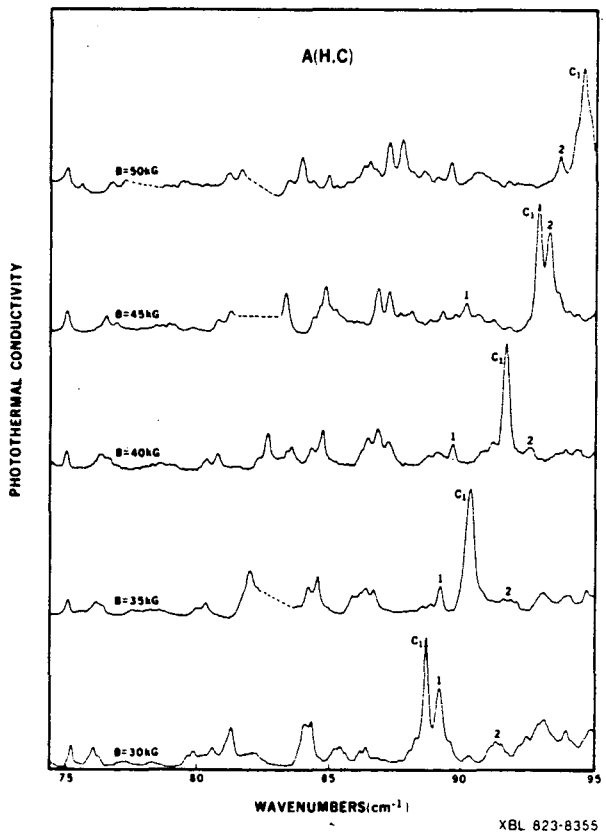

Figure 32 -- Crossing of Lines of the Same Symmetry

7.2 Ge:Be Spectroscopy

Samples were prepared for PTIS measurements from several Ge single crystals which were grown from Be-doped melts by N.M. Haegel and W.M. Hansen. These crystals contain Be doping ranging from 10^{14} to $5x10^{15}$ cm^{-3} and with residual background aluminum impurity concentrations of the order of 10^{11-12} cm^{-3}. Because of the strong oxidation strength of Be (which will reduce silica at the crystal growth temperatures), these crystals were grown under vacuum from a melt contained directly in the carbon susceptor. They are therefore very low in both oxygen and hydrogen concentrations. As a result we do not expect to be able to generate a hydrogen-related impurity complex center with Be in such a crystal, although such centers have been found in specially-produced crystals discussed in section 7.5. However, these samples provide the best possibility for high resolution spectroscopy of the Be double acceptor helium-like ground to excited state transitions (Cross et al, 1983) due to their excellent crystallography and moderate doping levels and compensation. This prevents broadening of the lines from inhomogeneous stress, impurity overlap, or Stark effect due to ionized centers. In the above referenced work the resolution was sufficient to show additional structure on the spectral lines, presumably due to a ground state splitting.

At intermediate cryogenic temperatures (8-10 K) photothermal ionization spectra of both the Be and the residual Al impurities were obtained simultaneously in the same sample. Surprisingly, the Be lines were relatively broad compared to normal high-resolution acceptor lines, which could have been due to excited state overlap even though the ground states should not be large enough to overlap at these concentrations. However, the aluminum line series, due to Al atoms distributed throughout the same bulk sample as the Be atoms, were extremely sharp, comparable to those of Al in ultra-pure Ge samples, with only a very slight inhomogeneous stress broadening (Figure 33). Since both Al and Be (and all other hydrogenic acceptors) have the same excited state wave functions, it is highly unlikely that excited state overlap is responsible for the broadening of the Be spectral lines without affecting the Al lines. One possible explanation for the Be broadening is the resonant transfer of excitation (virtual photon or polariton) between neighboring Be impurities at these moderately high impurity concentrations. Such a transfer does not couple the Be lines to the Al lines, nor do the Al centers couple to one another at the relatively low concentrations at which they exist. The result is a selective broadening of only the Be transition energies.

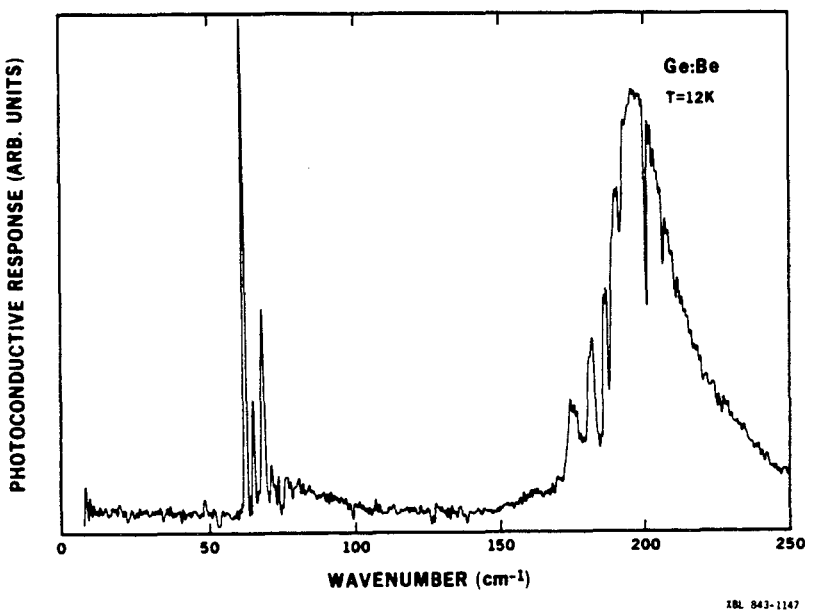

Figure 33 -- Ge:Al,Be PTIS Lines

An even more novel effect has been observed in these samples, for which both Be and Al spectra coexist. At low enough temperatures (below 6 K) the line series of the Be acceptors appear as absorptions in the continuum of the Al spectrum (Figure 34). As the temperature is increased the spectral lines of Be begin to change sign, indicating emission of a free hole which adds to the photothermal conductivity rather than absorption of holes (or the photons creating them) from the Al continuum. This effect has not, as far as we know, been observed before and is unusual in the sense of the Al acting as an internal photoconductor within the bulk of the same crystal in which the Be absorbers exist. The mechanism for such an absorption from

the Al continuum would have to include a non-radiative decay from the Be excited state to its ground state in order to reduce the flux of photons at the given transition energy (i.e., as in normal absorption spectroscopy). Again a resonant transfer of energy to a Be atom in its ground state, promoting it to a discrete excited state, could be involved; the difference here is that the initial excitation occurs in the Al atom and is a ground state to free state transition, one which in the absence of Be would contribute to the free hole conduction of the sample.

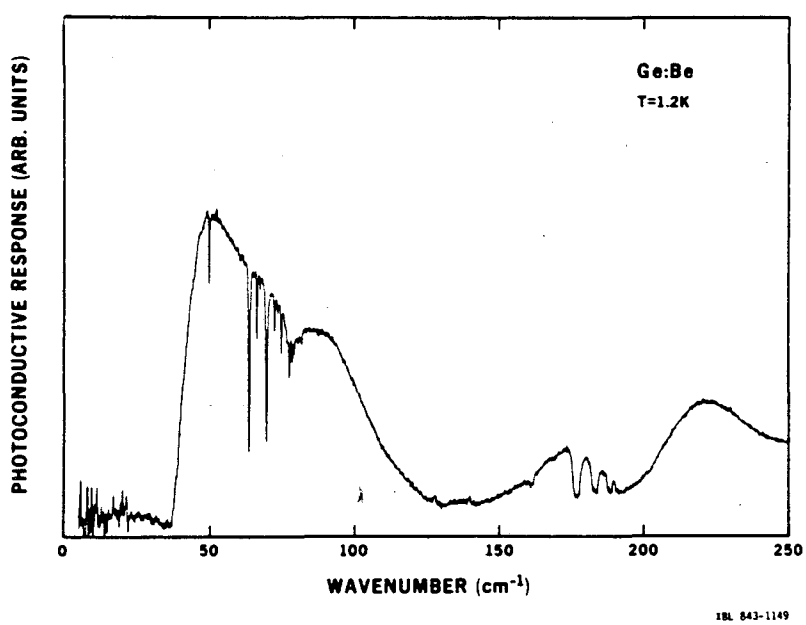

Figure 34 -- Be Absorption Lines in Ge:Al Continuum

An additional point worthy of mention here is the fact that the continuum peaks of both the Al and Be spectra are of approximately the same height, even though their

concentrations in the sample differ by at least three orders of magnitude. This is a manifestation of the fact that the matrix elements for the photon absorption depend on the overlap in k-space (near vertical photon transitions) of the ground states with the continuum final states. The shallow level (aluminum) ground state wave function is very large in real space, and so has a very small k-space extent. For the ground state 1s-like hydrogenic wave function with Bohr radius "a", in the spherical approximation and neglecting the valence band symmetry, the Fourier transformation of the wave function is:

$$\Psi(k) = (\pi a^3)^{-1/2}\int \exp(i\vec{k}\cdot\vec{r})\exp(-r/a)d^3\vec{r} = 8(a^3/\pi)^{1/2}(1+a^2k^2)^{-2}.$$

Since photon transitions are essentially vertical in k-space, the overlap integral with the parabolic band bottom is large, due to the large probability density near k=0. However, for the deeper levels, such as Be, the spatial extent "a" is small, leading to a broad k-space extent with low maximum probability density (that is, the probability is spread over a larger volume of k-space). This yields a smaller overlap integral with the top of the valence band, and so a smaller absorption cross section near the photoconductivity edge. This phenomenon also occurs for the ground state to bound excited state transitions, leading to smaller line strengths relative to the continuum strength for the deeper levels due to decreased overlap with the

excited states, which have the same spacial extent for both deep and shallow acceptors.

A calculation that is less hand-waving, although still an approximation, for the absorption transition rate for a hydrogenic atom in the (1s) state is given by Schiff (1968, section 35). Plane wave final state wave functions are used rather than true hydrogen continuum states, but the qualitative aspects of the solution are still correct. The transition rate as a function of k depends upon the Bohr radius "a" of the atom according to:

$$\omega \propto a^7/(1+k^2a^2)^6 \ .$$

At small k, near the band bottom for a semiconductor hydrogenic impurity, the overall height of the continuum absorption then scales as a^7, which indicates that a factor of only two in effective Bohr radius will produce more than two orders of magnitude of change in the relative continuum heights for the same concentrations of impurites. The integrated cross section over all k (proportional to the transition rate divided by photon energy for a given light intensity) is then approximately of order a^8. This is an extremely strong dependence on the size of the ground state orbit.

A more rigorous calculation, performed by Edwards and Fowler (1977), in which the 1/r dependence for true hydrogen continuum (scattering) states is used, gives a much more

exact fit to the experimentally observed shape of the absorption continuum. However, it is not as transparent from the form of their solutions that the height of the absorption scales with Bohr radius in the manner shown above. It is evident from the fact that agreement with experiment was reached only after allowing the charge and Bohr radius at small distances to differ from the free (screened) charge of the impurity, that there is indeed a large dependence on the central cell correction (or on the effective Bohr radius of the ground state) of the continuum strength.

7.3 A^+ Centers: Experimental

In the course of performing spectroscopy of Be-doped germanium samples, an unusual feature of the spectrum was noticed. It was highly temperature and filter dependent, and appeared to be a photoconductive continuum without line structure, but with an energy onset of only 40 cm^{-1} (5 meV). This was the shallowest continuum measured for an acceptor in Ge, and was even lower in energy than Ga under the maximum physically allowable uniaxial stress (before shattering the crystal). If such a spectrum were due to a shallow single acceptor it would be the shallowest ever discovered in Ge, and would be expected to have a significant thermal ionization at a temperature of 4.2 K.

The center responsible for this continuum was certainly related to the presence of Be in the sample, and was not correlated with the underlying Al concentration, as demonstrated by spectroscopy of samples taken from different crystals with different impurity concentrations.

Spectroscopy at pumped liquid helium temperatures (down to 1.2 K for normal ^{4}He at pressures below 1 torr) revealed that the continuum peak height increased substantially at lower temperatures. This confirmed the thermal ionization assumption postulated above for such a shallow level. At low temperatures the peak of the continuum is actually higher than that of the shallow levels Al and B. Additionally, below temperatures of 3-4 K the bound-state transition lines of B and Al, which all require at least 8 meV of photon energy, appear as absorption lines from the shallow 5 meV continuum (Figure 35). This phenomenon is analogous to the Be absorption lines from the shallow single acceptor continuum spectra. However, the absorption is exceptionally strong, as much as 50% for a sample of only 4 mm thickness, even though the absolute concentration of shallow levels is known to be only approximately 10^{11} cm^{-3}.

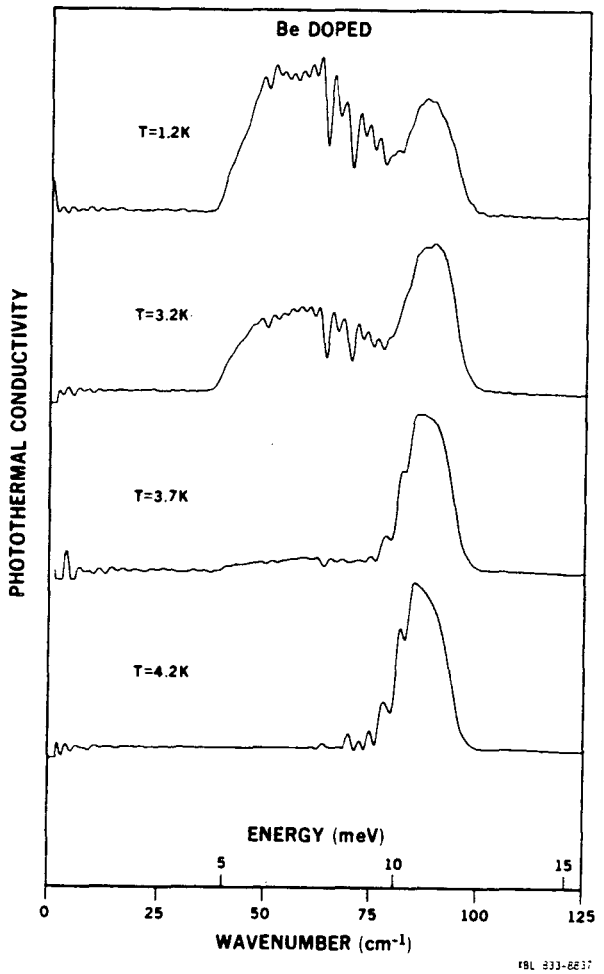

Figure 35 -- Ge:B,Al Absorption Lines in the Continuum

In order to understand the nature of the experimentally observed phenomena, a series of experiments were performed in which the temperature, sample compensation, and far-infrared filter cut-off frequency were changed. The response of the new shallow continuum was found to be eliminated by a filter cut-off frequency above the 5 meV onset but below the shallow acceptor ionization energies of B and Al. This is a strong indication of a center which

requires optical pumping of neutral shallow acceptors to produce free holes, in order to maintain a finite equilibrium concentration. Experimental evidence for Be-doped samples indicates that the pumping may be either from shallow levels Al and B or from the deeper Be centers, only requiring the presence of free holes to create this new acceptor continuum. Spectroscopy of samples compensated with Li (Figure 36) at concentrations above the shallow residual impurity concentration demonstrates that these shallow centers are not necessary for the production of the new continuum if free holes are generated from Be acceptors. However, for these samples the use of a filter with cut-off frequency below the Be ionization energy surpresses the generation of free holes and clearly eliminates the new center. All of this spectroscopic information points to an impurity center formed by the binding of a free hole to a neutral Be center, which exists in large concentrations in low-compensation samples. This produces a double acceptor with an extra positive charge (denoted as Be^+). Such a center would be expected to have, in analogy to the H^- atom, a very much reduced ionization energy for the extra hole. A further point is the question of whether or not bound excited states for such a system should exist. We have no experimental evidence for the existance of bound states.

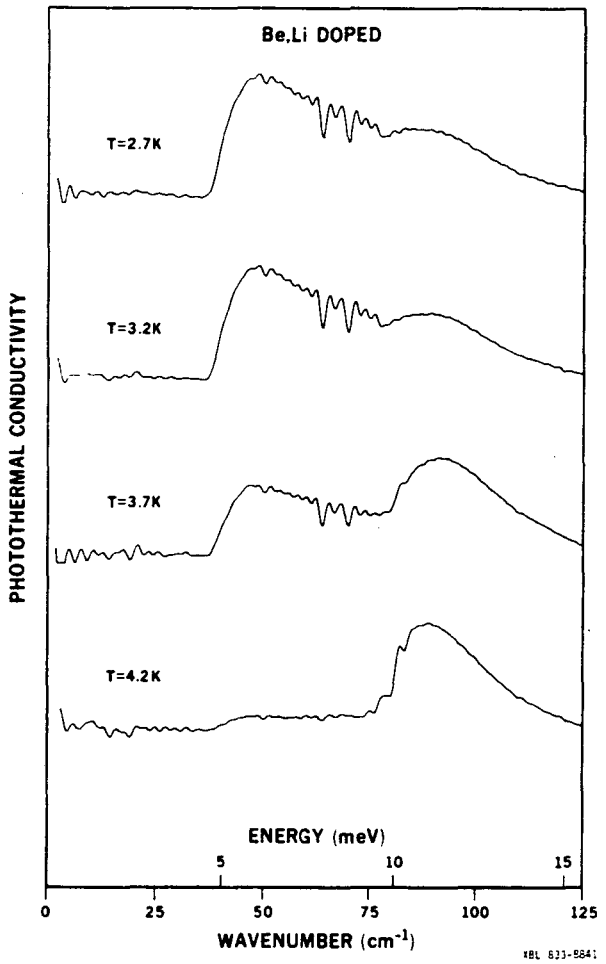

Figure 36 -- Li Compensated Ge:Be Spectra

The binding mechanism for such an impurity center will be discussed theoretically in the next section, but it is important to point out here that there are three holes weakly bound to a single substitutional Be atom in the lattice which give rise to this new shallow continuum. This is an entirely new phenomenon, never before reported for any hydrogenic system. It is not at all the same phenomenon as the binding of multiple bound excitons to a charged

impurity, which instead involves both holes and electrons. In this positively charged multiple acceptor, a neutral double acceptor (Be) binds a third hole to create a hydrogenic state of occupation $(1s)^3$. This is possible for hole states in an elemental semiconductor where the valence band has $p_{3/2}$ symmetry, with the holes behaving as fermions with 3/2-spin, having four possible magnetic quantum numbers (spin projections). However, the degeneracy of such a state can be broken by application of an external uniaxial stress. In general, the four-fold degeneracy splits into two Kramers doubly degenerate states, one at slightly lowered energy and one slightly elevated. When the stress is sufficiently strong, the energy splitting will become more than the small binding energy for the third hole, and as a result it will no longer be bound. This is indeed experimentally observed (Figure 37), wherein a moderate uniaxial stress along the ⟨111⟩ axis causes the Be^+ acceptor to vanish.

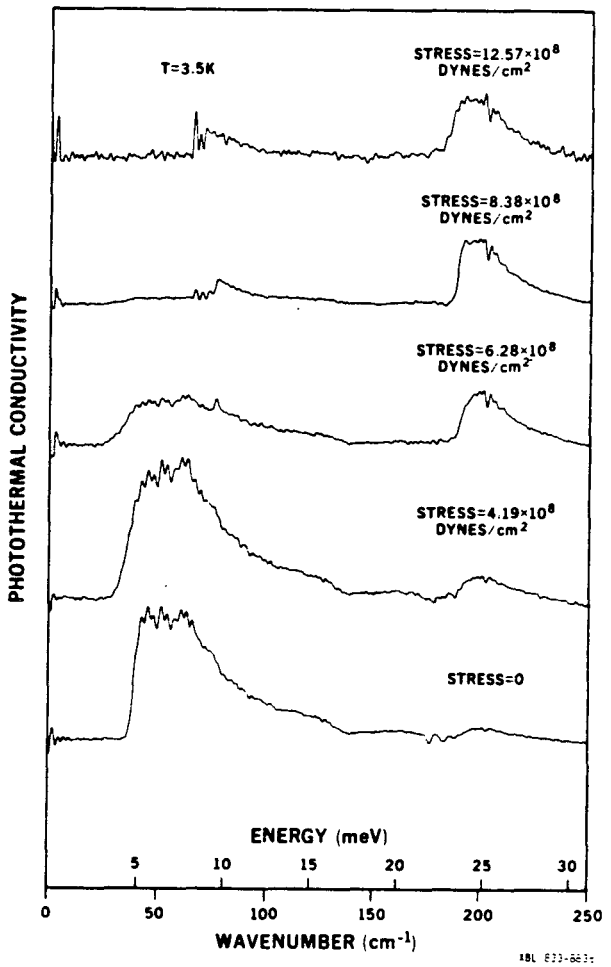

Figure 37 -- Stress Removal of Acceptor-plus Centers

In addition to the Be^+ centers already discussed, many other substitutional acceptors in elemental semiconductors exhibit the formation of A^+. In fact, all acceptors measured showed this behavior. A listing of the various group II and the group I Cu impurities, with both experimentally measured and theoretically fit values of ionization energies, is given in Table 2. This table contains only the multiple-acceptor impurities for which the

$(1s)^{3 \text{ or } 4}$ model discussed in the next section applies. Several group III acceptor-plus centers have also been measured, including Ge:Ga, Si:B, and Si:In. These states are analogous to the H^- atom and have the $(1s)^2$ configuration.

Acceptor	$E(A^+)$		$E(A^\circ)$	$E(A^-)$	
	Exp	Theory	Exp=Theory	Exp	Theory
Be	5.1	3.4	24.81	58.02	56.07
Zn	4.1	4.5	32.98	86.51	74.53
Mg	2.9	4.9	35.85	--	81.02
Mn	3.2	7.5	55	~100	124.3
Hg	12.2	12.6	91.88	~230	207.6
Cu	2.0	10.4	43.21	330	87.8

Table 2 -- Multiple Acceptor Plus Centers

7.4 A^+ Centers: Theory

A qualitative understanding of the behavior of positively-charged double acceptors such as Be^+ can be obtained from the hydrogenic model, in which the number of identical particles allowed by the Pauli exclusion principle to occupy the same spatial state is determined by the particle's spin. For a hole at the top of the valence band, which has four-fold degeneracy, the particle acts as if it

had 3/2-spin, with four possible projections. This means that in principle up to four such valence band holes could occupy the identical ground state spatial wave function, which must then be taken as a totally symmetrized linear combination of particle states under the permutation of coordinates (Slater determinant). The additional holes bind to the impurity center if the total energy of the new state (with an extra hole) is lower than the total energy of the original state (without the extra hole). This fact leads us then quite naturally into a variational calculation to determine upper limits on the total energy of states of one to four holes, all in the (1s) hydrogenic envelope function, binding to a single charged impurity.

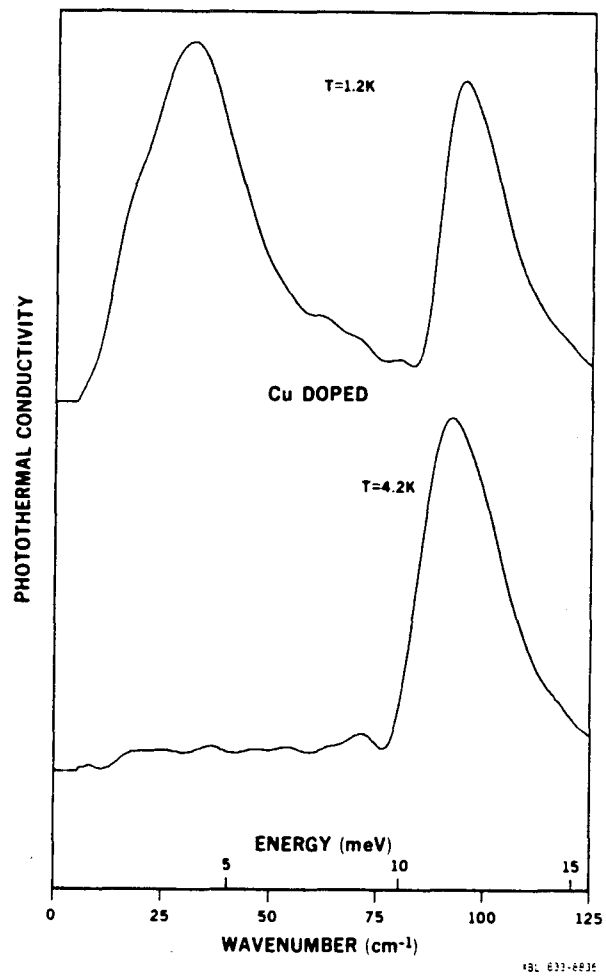

Figure 38 -- Ge:Cu-plus Center

The analogy to be made in the case of an extra hole bound to a single acceptor, such as Ga, is to a hydrogen atom with two electrons in the (1s) state, H^-. This system is also an analog of the negatively-charged donor systems (D^-) which can, like hydrogen, have at most two spin-1/2 electrons in the (1s) state. Many such D^- centers have been reported, particularly in Si, but results for A^+ centers are much less abundent. Also, the only A^+ centers reported were

due to two holes bound to a single acceptor (B in Si, Ga in Ge by Gershenzon et al, 1971). In these cases the more advanced model of allowing up to four holes to occupy the (1s) state was never proposed, as it was not needed. For the group II impurity centers, such as Be, Mg, Zn, and even Hg, which form substitutional double acceptors in Ge, and also for the group I impurities which form triple acceptors, such as Cu in Ge (shown in Figure 38), this new idea is crucial. All of these impurities have been found to exhibit the A^+ behavior, a discovery which was made in these photothermal ionization studies (McMurray, 1984; Haller et al, 1984). Additional group III centers of this type have also since been identified, although they do not require the four-fold degenerate spin statistics in order to exist. A comparison of three A^+ centers in Ge, formed from group I, II, and III acceptors, is shown in Figure 39.

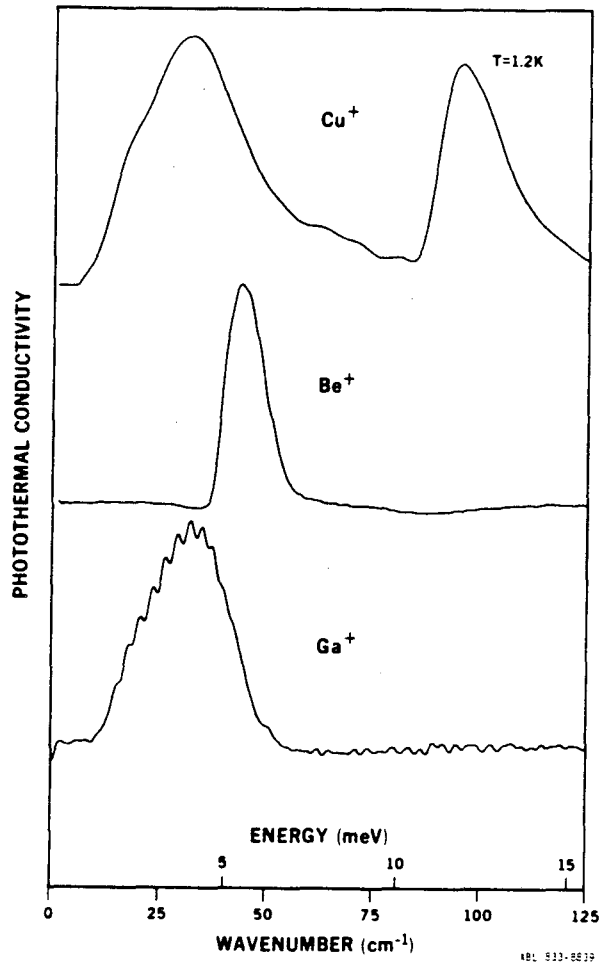

Figure 39 -- Comparison of Group I,II,III-plus Centers

A first-order approach to the variational calculation utilizes a symmetrized product wave function of single-particle states with the same screening parameter in the exponential of the (1s) wave function for all particles (an effective one-electron Coulomb charge in the presence of all other electrons). This approach works very well for the case of two particles bound to a doubly-charged nucleus, as in neutral He (Schiff, 1968, section 32). It does not,

however, lead to binding for the case of the over-charged atom H^-, which is known to exist in nature, or for the case of He^- with imaginary spin-3/2 electrons all in the (1s) spatial state, which is the case of interest for the Be^+ atomic analog. It is obvious that since a variational calculation gives only an upper bound for the total energy (the lowest possible energy is that of the eigenvalue obtained from the true eigenfunction), we must improve the variational wave function in order to more closely reproduce the true ground state.

The simplest improvement that can be made easily is to allow each of the single-particle wave functions to have a different screening parameter in the exponential. This allows more degrees of freedom in the many-particle variational calculations, and should produce a better ground state wave function and energy. For the three-particle case of He^-, the third particle is in fact bound, although by a very small energy. It can be seen in general (Table 3) that all of the singly-overcharged centers do bind by a small but definite amount. Improved calculations including angular correlations between the particles in a multi-particle wave function (Wu and Falicov, 1984) give a lower upper bound for the total energy, and thus a larger binding energy for the last particle. Monte-Carlo calculations, which do not give an upper bound but are accurate to within statistical errors

only (Kalia, Vashista and Lee, 1984), show only slight improvement over the Wu and Falicov method but allow for the possibility of energy calculation for virtually any form of impurity potential. This method may thus be useful in the future to calculate explicitly the central cell corrections due to different impurity atoms.

Energy	n=1	n=2	n=3	n=4
Z=1	0.500	0.514	-	-
Z=2	2.000	2.885	3.006	-
Z=3	4.500	7.259	8.617	8.945

Table 3 -- Variational Calculation of Energies (Hartrees)

7.5 Ge:Group II-Hydrogen Impurity Complex Acceptors

Two new hydrogen-related shallow acceptor centers have been discovered recently in germanium doped intentionally with group II impurities (McMurray et al, 1984). Specifically, in crystals grown in a hydrogen atmosphere from zinc-doped and beryllium-doped melts, the new centers denoted A(Zn,H) and A(Be,H) were discovered by PTIS. This was the result of an intentional search to find such hydrogen-related centers with group II impurities. Each of these complexes forms single acceptor levels with hydrogenic spacings of the excited states. Many of the properties of the tunnelling-hydrogen species of Figure 14 are shared by

these new centers, but there exists a fundamental difference in the behavior of the hydrogen atom in the complex. Although it is assumed to still provide an extra internal degree of freedom from nuclear motion, hydrogen no longer provides an empty electron orbital. In these two cases, and maybe others as well, the hydrogen gives up its electron, causing a shift from double acceptor to single acceptor of the group II atom. This requires that the electron energy levels of H are all above the Fermi level for electrons in the crystal. This is quite different from the previous cases, and is the reason for the reversal in the ordering of the two elements in the notation A(X,H).

Spectroscopy of the acceptor A(Be,H) is shown in Figure 40. It can be seen from these spectra that the beryllium-hydrogen center exhibits two series of lines, much like the cases of A(H,C) and A(H,Si). It is also seen, in the upper trace, that the strength of these line series, relative to the residual aluminum impurity concentration, decreases with high-temperature annealing (annealing performed by N.M. Haegel). This is presumably due to the break-up of some of the impurity complexes, which aquire sufficient thermal energy to overcome the binding force of the hydrogen to the beryllium. In Figure 41 it is further seen that the two series of lines exhibit a thermal population from one ground state in the manifold to the

other as the sample temperature is changed. This is again reminiscent of the previous acceptor complexes, and proves that both line series are due to a single center.

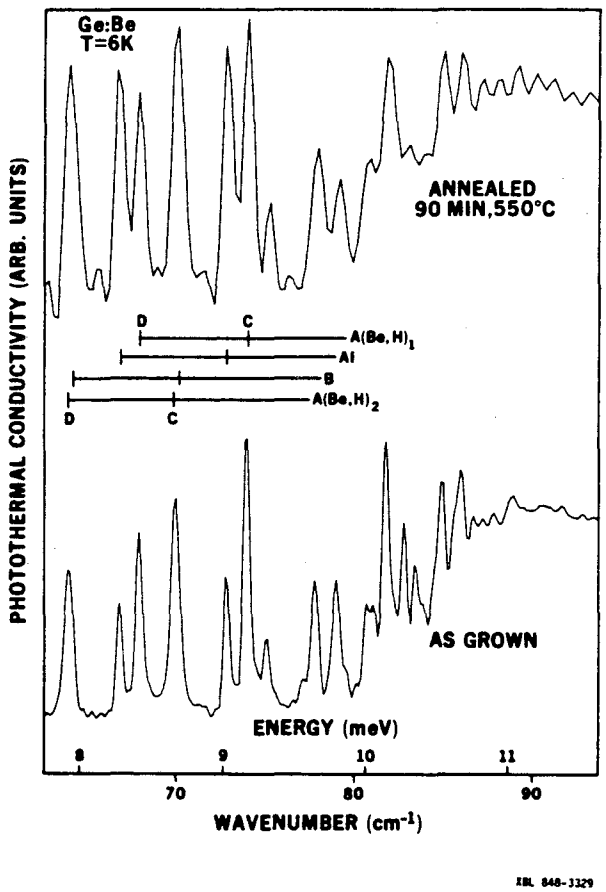

Figure 40 -- PTIS of A(Be,H)

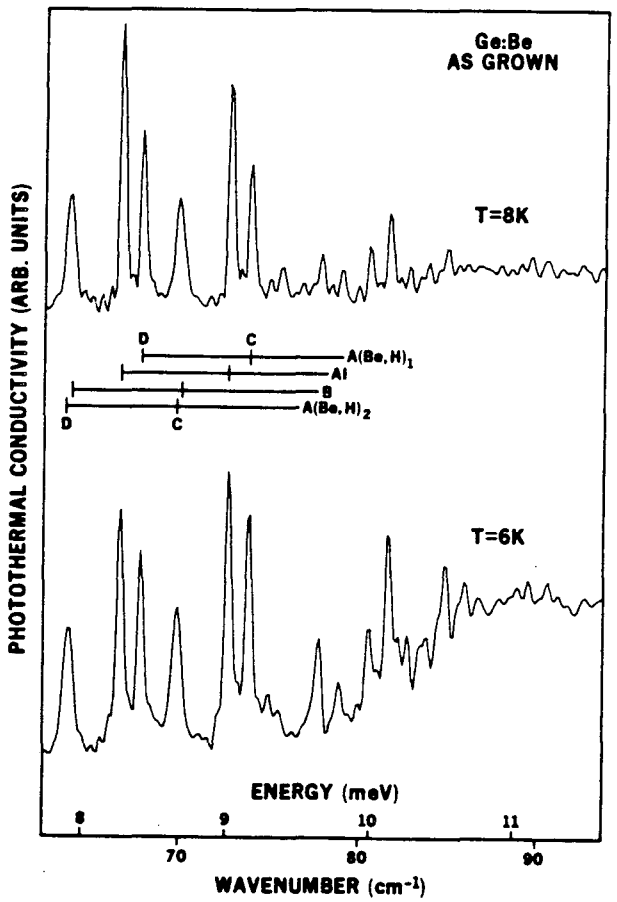

Figure 41 -- Thermal Population of A(Be,H)

Uniaxial stress was applied to a germanium sample containing the A(Be,H) centers, along an arbitrary stress axis (non-symmetry direction). For elemental substitutionals like aluminum, the spectral lines split with stress. However, for the lines of the two A(Be,H) series, only a minor broadening of the ground state at the higher stresses is observed (Figure 42). This again implies that the two line series are due to Kramers doublet states, as in

the previous cases. It is our assumption that a system similar to the ordinary tunnelling-hydrogen cases exists for these centers as well. The symmetry of the ground state manifold is that of at least two doublets with the full tetrahedral symmetry which exhibit thermal population. The average energy of the two ground-state manifold doublets is 11.04 meV, very much effective-mass like (similar to the elemental single acceptors).

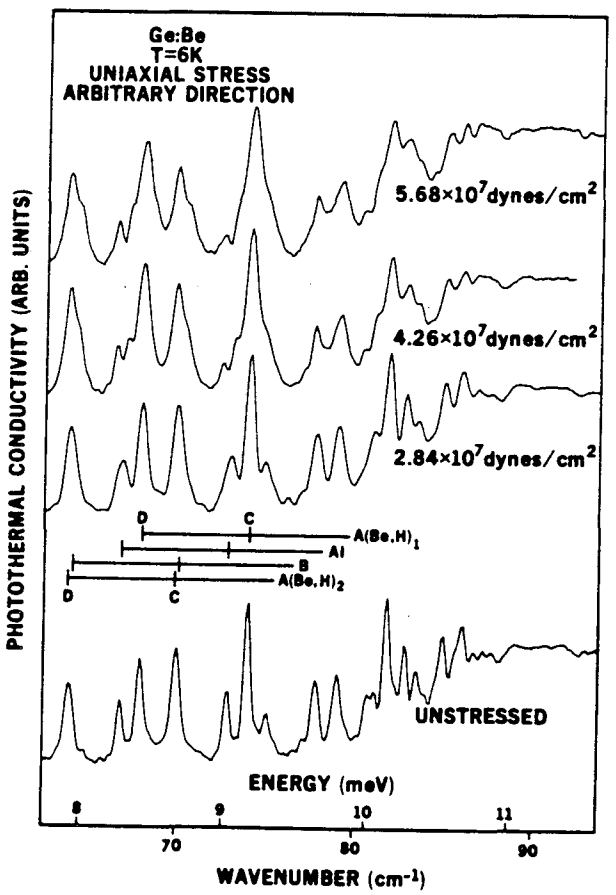

Figure 42 -- PTIS of Stressed Ge:A(Be,H)

A similar situation exists for the Zn-doped crystals, which display A(Zn,H) centers in the as-grown samples, as seen in Figure 43. This line series is also hydrogenic, but the ground state is substantially deeper in energy (ionization energy=12.53 meV) than effective mass theory predicts. This may be because there is a second energy level in the manifold that is substantially shallower than the effective mass energy (again by about 2 meV) so that the average of the two is in the 10-11 meV range. If such a state exists, it is not seen spectroscopically by thermal population, even at temperatures as high as 15 K. The upper trace of Figure 43 shows that the A(Zn,H) acceptor also disappears with thermal annealing, but that the times and temperatures required are substantially higher than for A(Be,H). This implies a larger binding energy of the hydrogen atom to the zinc than to the beryllium atom. This trend seems to continue as one moves to deeper acceptors. The copper-hydrogen complex is much more difficult to dissociate than Zn-H, as evidenced by the fact that at high annealing temperatures (700°C and above) copper contamination results in destruction of the Zn-H complex, but formation of A(Cu,H).

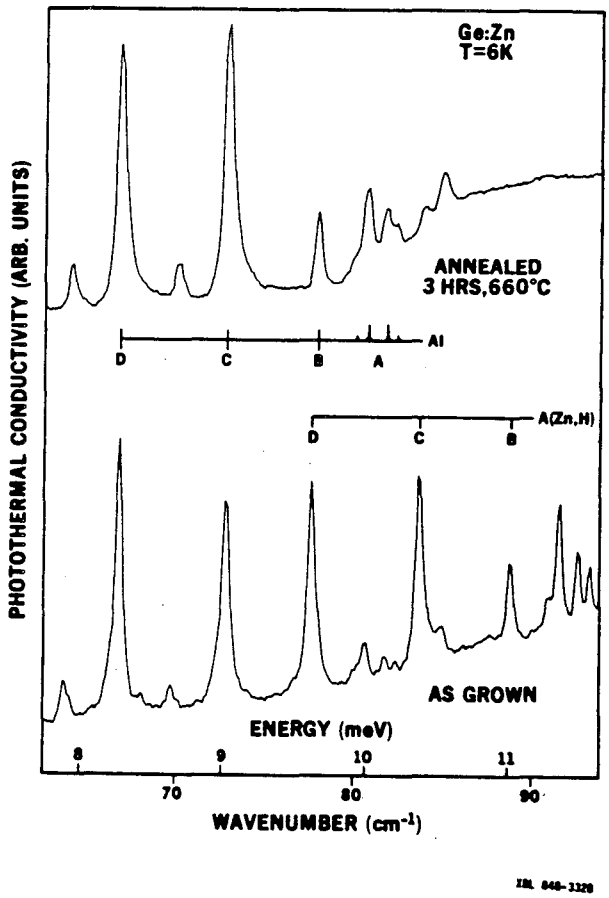

Figure 43 -- PTIS of A(Zn,H)

Figure 44 shows that the line series due to the zinc-hydrogen acceptor is again stress-insensitive for arbitrary uniaxial stress axis. Once again this means that the ground state is a Kramers doublet with full tetrahedral symmetry. This remains in accordance with the previous models, although the additional levels in the ground-state manifold are not seen.

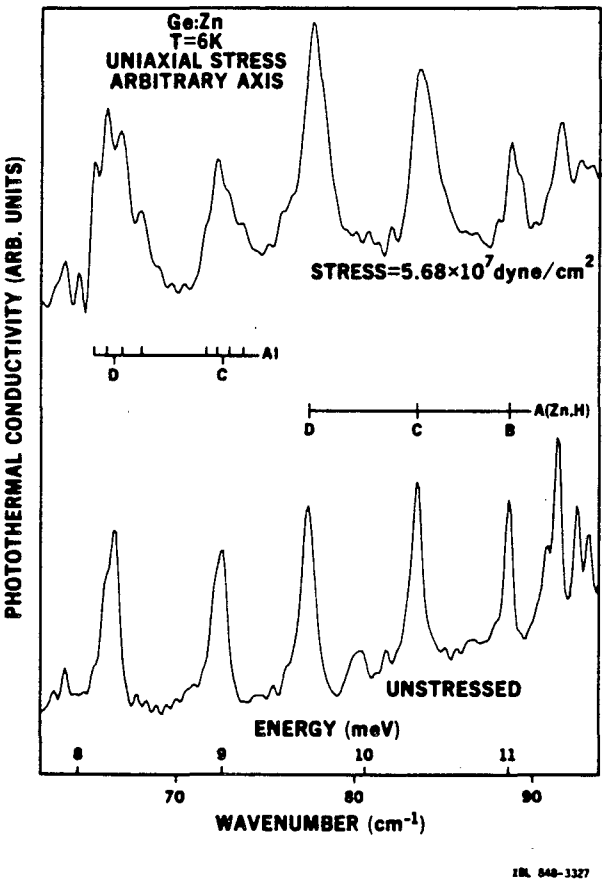

Figure 44 -- PTIS of Stressed A(Zn,H)

Isothermal annealing studies were performed by N.M. Haegel on the Zn-H center at two different temperatures, as shown in Figure 45. This study shows clearly that the rate of decay follows a simple first-order exponential process, giving the straight-line fits in the Arrhenius plot. From the slopes of the two lines at the two different annealing temperatures, an excitation energy for the A(Zn,H) dissociation of 3.0 eV can be obtained, with a rate prefactor of 3×10^{12} sec^{-1}. Variable-temperature Hall effect

measurements were made to verify that it was indeed the shallow Zn-H impurities that were disappearing with annealing, and results are shown in Figure 46. Note that after 3 hours at 659°C the sample shows over-compensation of the shallow acceptors by donors.

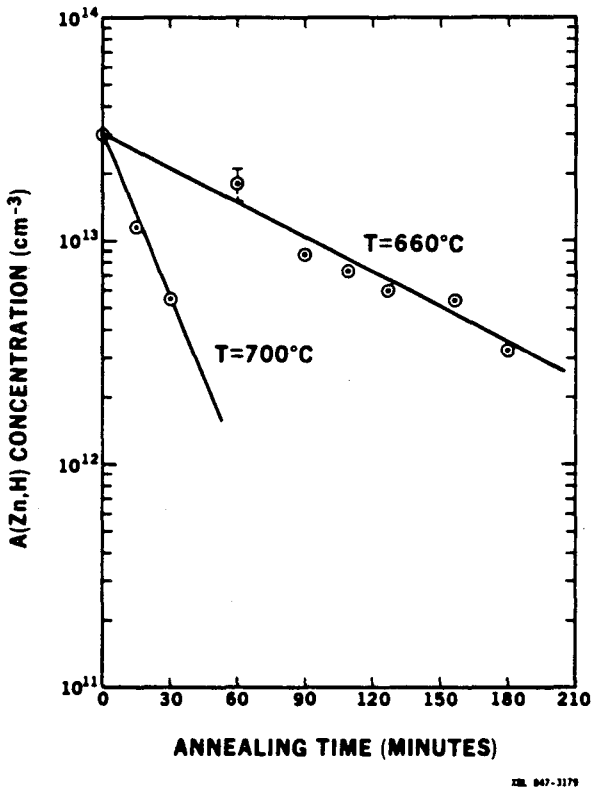

Figure 45 -- Isothermal Annealing of A(Zn,H)

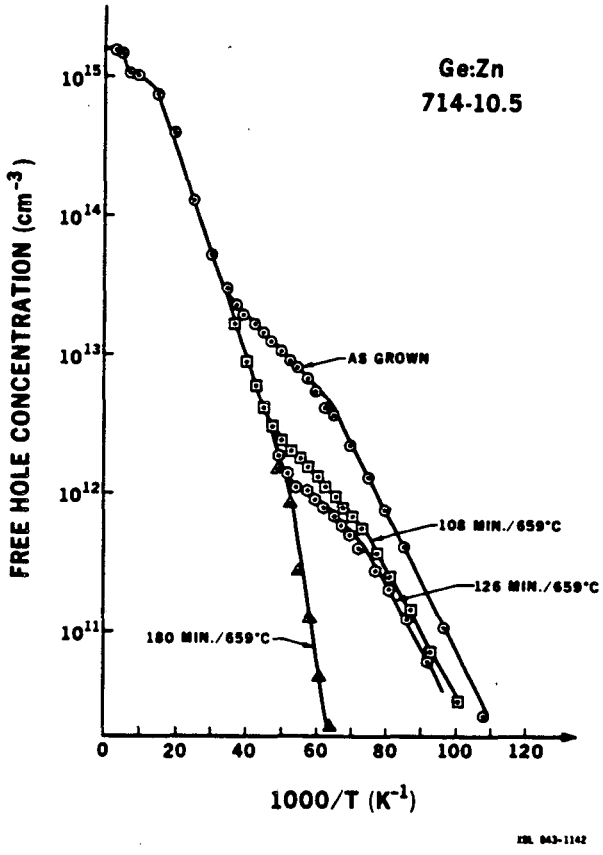

Figure 46 -- Variable-temperature Hall Effect of A(Zn,H)

7.6 Absorption Spectroscopy Using A^+ Photoconductors

Experiments with A^+ centers in Ge has lead to the use of samples containing such centers as photoconductors. This is advantageous because the photoresponse begins at much lower energies than with elemental dopants, as shown in Figure 47. It is therefore possible to obtain absorption lines from the bound-state transitions of the elemental shallow levels using such a photoconductor.

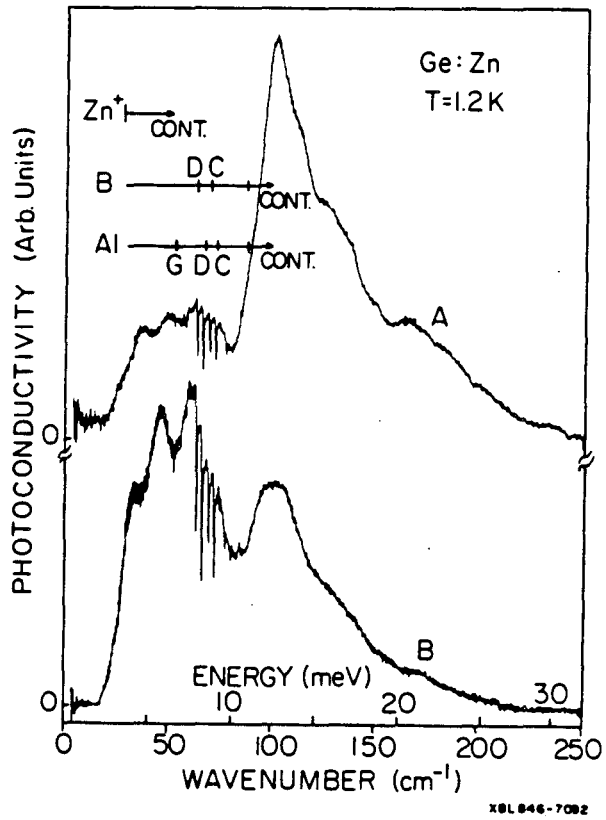

Figure 47 -- PTIS of Zn^+

It can be seen in the lower trace of Figure 47 that the Zn^+ center responds with a continuum strength larger than that of the residual boron and aluminum together when optically pumped by the blackbody radiation from a room-temperature filter. Even with a 4.2 K filter, there is significant pumping of the neutral Zn atoms to form free holes, necessary for the creation of the plus-center, as shown in the upper trace. In either case, the line spectrum due to the residual acceptors can be easily seen, even though they exist only in concentrations in the 10^{11} cm^{-3}

range. This was unexpected based on published values for absorption coefficients of shallow levels in semiconductors (Jones and Fisher, 1965). Initially, one might try to explain the discrepancy by some sort of resonance mechanism, as was mentioned in section 7.2. This phenomenon would have been of great interest if it would occur, but it seems that the explanation is simply the fact that the older published measurements were not performed at sufficiently high spectral resolution. The broadening of the lines due to the instrumental linewidth caused a non-linear correction to the published values of the absorption coefficient. It is thus actually possible to now measure samples with these low concentrations of impurities, even though it had been suggested in the past that orders of magnitude higher concentrations were required.

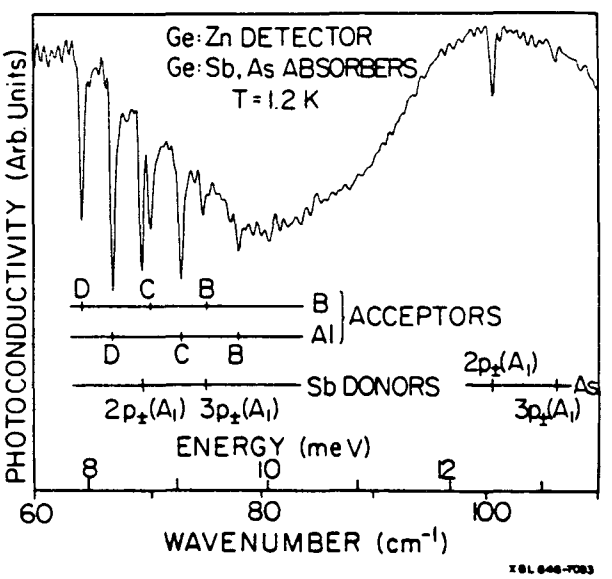

Figure 48 -- Absorption Spectrum of Ge:Sb,As

This fact is demonstrated quite clearly in the spectrum of Figure 48, in which the Zn-doped sample was used as a photoconductor for the measurement of the absorption spectrum of an external slice of Ge:Sb,As. The dopant concentrations in this transmission sample, as measured by Hall effect, were only [Sb]=1.6x10^{12} cm^{-3} and [As]=0.4x10^{12} cm^{-3}. As can be seen, the arsenic lines are easily detectable, causing roughly 10% absorptions in the continuum height for a slice of only four mm thick. The lower limit of detection would then appear to be an order of magnitude lower in concentration than this.

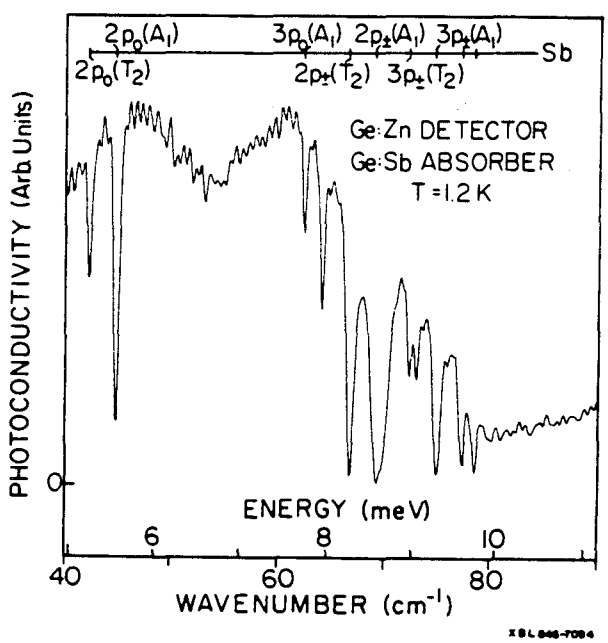

Figure 49 -- Absorption Spectrum of High Concentration Sb

Another absorption experiment was performed using the same photoconductor with a 1.2 mm thick sample of Ge doped

with [Sb]=3x10^{14} cm^{-3}. This concentration is similar to the ones used in the published absorption experiments (Jones and Fisher, 1965). It can be seen from the spectrum in Figure 49 that the absorption strength for several lines is so large that the transmittance is practically zero. This makes it extremely difficult to determine accurately a linear absorption coefficient for these lines, and in fact Figure 50 shows the calculated coefficient for all but the very strongest of the transition lines because of this problem. These spectra demonstrate that at high resolution it is best to perform such absorption experiments with more lightly-doped samples in order to remain in the linear region of the exponential absorption curve.

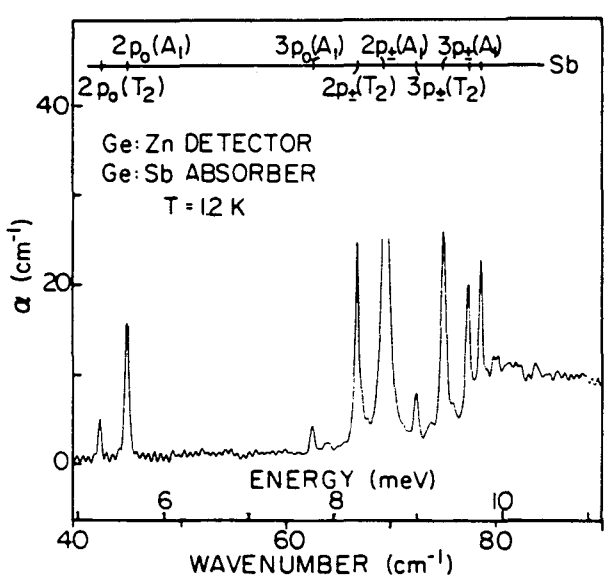

Figure 50 -- Linear Absorption Coefficient of Ge:Sb

Chapter 8 -- Discussion, Conclusions, and Future Work

Photothermal ionization spectroscopy of shallow centers in ultra-pure and in intentionally-doped Ge has been a very fruitful technique, yielding many new results for impurity complexes and over-charged acceptors. These results will be summarized here, as well as the inadequacies of the proposed models for each of the observed phenomena. The experimental observations contribute greatly to the process by which the physics of these impurities is finally understood. It is a process in which the experiment and theory go hand in hand, interacting with one another in such a way as to guide one to new experiments and to new theoretical models for the underlying physical phenomena. The feedback obtained in this way has enabled a number of conclusions to be reached regarding microscopic models and symmetries of ground-state configurations. These conclusions will be stated here, in addition to speculations regarding new impurity centers as yet undiscovered. In addition, mention will be made of on-going and future projects related to the physics underlying the properties of known acceptor complexes.

8.1 Effectiveness of the Current Models for Tunnelling-hydrogen Complexes

In the cases of impurity complex centers which are expected to be of the form shown schematically in Figure 14, the hydrogen atom can be thought of as a source of a half-empty orbital which can contain one additional electron. The assumption is therefore that the energy of this orbital lies below the Fermi level in each such system. This model then accounts for the impurity type (n or p) for each of the observed complexes. The effect of the hydrogen atom is to shift the impurity to an effective position in the periodic table that is one atomic number lower, to the left of the actual elemental species.

The newest hydrogen-related impurity complexes, those of the group II-hydrogen centers discussed in section 7.5, behave somewhat differently from the above cases. In these impurities the hydrogen atom is a source of an extra electron for the impurity, so that the energy of the orbital is obviously above the Fermi energy of the system. In such a case, the effect of the hydrogen is to shift the substitutional acceptor one position to the right in the periodic table, toward a higher atomic number. This reduces the number of holes in the acceptor state by one for each hydrogen atom involved. This may also occur for the case of group I or group III atoms as the substitutional acceptor.

The internal degree of freedom provided by the additional nuclear position in the complex center causes a change in symmetry for the shallow level wave functions. In particular, this accounts for the stress insensitivity in that the ground state of a shallow acceptor can now be a Kramers doublet, which is unsplittable and does not shift with stress, as opposed to the quartet ground state of an elemental acceptor. For the donor case, again the new symmetry of the ground state causes a situation in which stress splitting should not be and is not observed. The fact that an entire manifold of states now exists where the elemental impurity has a single ground state accounts for the observed thermal population of the next higher-lying doublet of the manifold. Also, the presence of an isotope shift in the ground state energy for two of the known tunnelling-hydrogen centers (one acceptor, one donor) when deuterium is substituted for hydrogen during crystal growth, confirms the presence of one and only one hydrogen atom in the impurity complex.

One of the inadequacies of the current theory is its inability to determine a priori the ordering of the states in the ground-state manifold. It is especially concerning that in each case of a tunnelling-hydrogen impurity acceptor complex the lowest lying two states are the two Kramers doublets, and that none of the three quartet states have

been observed experimentally. It is conceivable that these states are sufficiently higher-lying in energy that they cannot be substantially thermally populated before ionization of the ground state to the band occurs. For single shallow acceptors this would require an energy difference of only 3-4 meV above the lowest-lying state of the manifold. In fact, if the quartet states were somewhat higher in energy than this, perhaps 7 meV above the ground-state, PTIS would be possible into the very weakly-allowed s-like higher energy state from the ground-state doublet. Such transitions are not observed, so one must conclude that either the three quartets all exist in the energy range 3-7 meV above the ground state or they are much higher in energy, at least near the very bottom of the continuum band and so are not observed as discrete transitions.

8.2 Models for C-N Impurity Complexes and their Predictions

In the case of the two models proposed to explain the features of the C-N impurity complex centers, essentially all of the experimental facts are accounted for, again with the exception as above of not observing the extra states of the multiple ground-state manifold. Specifically, the model explains the stress-insensitivity of the $A_{3,5}$ acceptor spectral lines. This effect is due to the doublet nature of

the two lowest-lying states in the ground-state manifold, which can have the same symmetry for a diatomic center having six equivalent orientations. It is again true, as above for the tunnelling-hydrogen case, that the specific symmetry-group representation of the doublet has not been determined.

The interconversion phenomenon is explained by the fact that two possible configurations exist, because of the internal bonding arrangements of a C-N center, which are both single acceptor states. This is a unique situation in that an impurity in both a substitutional and an interstitial configuration can exhibit the same overall charge state in the lattice. The fact that an internal bonding mechanism exists accounts for the low energy barrier for conversion from substitutional to tetrahedral interstitial sites. It should be pointed out here that the C-N acceptor in the form A_4 is the first reported interstitial shallow acceptor in an elemental semiconductor. Since the cyanide ion is chemically very similar to a group VII elemental atomic species, it might be anticipated that, if their solubilities were sufficient, group VII atoms would exist in an elemental semiconductor lattice as free interstitials which form singly-charged shallow acceptors. However, they have not been observed experimentally.

A striking feature of the trio of spectral line series due to the C-N acceptors is the fact that, to within experimental error determined by linewidths, the energy of the A_4 acceptor is exactly equal to the average (center of the splitting) of the A_3 and the A_5 line series initial state energies. A non-quantitative model description based on group theory alone cannot account for the ordering nor the size of the splittings in the multi-level manifold. It is also true for both the A(H,C) and A(H,Si) cases that the average of the two Kramers doublet energies is very near to the hydrogenic value, i.e. the energies of substitutional single acceptors.

8.3 Comparison of Acceptor-plus Centers to Atomic Models

The model for over-charged acceptor centers with up to a total of four bound holes existing in the (1s) hydrogen-envelope ground state accounts very well for the physical phenomenon observed; that is, the prediction that each central charge (single, double, or triple) can in general bind one more shallow hole state than the number required for neutrality. These bound state energies for group II impurities fit very well with the effective Rydberg predictions from pseudo-He^- free atom states with virtual 3/2-spin electrons. However, the usefulness of an effective Rydberg approach for deep levels, such as the group I atoms,

is questionable. For the case of copper in Ge, the A^+ center binds the fourth hole with much less energy than would be predicted by the model. Presumably the breakdown in the approximation occurs because of the large central cell correction for such deep levels.

8.4 Absorption Spectroscopy Using A^+ Photoconductors

Considering the very low concentrations of electrically-active absorbers that one is able to detect using even a very non-optimized $Ge:Zn^+$ photoconductor, it should in principle be possible to perform very high-resolution studies of rather pure samples. The purity is very important here because it determines whether or not the impurities will overlap or otherwise interact. In the past absorption spectroscopy had not been considered for samples with low impurity concentrations ($\sim 10^{11}$ cm^{-3}). Since it now appears possible, very precise measurements of the oscillator strengths of isolated impurities should be performed in the near future for the entire set of acceptors and donors in pure elemental semiconductors.

8.5 Future Plans and Speculations

Experiments involving diffusion of isotopically pure KCN species of various isotopes have thus far not provided any new information, such as an isotope shift in the

far-infrared spectrum, or a statistically significant presence of radioactive tracer material in the sample in order to prove the in-diffusion assumption for the cyanide species. Such experiments are still progressing, and it is hoped that in the future, perhaps through diffusion or crystal growth in an atmosphere of HCN gas, sufficient concentrations of A(C,N) impurity complexes can be attained to perform absorption spectroscopy of the vibrational states of the C-N molecule. Also, samples with sufficiently high ^{14}C concentrations from labelled radiotracer $K^{14}CN$ diffusion could be used to form a Li-drifted nuclear radiation detector in order to self-count the internal radioactive decays.

One hope for a new set of experiments in elemental semiconductors would be the search for a series of stress-independent hydrogen-related impurity centers in Si. Such centers are expected to exist in ultra-pure Si single crystals containing sufficient hydrogen concentrations. Unfortunately, at the present time the purest available material is vacuum-grown (float-zoned) and attempts to introduce hydrogen from a plasma have not produced such centers. It may be possible in the future to introduce sufficient quantities of hydrogen to form tunnelling-hydrogen centers such as A(H,C) in Si. The lattice mismatch for C in Si is almost as large as for C in

Ge, so that the hydrogen binding mechanism would be expected to be similar. It is not clear whether or not a center such as A(H,Ge) in Si would be expected, as the lattice relaxation around the impurity is in the opposite direction as for the smaller C atom. A search for such a larger-atom complex with hydrogen in Ge, using Sn-doped Ge samples rapidly quenched from 400 ^{o}C, gave negative results. This was taken to indicate that the binding of the hydrogen atom required a strain field from a smaller impurity atom than the host.

In addition it will be worthwhile to explore whether or not the C-N system, which does not require the strain-field binding of a hydrogen atom, will appear as an acceptor complex in Si. The behavior of cyanide as an inhibitor of deep level diffusion has not been explored for Si, where the diffusion temperatures required tend to be several hundred degrees higher than for Ge. If CN protects the Si wafer from the entry of Au and other deep-level impurities, it could be an issue of large technological importance.

As a final note, it may also be possible to perform such impurity complex studies on non-elemental systems such as GaAs. In such a semiconductor an impurity complex such as C-N should appear as a single acceptor in its interstitial form, although it may have two different energy levels due to the difference in the surrounding atoms

(anions or cations) in the two types of tetrahedral hole sites. However, in its substitutional configuration, if it occupies the Ga site, it would be an isoelectronic (neutral) impurity center, similar to an elemental group III atom.

Appendix A -- Effective Mass Theory of Acceptors

The effective mass approximation is a mathematical method in which the effects of the periodic crystal potential on an impurity state are replaced by an equivalent tensor quantity in the effective one-electron equation of motion. This tensor acts as an inverse mass in the kinetic energy term of the Hamiltonian, and its elements are determined by the band structure parameters of the unperturbed system (Luttinger and Kohn, 1955). The components of this tensor are determined experimentally by cyclotron resonance measurements (Dresselhaus, Kip and Kittel, 1954). For a single non-degenerate band, such as a direct gap semiconductor (i.e., GaAs) conduction band, the formalism of Wannier (1937) can be applied directly to the Hamiltonian to produce a Schrödinger equation for the effective screened one-electron potential. However, for the case of degenerate bands, such as the valence bands of the diamond-lattice or zinc-blende semiconductors, a more complicated formalism must be adopted.

The valence bands for Ge and Si consist of two warped or fluted spheres which become degenerate at the Γ point, k=0. This band structure can be written in its most general form, to order k^2 (Kittel and Mitchell, 1955), as

$$E_{h,l}(\vec{k})=Ak^2\pm[B^2k^4+C^2(k_x{}^2k_y{}^2+k_y{}^2k_z{}^2+k_z{}^2k_x{}^2)]^{1/2}$$

and $$E_{so}(\vec{k})=-\lambda+Ak^2$$

where λ is the value of the spin-orbit splitting and the zero of energy is taken to be the valence band top. The degenerate energy maximum for the electron states (energy minimum for holes in the electron distribution) gives rise to coupled differential equations of motion, which can be parameterized by a few effective values (Shockley, 1950). One must in this case diagonalize both the unperturbed crystal Hamiltonian H_o and the impurity potential $V(r)$ simultaneously. In addition, spin-orbit coupling must be included in the initial Hamiltonian (Elliot, 1954). Since the coulomb impurity potential $V(r)=-e^2/\varepsilon r$ is invariant under time-reversal, Kramers theorem states that solutions for the energy eigenvalues will always produce doublet pairs (spin degeneracy) in the absence of a magnetic field.

A derivation of the effective mass Hamiltonian for the simple non-degenerate case is given here, following Luttinger and Kohn (1955). The wave function Ψ for the impurity state satisfies

$$(H_o+V)\Psi = E\Psi \quad .$$

Ψ may be then expanded in a complete set of Bloch functions which are states of the unperturbed crystal Hamiltonian, so that

$$\Psi(r)=\int C(k)\psi_k(r)d^3k \quad \text{where} \quad H_o\psi_k=E(k)\psi_k \quad .$$

Therefore one can write

$$[E(k)-E]C(k)+\int V(k,k')C(k')d^3k'=0$$

with $\quad V(k,k')=\int\psi_k V\psi_{k'}d^3r=\int(u_k{}^+u_{k'})Ve^{i(k'-k)r}d^3r \quad .$

This last expression for $V(k,k')$ is just a Fourier transform of the impurity potential $V(r)$ times a product of Bloch states. If the potential does not vary rapidly with distance (the assumption of a gentle variation on the scale of the lattice constant) so that it is reasonably constant over any one unit cell, then it will only have Fourier components corresponding to very small k, i.e. wavelengths long compared to the lattice spacing. In this case, the kernal function $V(k,k')$ is negligibly small except when $k\simeq k'$, for which

$$V(k,k')=(2\pi)^{-3}\int V(r)e^{i(k'-k)r}d^3r=V(k-k') \quad .$$

The equation for the energy eigenvalues can now be written as

$$[E(k)-E]C(k)+\int V(k-k')C(k')d^3k'$$

with $\quad E(k)=\Sigma\alpha_{ij}(k_i-k_i')(k_j-k_j') \quad .$

Introducing the radial function $F(r)$ as

$$F(r)=\int C(k)e^{i(k-k')r}d^3k$$

we can now write this as the effective mass equation

$$[\Sigma\alpha_{ij}(\tfrac{1}{i}\nabla_i)(\tfrac{1}{i}\nabla_j)+V(r)-E]F(r)=0$$

where α_{ij} are constants determined by the symmetry of the lattice. These constants are then the effective mass parameters, as they take the place of the coefficient $\hbar^2/2m$ in the kinetic energy term for the impurity eigenfunction

equation. The wave function is a product of a set of Bloch states times a modulating function F(r). The envelope function is a state of good parity of the perturbed Hamiltonian, while the Bloch states are not. Thus, weakly allowed $1\Gamma_8^+ \rightarrow 2\Gamma_8^+$ (E line of Jones and Fisher) can be seen.

For the case of Ge, we can write the effective mass Hamiltonian with spin-orbit coupling (Baldereschi and Lipari, 1970) as

$$H=[\frac{\gamma_1}{2m}p^2-\frac{e^2}{\varepsilon r}]-\frac{1}{9m}[\gamma_3-(\gamma_3-\gamma_2)\delta_{ij}]P_{ij}J_{ij}$$

in terms of the Luttinger valence band parameters (1956), where m is the free-electron mass. The operators P and J are traceless reducible second-rank symmetric tensor operators, and have no first-rank (vector) components due to the tetrahedral symmetry of the lattice. The terms can be given in irreducible components of the tensors, and written in such a way as to display the parts with full spherical symmetry separately from those with only cubic symmetry. This rearrangement points to a better set of parameters. Keeping the constant γ_1, we use

$$\mu=(6\gamma_3+4\gamma_2)/5\gamma_1$$

for the strength of the spherical spin-orbit interaction, and the cubic coupling parameter

$$\delta=(\gamma_3-\gamma_2)/\gamma_1$$

for the cubic contributions. Since these are small for Ge (δ=0.1 using the Luttinger parameters given by Lawaetz,

1971) they can safely be treated as a perturbation. In any case, the cubic terms do not contribute to the energy of the (1s)-like ground state.

If we define an effective Rydberg for the germanium lattice by

$$R_o = e^4 m/2\hbar^2 \varepsilon^2 \gamma_1$$

the value of R is then calculated to be 4.3 meV by Baldereschi and Lipari (1973). They further show that for the case of Ge (μ=0.766) the spin-orbit interaction strength is such that the binding energy of the ground state ($1S_{3/2}$) becomes 2.284R, as interpolated from their table of values in the strong-coupling limit. This is then a binding energy of 9.82 meV for the hydrogenic effective-mass one-hole acceptor state. The value for silicon (μ=0.483) is taken from the weak-coupling limit table (spin-orbit energy splitting $\simeq$ binding energy) as 1.418 times the effective Rydberg of 24.8 meV, or a binding energy of 35.17 meV; in the strong coupling limit it becomes 1.336(24.8 meV)=33.13 meV. The value quoted in the paper is 31.6 meV.

References

Ahlburn, B.T., and Ramdas, A.K., 1968, Phys. Rev. 167, 932-42; and 1969, Phys. Rev. 187, 717-29.

Baldereschi, A. and Lipari, N.O., 1970, Phys. Rev. Lett. 25, 1660-4.

Baldereschi, A. and Lipari, N.O., 1973, Phys. Rev. B8, 2697-709.

Baldereschi, A. and Lipari, N.O., 1974, Phys. Rev. B9, 1525-39.

Baldereschi, A. and Lipari, N.O., 1976, "Physics of Semiconductors", ed F.G. Fumi (Rome:Tipografia Marves), 595-8.

Barraf, G., Schluter, M., and Allan, G., 1982, Phys. Rev. Lett. 50, 739-42.

Bell, R.J., 1972, "Introductory Fourier Transform Spectroscopy" (New York: Academic)

Broecx, J., Clauws, P., Van Den Steen, K., and Vennick, J., 1979, J. Phys. C: Solid St. Phys. 12, 4061-79.

Bykova, E.M., Lifshits, T.M., and Sidorov, V.I., 1973, Sov. Phys. Semicond. 7, 671-2.

Collins, A.T., and Lightowlers, E.C., 1968, Phys. Rev. 171, 843-55.

Cross, J.W., Ho, L.T., Ramdas, A.K., Sauer, R., and Haller, E.E., 1983, Phys. Rev. B28, 6953-60.

Darken, L.S., 1982, J. Appl. Phys. 53, 3754-64.

Darken, L.S., and Hyder, S.A., 1983, Appl. Phys. Lett. 42, 731-3.

Dresselhaus, G., Kip, A.F., and Kittel, C., 1954, Phys. Rev. 95, 568-9.

Edwards, A.H., and Fowler, W.B., 1977,Phys. Rev. B16, 3613.

Elliot, R.J., 1954, Phys. Rev. 96, 266-87.

Evwaraye, A.O., Hall, R.N., and Soltys, T.J., 1979, IEEE Trans. Nucl. Sci. 26, 271.

Faulkner, R.A., 1969, Phys. Rev. 184, 713-21.

Frank, W., Seeger, A., and Gosele, U., 1981, MRS Symposia Proceedings Vol. 2, "Defects in Semiconductors", ed. J. Narayan and T.Y. Tan, 31-54.

Gershenzon, E.M., Gol'tsman, G.N., and Mel'nikov, A.P., 1971, JETP Lett. 14, 185.

Hall, R.N., and Soltys, T.J., 1977, GE Res. Rep No. 9, 7.

Haller, E.E., 1978, Phys. Rev. Lett. 41, 1192-4.

Haller, E.E., Hansen, W.L., and Goulding, F.S., 1981, Advances in Physics 30, 93-138.

Haller, E.E., and Falicov, L.M., 1978, Phys. Rev. Lett. 41, 1192-9.

Haller, E.E., Joos, B., and Falicov, L.M., 1980, Phys. Rev. B21, 4729-39.

Haller, E.E., McMurray, R.E. Jr., Haegel, N.M., and Falicov, L.M., 1984, Proc. of XVII Int. Conf. on Phys. Semi.

Jones, R.L., and Fisher, P., 1965, J. Phys. Chem. Solids,

1125-31.

Joos, B., Haller, E.E., and Falicov, L.M., 1980, Phys. Rev. B22, 832-41.

Kalia, R.K., Vashista, P., and Lee, M.A., 1984, Bull. of Amer. Phys. Soc. Series II 29, 292.

Kane, E.O., 1960, Phys. Rev. 119, 40-2.

Kittel, C. and Mitchell, A.H., 1954, Phys. Rev. 96, 1488-93.

Kogan, S.M., and Sedunov, B.I., 1967, Sov. Phys.-Solid State 8, 1898.

Kohn, W., 1957, "Solid State Physics" vol. 5, ed. F. Seitz and D. Turnbull (New York: Academic), 257-320.

Lawaetz, P., 1971, Phys. Rev. B4, 3460-7.

Lang, D.V., 1974, J. Appl. Phys. 45, 3022.

Lifshits, T.M., Likhtman, N.P., and Sidorov, V.I., 1968, Soviet Phys. JETP Lett. 7, 2076.

Lifshits, T.M., and Nad', F.Y., 1965, Soviet Phys. Dokl. 10, 532.

Luttinger, J.M., 1956, Phys. Rev. 102, 1030-41.

Luttinger, J.M., and Kohn, W., 1955, Phys. Rev. 97, 869-88.

McMurray, R.E. Jr., 1984, Proc. of Spectr. of Shal. Cen. in Semicond., to be pubished in Solid State Comm.

McMurray, R.E. Jr., Heagel, N.M., Kanh, J., and Haller, E.E., 1984, Proc. of Spectr. of Shal. Cen. in Semicond., to be published in Soid State Comm.

Ramdas, A.K., and Rodrigues, S., 1981, Rep. Prog. Phys. 44, 1297-1387.

Reuszer, J.H., and Fisher, P., 1964, Phys. Rev. 135, A1125-32.

Schiff, L.I., 1968, "Quantum Mechanics", 3rd ed. (New York: McGraw-Hill).

Shockley, W., 1950, Phys. Rev. 78, 173-4.

Tokumoto, H., and Ishiguro, T., 1977, Phys. Rev. B15, 2099-117.

Van der Pauw, L.J., 1958, Philips Research Rep. 13, 1.

Van de Steeg, M.J.H., Jongbloets, H.W.H.M., Gerritsen, J.W., and Wyder, P., 1983, J. Appl. Phys. 54, 3464-74.

Wannier, G.H., 1937, Phys. Rev. 52, 191-7.

Wu, Y., and Falicov, L.M., 1984, Phys. Rev. B29, 3671.

This report was done with support from the Department of Energy. Any conclusions or opinions expressed in this report represent solely those of the author(s) and not necessarily those of The Regents of the University of California, the Lawrence Berkeley Laboratory or the Department of Energy.

Reference to a company or product name does not imply approval or recommendation of the product by the University of California or the U.S. Department of Energy to the exclusion of others that may be suitable.

TECHNICAL INFORMATION DEPARTMENT
LAWRENCE BERKELEY LABORATORY
UNIVERSITY OF CALIFORNIA
BERKELEY, CALIFORNIA 94720